1981

Nonphotochemical hole burning and the nature of amorphous solids

Roland Paul Stout
Iowa State University

Stout, Roland Paul

NONPHOTOCHEMICAL HOLE BURNING AND THE NATURE OF AMORPHOUS SOLIDS

Iowa State University PH.D. 1981

Nonphotochemical hole burning and the nature of amorphous solids

by

Roland Paul Stout

A Dissertation Submitted to the
Graduate Faculty in Partial Fulfillment of the
Requirements for the Degree of
DOCTOR OF PHILOSOPHY

Department: Chemistry
Major: Physical Chemistry

Approved:

Signature was redacted for privacy.

In Charge of Major Work

Signature was redacted for privacy.

For the Major Department

Signature was redacted for privacy.

For the Graduate College

Iowa State University
Ames, Iowa

1981

TABLE OF CONTENTS

	Page
DEDICATION	iii
CHAPTER I. INTRODUCTION	1
Review of Optical Hole Burning	1
Nonphotochemical Hole Burning: The Mechanism	12
Amorphous Solids	25
CHAPTER II. THEORY	28
Effects of Two Level Systems on Hole Burning	28
Connections with Other Theories	39
CHAPTER III. EXPERIMENTAL	43
Sample Preparation	43
Cryogenic Equipment	50
Optical System and Light Sources	51
CHAPTER IV. RESULTS AND DISCUSSION	55
Survey of Nonphotochemical Hole Burning	55
Thermal Effects of Nonphotochemical Hole Burning	86
Computer Modeling	108
CHAPTER V. CONCLUSION	120
Nonphotochemical Hole Burning	120
REFERENCES	127
ACKNOWLEDGMENTS	133
APPENDIX	134

DEDICATION

To my parents, J. Dean and Betty Stout, who planted the seeds of curiosity, and to the teachers who nurtured them along the way.

CHAPTER I. INTRODUCTION

Review of Optical Hole Burning

The optical hole burning phenomenon, in which monochromatic excitation into an optical transition causes a localized decrease in the intensity of that transition centered at the excitation frequency, may be understood to be due to a decrease in the population of the initial state for the transition at the excitation frequency. One consequence is that since holes are localized around the excitation frequency, the transition involved must be inhomogeneously broadened. One may hope to use optical hole burning to reduce or eliminate the inhomogeneous broadening of spectral lines and obtain information about dynamical processes.

Within this broad definition, hole burning may be divided into two types: the first associated with depopulation of the lower (usually the ground) level of a transition yielding holes in the absorption spectrum of the system, and the second associated with depopulation of the upper (excited) level producing holes in the emission spectrum. Ironically, optical hole burning was first observed in emission spectra when an intensity decrease at the peak of the gain curve, (ω_0), of high-power ruby lasers was observed (1,2). This "spectral hole" was explained as selective depletion of excited states resonant with ω_0 since this is the most probable lasing frequency. A later interpretation (3,4) suggested that the holes, formed spatially as excited states resonant with ω_0, were depleted at positions of maximum amplitude of the standing optical

wave in the laser cavity. A similar decrease in lasing intensity, observed in the output of a helium-neon laser (5), was explained (5,6) as the depletion of excited neon atoms with velocities near the peak of the Doppler profile for the laser transition. Holes burned by saturating a transition of a gaseous sample are now known as Lamb dips Danielmeyer provides an insightful interpretation of saturation hole burning of laser transitions which considers the effect of drift and diffusion of excited states on hole burning in lasers (7).

That optical holes were first observed in emission (laser) lines was a consequence of the intense research activity on the properties of laser systems after their inception in 1954. More recently, lasers are being used as intense, monochromatic light sources, resulting in observations of hole burning by depletion of the ground state population. These now far outnumber examples of hole burning by depletion of the excited state. The first such example (8) was observed by the Lamb-dip method, saturating an absorption transition of neon at low pressure using a helium-neon laser. This type of Lamb-dip spectroscopy has been used to obtain ultrahigh-resolution spectroscopic data (9).

The first example of saturation hole burning in the absorption spectrum of a solid was obtained in ruby (10) and has since been used to obtain high-resolution absorption (10-17), Zeeman (10,11), Stark (12-16) and hyper-fine (17) spectra of metal atoms in solid systems at low temperatures. Saturation hole burning has also been observed in solutions of organic dyes (18) (which has now found wide use in the passive mode-locking of lasers (19)), in solutions of aromatic

hydrocarbons (20), and in the zero-field microwave spectra of triplet states (21,22), in each case providing new information about the energetics and dynamics of the systems studied. A related hole burning method, population hole burning, has been observed (23-25) in which the triplet population builds up at the expense of the ground state population.

All these examples of hole burning are transient in nature. The burned holes decay (fill) rapidly as the equilibrium population densities are reestablished by, for example, decay of the states produced in saturation hole burning. For hole burning of emission transitions, the holes are filled by optical pumping to repopulate the excited state or by diffusion of excited states into the region of the hole (7).

To burn permanent holes, the processes which allow holes to fill must be removed. Permanent holes, only possible in absorption transitions, are burned when the species absorbing at the excitation frequency are removed, either by destruction or by causing them to absorb at another frequency by interaction with the exciting field. To prevent these holes from filling (or being annealed out), the diffusion processes in the sample must be halted by using a rigid sample at low temperatures.

The most obvious way to remove the absorbing species is to destroy or alter it photochemically. Because of the required rigidity of the samples, photochemistry involving gross molecular rearrangement cannot occur and highly reactive species formed by photochemical fragmentation

cannot diffuse apart and sometimes recombine. The types of photochemical reactions which form holes, then, are those photoreactions forming stable products and rearrangements not involving gross structural changes. Even these permanent holes may be annealed if the sample is not sufficiently rigid to prevent diffusion or if the sample temperature is raised, allowing diffusion to begin.

Photochemical hole burning (PHB) by dissociation and by molecular rearrangement have each been observed (26,27). The first dissociative photochemical holes were observed by deVries and Wiersma (26) for s-tetrazine in a durene host crystal. Combining their data with others', they studied the dynamics of vibrational relaxation for the excited and ground states of s-tetrazine. Similar photochemical holes have been observed by Cuellar and Castro for dimethyl-s-tetrazine in a polyvinyl carbazole film (28). Photochemical holes by molecular rearrangement were first observed by Gorokhovskii et al. for H_2-phthalocyanine in n-octane (27) where the rearrangement is the photo-induced tautomerism of the inner protons of the phthalocyanine ring. PHB has now been studied in many free-base porphine type molecules in Shpolskii matrices (29-34) and crystals (38-40). These studies have shed light on the thermal broadening of electronic transitions (31-33,35), the homogeneous linewidths for purely electronic (29,35) and vibronic transitions (36), matrix effects on electronic transitions (40), inhomogeneous broadening of vibronic transitions (30,34), vibrational frequencies large molecules in solid matrices (38), and the coupling of excited states as studied using the Zeeman effect (37).

Recently, similar THB results have been observed in chlorin (7,8-dihydroporphine), the parent molecule of the chlorophyll system, in n-alkane hosts (41,42), and in C-phycocyanin (43) and C-phycoerythrin (44), the light harvesting pigments of blue-green and red algae, respectively, in glasses. These studies have shown photochemical hole burning to be a useful tool for obtaining information on the conformation, photochemistry and dynamics of these molecules, which is useful for understanding their role in photosynthesis.

Another type of PHB which has been observed involves the photoejection of electrons. Holes have been observed for photoejection of trapped electrons in organic glasses (45) and from F_3^+ color centers in NaF (24). Similarly, PHB by photoionization has been observed for resorufin in polymethyl methacrylate (46).

There have been many reports of photochemistry of small molecules in rare gas matrices of which the photochemistry of $Fe(CO)_5$ is typical. Ultraviolet irradiation of $Fe(CO)_5$ in argon produces $Fe(CO)_4$ + CO which remain trapped together. Infrared irradiation into the CO stretching region of $Fe(CO)_4$ causes the reaction to be reversed yielding $Fe(CO)_5$ (47). In particular, IR laser irradiation into a particular band in the $Fe(CO)_4$ spectrum converts the molecules absorbing in that band but leaves other bands in the same region unchanged (48,49). While this does not create well-defined holes within a band, but rather burns out the entire band, it is still an example of PHB since the absorption has been decreased at a selected frequency by a photochemical reaction.

The PHB of hydrogen bonded dihydroxyquinones is especially interesting since it is in many ways similar to nonphotochemical hole burning, the subject of this dissertation. Haarer and coworkers at IBM San Jose have studied the series of hydroxyquinones from 2,5-dihydroxy-p-benzoquinone through 6,11-dihydroxy-5,12-tetracenequinone and some related molecules in various hosts (50,51). They found that in non-hydrogen bonding hosts at low temperatures, the laser-excited fluorescence spectra are line-narrowed showing no Franck-Condon shifts and that no PHB occurred. From this, they concluded that intramolecular proton transfer (tautomerization) was not occurring.

When several of these dihydroxy-p-quinones, of which 1,4-dihydroxy-anthraquinone (quinizarin) is a typical example, were doped into proton acceptors (polymethylmethacrylate) or into hydrogen bonding systems (ethanol, polyvinylalcohol) PHB was observed in moderate to high yield. Diffuse laser irradiation into the (0,0) band of quinizarin in 3:1 ethanol/methanol at 2K caused the absorption in the region of the laser frequency to decrease while the absorption increased 3000 cm^{-1} to higher energy. Warming the sample to 60-80K caused the original (unburned) spectrum to reappear. Irradiation of the sample with a weak, broad band light source also caused the holes to disappear. In contrast to the highly structured fluorescence spectrum of quinizarin in the nonhydrogen bonding solvent n-heptane, the fluorescence of quinizarin in the alcohol glass showed a complete lack of vibrational structure and a blue shift of 220 cm^{-1} with respect to the n-heptane spectrum. The interpretation of these data is that PHB occurs in these systems via the breaking of

an intramolecular hydrogen bond and the formation of an intermolecular hydrogen bond to the matrix as depicted below for quinizarin. That

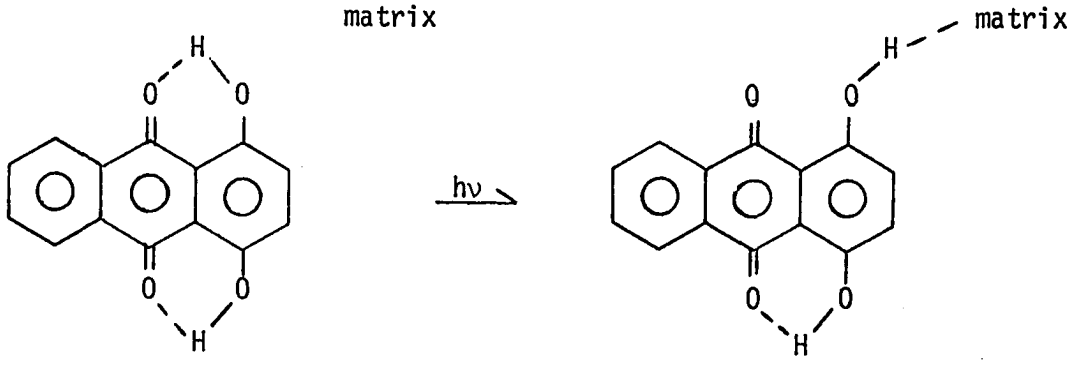

this tautomerization is reversible is indicated by the disappearance of the holes by warming or by exciting into the product's absorption with even a weak light source.

Holes burned with a weaker, narrower laser were found to be Lorentzian with widths of 1.5-3.0 cm^{-1} for holes burned around 2K (50, 51). These widths indicate the existence of a relaxation process with a relaxation time of 5-10 ps (51) in the glassy media. The authors do not distinguish between T_1 (lifetime[1]) or T_2' (dephasing[1]) processes,

---

[1]If an ensemble of molecules is excited with an incoherent source, the only relaxation process is decay of the excited state, a lifetime or T_1 process. If the ensemble is excited with a coherent (i.e., laser) source, the prepared excited states are in phase with each other. Processes which destroy the phase coherence of the excited ensemble are called dephasing or T_2' processes. A good example is due to Macomber (52). Consider a group of soldiers marching to a drill sergeant's call on a hot parade ground. While they march to the cadence, the soldiers are in phase. If the sergeant ceases his cadence and the soldiers' memory of the cadence is imperfect, the soldiers will eventually fall out of step until the unit is scattered over the entire parade ground. The unit has lost its phase coherence and has been dephased; a T_2' process. If after some longer time the soldiers collapse from heat exhaustion, the unit has undergone a T_1, lifetime, relaxation.

but they seem to imply that a T_2' process is more likely. They postulate that the hydrogen bond to the matrix may provide relaxation pathways which are absent in other systems (51).

The photochemical back reaction was found to be phonon selective in that molecules with strong electron-phonon coupling underwent the back reaction with more facility than those with weaker coupling (53). This phonon selectivity allows the experimental discrimination between sites of differing electron-phonon coupling strength. One consequence of the phonon selectivity of the back reaction is that the relative phonon coupling strength for a reactive center does not change in the tautomerization process, but is determined by the local structure of the glass around the quinizarin molecule. The PHB of quinizarin has been used to investigate electron-phonon coupling in organic glasses (54). The PHB of dihydroxyquinonens and how it relates to nonphotochemical hole burning will be discussed in a later section.

As was stated above, there are two ways to produce permanent holes. The first method, to destroy or alter the absorbing molecule photochemically, has been discussed. The second method, causing the absorption energy of a molecule to change through interaction with the exciting field, leads to nonphotochemical hole burning (NPHB) or photophysical hole burning. NPHB was first observed indirectly in 1972. Personov et al. (55,56) reported the first laser-induced fluorescence line narrowing for organic molecules in glasses, noting

that at high laser powers (30 mW)[2] the line-narrowed fluorescence intensity decreased with time to one third its original intensity after five minutes. If the laser power was lowered to 0.3 mW, no fluorescence intensity decrease was observed. The first direct observation of NPHB was made in 1974 when, after laser-irradiation of perylene or 9-amino-acridine in ethanol at 4.2K, a stable hole in the absorption spectrum was observed at the laser frequency (57). The hole was found to be stable in the dark at the burn temperature (T_B = 4.2K). Warming to 30K and cooling back to T_B eliminated the hole, as did irradiation with an intense white light at T_B. Investigation of this hole showed it to have a width of 0.7 cm^{-1} which, after deconvolution of the laser profile, gave a width for the absorption of a single impurity center (site[3]) of 0.3 cm^{-1} or 0.6 cm^{-1} for a Gaussian or Lorentzian line shape (57,58).

The kinetics of the burning were studied in an attempt to determine the mechanism. The fluorescence intensity decrease was found to be non-exponential due to the fact that fluorescence was observed from all sites which absorbed at the laser frequency but which burn out at different rates (58). Kinetic modeling of the fluorescence decrease showed the burning to be a one-photon process (58), disproving the suggestion (55,56) of a two step ionization via the triplet state,

---

[2]NPHB depends on laser flux rather than power, but Personov et al. (55,56) do not report the flux used.

[3]For purposes of this dissertation, a site is defined as an impurity molecule and its immediate surroundings in the amorphous matrix.

giving rise to the theory that the mechanism involved a reorientation of the excited impurity molecule in the matrix (58).

Fine structure observed in the hole burned spectra of organic molecules in glasses (58), was interpreted as the vibronic spectra of the sites burned at the laser frequency. (NPHB alters the density of sites in the ground state. This altered density not only produces holes in absorption at the laser frequency, but also in other vibronic transitions of the impurity molecule.) This has been suggested as a means of obtaining the vibronic spectra of large molecules in glasses (59,60) and is experimentally identical with the method proposed for obtaining the vibronic structure of molecules in Shpolskii matrices by PHB (38).

NPHB in infrared vibrational transitions was observed by Dubs and Günthard after irradiation into the ν_{17} band of trans-1,2-difluoroethane in solid argon or krypton using a diode laser (61,62). For an argon matrix deposited at 17K, a hole burned at 6K has a Lorentzian profile of width 0.006 cm^{-1}. The homogeneous widths indicate a relaxation time of 3.5 ns which is interpreted as a vibrational lifetime with no contribution from dephasing at 6K. The hole widths depend strongly on the matrix deposition temperature and annealing history of the sample, being narrower for matrices deposited at higher temperatures. The holes are unstable and disappear with time, more quickly at higher temperatures. This annealing was shown to be thermal in nature, arising from thermal radiation entering through the dewar windows. It was postulated that the formation of the holes was due to a shift of the vibrational

frequency of an excited molecule within the inhomogeneous distribution of frequencies. This shift, it was suggested, could be caused by a temporary local heating of the molecular environment, resulting in a change in the local structure of the matrix.

NPHB has also been observed in dimethyl-s-tetrazine in a polyvinylcarbazole film (28). When a sample is irradiated with an intense pulsed dye laser, photochemical holes were burned whose widths were laser limited. When much less intense ($\sim$ 8 mW[4]), narrower (0.01 cm^{-1}) cw laser was used, nonphotochemical holes were burned. These holes were Lorentzian with a width of 0.44 cm^{-1} for a burn temperature of 1.8K. The nonphotochemical holes were found to be unstable, decreasing in depth with time for samples held at or below T_B. This decay was fit by an expression of the form $h = at^b$ where a and b are constants and h is the hole depth. For T_B = 1.8K, a and b were found to be 6.2 and -0.25, respectively.

Edelson et al. have observed nonphotochemical holes burned with one photon in the one-photon and two-photon spectra of phenanthrene (63). They suggest that this method may be useful for studying the vibronic spectra of large, biologically important systems whose substitution into crystalline hosts is not feasible.

At the beginning of 1978, all that was known about the mechanism of NPHB was that it was a one-photon process (58). In a series of

---

[4]Again, the laser flux was not reported.

three papers in 1978-1979, Hayes and Small discussed the salient properties of NPHB, its relation to the nature of organic glasses and a NPHB mechanism (64-66).

Nonphotochemical Hole Burning: The Mechanism

Fluorescence line narrowing (FLN) and NPHB are intimately connected. NPHB was discovered in the course of FLN studies of molecules imbedded in organic glasses (55,57). When NPHB occurs, FLN is usually observed as well (55-60, 63-66), and each has been used to probe the inhomogenities present in amorphous solids and to observe narrow spectroscopic features in the presence of site inhomogeneous broadening (55-66). The similarities between FLN and NPHB occur because both processes share a common first step, the site-excitation-selection step.

Site-excitation-selection can be understood by considering Figure 1. A broad absorption such as those typical of solutions or glasses may be thought of as a superposition of narrower absorptions due to individual sites which are inhomogeneously distributed across the entire band. This distribution occurs because of the random nature of the environment around each absorbing molecule. If the broad absorption is irradiated with a narrow source such as a laser, only those sites which absorb at the excitation frequency, the shaded site in Figure 1, are selected. The sites absorbing at the excitation frequency share the common transition energy, but they need not be

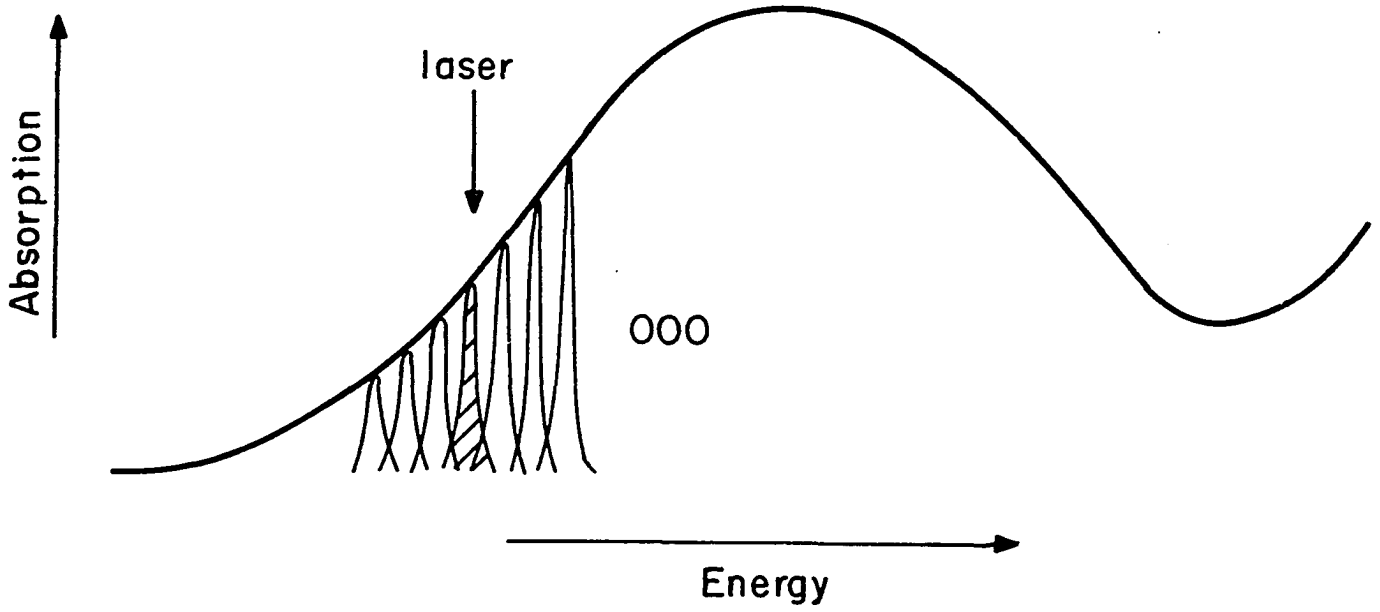

Figure 1. A schematic representation of a glass absorption spectrum showing the narrow site absorptions which are inhomogeneously distributed in energy across the band. Irradiation with a narrow laser as shown excites only the shaded site resulting in energy site selection

geometrically equivalent, thus the term site-excitation-selection.[5] In liquid samples, the molecular motion allows the excitation to spectrally diffuse across the entire band. If the sample is rigid, preventing bulk diffusion, and if other spectral diffusion processes are absent, the excitation will remain localized at the excited site. This site can then emit a photon into a line-narrowed fluorescence band, or undergo a hole burning reaction to become part of a narrow hole.

When NPHB is observed for a sample, FLN has usually been observed as well. The converse is not true. FLN has been observed from mixed crystals, rare gas matrices, and Shpolskii matrices, but NPHB has not been found to occur in these hosts.[6] NPHB has generally been observed in glasses and, in a few cases, random polymers or rare gas matrices. All of these hosts, in which NPHB is known to occur, are random or amorphous in nature.

Nonphotochemical holes are not generally deep, usually saturating (ceasing to burn) around 10-20% of the original optical density at the excitation frequency. Once burned, nonphotochemical holes are typically persistent[7] if kept in the dark. Irradiation with an intense

---

[5]Hereafter the term site-selection will be used, with the understanding that the sites are being excitation energy selected.

[6]The hole burning reported by Dubs and Günthard (61,62) in rare gas matrices was done on vibrational bands from which fluorescence does not occur. Most examples of NPHB occur in electronic transitions and such hole burning has not been observed in rare gas matrices.

[7]By persistent, it is meant that the integrated intensity or profile of a hole does not change on the time scale of the experiment (many hours) if the sample is kept at or below T_B.

white light or warming the sample removes the holes. Nonphotochemical holes are most often burned with relatively low laser powers, less than 50 mW. At higher laser powers, 50-200 mW, holes are found to be broader than those burned with lower powers and at even higher powers, above 250 mW, no holes are burned and existing holes are removed. These power effects are thought to arise from bulk heating of the sample by the laser (28,64).

The persistence of holes and the effects of laser power actually vary widely. The holes observed in a vibrational band of difluoroethane decreased with time at T_B (61,62), which was shown to be a thermal effect due to the background thermal radiation. Nonphotochemical holes burned in dimethyl-s-tetrazine in polyvinylcarbazole also disappeared with time and showed broadening at relatively low laser powers (< 40 mW) (28). On the other hand, holes burned in tetracene in 4:1 ethanol/methanol (64) and in tetracene in 2:1:1 glycerol/dimethylsulfoxide/N,N-dimethylformamide (*vide infra*) are persistent at T_B and do not show any broadening until powers in excess of 50 mW are reached. Within limits appropriate to the system under study, the general observations given above for persistence and broadening are valid.

Hayes and Small (64) have observed that the FLN spectrum of tetracene in 3:1 ethanol/methanol exhibited a strong linear electron-phonon coupling as indicated by strong phonon wings on the fluorescence lines while tetracene in 5:2 ethyl ether/isopropanol exhibited much weaker phonon wings and electron-phonon coupling. Yet, each of these samples exhibited NPHB with comparable efficiencies. It was concluded

that NPHB was not correlated with the linear electron-phonon coupling strength as exhibited in fluorescence spectra.

Nonphotochemical (and photochemical) holes generally consist of two parts. A relatively narrow hole appears at the excitation frequency and a broader hole appears to lower energy. The entire hole looks highly reminiscent of the zero-phonon and phonon side bands often seen in the absorption spectra of crystals except that here the side band (hole) lies to lower rather than to higher energy. To understand this effect, note that the absorption of a site, in general, consists of a zero-phonon line (ZPL) and a phonon side band (PSB) to higher energy as depicted in Figure 2a. A zero-phonon hole is produced when sites absorbing at the excitation frequency, ω_0, through their ZPLs undergo hole burning. The PSB hole to lower energy is the convolution of all sites which absorb at ω_B through their PSB and relax to the zero-phonon level before undergoing hole burning. (One such site is shown as the dashed curve in Figure 2b.) The intensity of the PSB hole, more properly called a pseudo-PSB hole, at $\Delta\omega = \omega_B - \omega$ traces out the absorption intensity of sites which absorb at ω_0 through phonons of frequency $\Delta\omega$. From this model, one would expect to see a true PSB hole to higher energy due to the PSBs of sites absorbing at ω_B through their ZPLs.

The existence of zero-phonon holes implies that NPHB does not depend on the linear electron-phonon coupling through the direct excitation of a phonon (67). This indicates that a phonon assisted

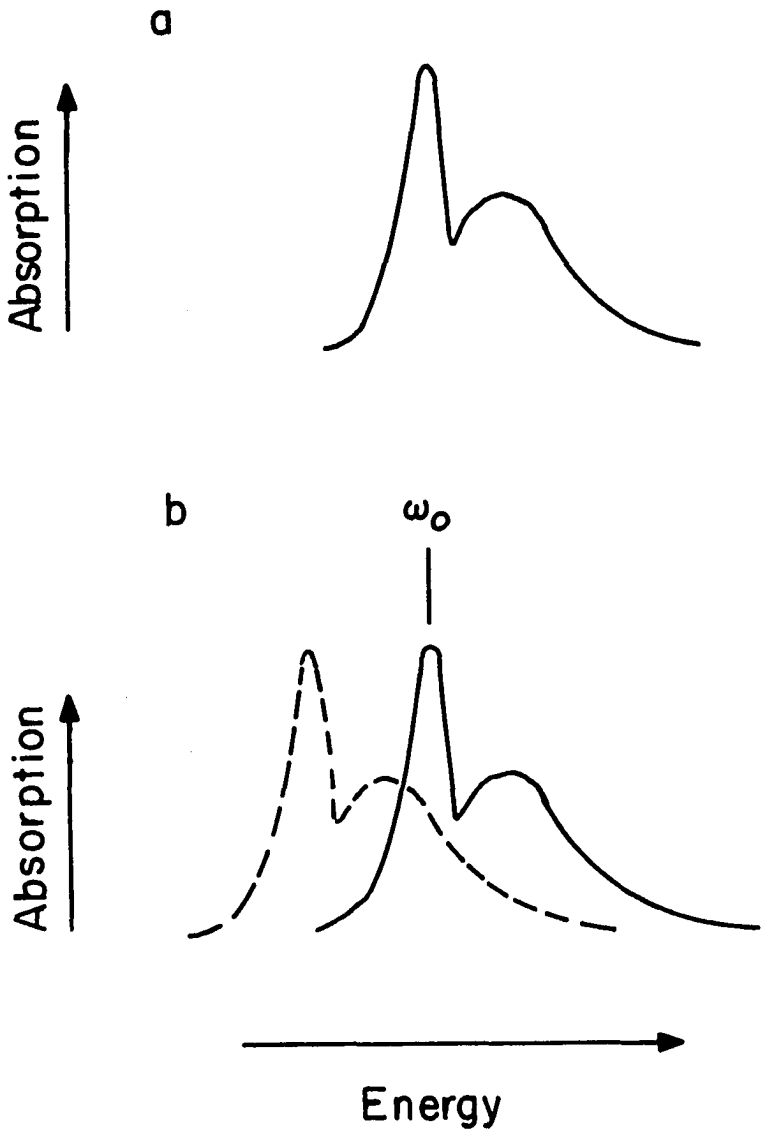

Figure 2. Site absorption profile. (a) A schematic representation of the absorption spectrum of an individual site showing the sharp zero-phonon absorption and the broader phonon side-band absorption to higher energy. (b) Irradiation at ω_o excites some sites through their zero-phonon line (solid curve), and other sites, and zero-phonon lines of which lie to lower energy, through their phonon side band (dashed curve)

site interconversion process of the type observed by Small (68) for tetracene in p-terphenyl is not the mechanism for NPHB.

Friedrich et al. (54) have considered the effect of electron-phonon coupling for photochemical hole burning and predict that a PSB hole should be observed to higher energy. They point out, however, that phonon holes will be as intense as pseudo-PSB holes only for weak coupling and very short burn times. They observe this situation for a burn time of 16 seconds. For longer burn times, the pseudo-PSB hole is observed to overwhelm the PSB hole because the ZPL and its associated PSB hole saturate while the pseudo-PSB hole continues to burn.[8] This is explained (54) by assuming a distribution of electron-phonon coupling strengths. The PSB hole is produced by weakly coupled sites which absorb at ω_B through their ZPLs. The pseudo-PSB hole is produced by more strongly coupled sites giving rise to a deeper pseudo-phonon hole. The PSB holes, to higher energy of the ZPL, are seldom seen in NPHB perhaps because of the longer burn times, or perhaps, as Friedrich et al. (54) suggest, the sites burned away at ω_B have new absorption energies only slightly removed from ω_B (vide infra) and interfere with the ZPL saturation.

Until now, we have been blithely speaking of nonphotochemical hole burning (NPHB) without having shown that it is indeed not photochemical in nature. There are several points which speak to this

---

[8]This is also true for strong electron-phonon coupling (69, vide infra).

question. Most absorbing molecules used in NPHB, perylene, 9-amino-acridine, tetracene, 1,2-difluoroethane, etc., are photostable in room temperature solutions. While hole burning is observed for these molecules in glassy solids, no holes have been observed for these molecules in crystals, Shpolskii matrices, or rare gas matrices[9] under similar conditions. If the hole burning were photochemical, a photoproduct's absorption would be expected well removed from the excitation frequency. No such photoproduct has been observed. The most telling evidence is provided by the hole filling experiments of Hayes and Small (64). They burned a hole at 21041 cm^{-1} into the origin absorption band associated with tetracene's lowest excited singlet state, S_1. Another hole burned at 21038 cm^{-1} did not change the first. A third hole, burned at 21039.5 cm^{-1} midway between the first two, reduces their intensity by 25%. Further burning at this intermediate frequency reduces the original two holes by another 15%. From analysis of the hole areas, it was concluded that $\sim$45% of the sites burned are shifted to sites differing in energy by < 2 cm^{-1}.

To review, the mechanism for NPHB must explain the observations that:

1) NPHB occurs only in amorphous solids.

2) NPHB does not depend on the direct excitation of a phonon.

---

[9]We are considering here NPHB into electronic transitions. See also footnote 6.

3) A zero-phonon hole appears at the excitation frequency.
4) A broad pseudo-phonon hole may be produced to lower energy from the excitation.
5) Holes do not burn completely, but are persistent.
6) Holes burned at any given temperature are irreversibly eliminated by warming the sample sufficiently.

The mechanism of Hayes and Small (64-66) for NPHB is based on the proposal that a glass contains a distribution of asymmetric intermolecular double well potentials or, as they are frequently called, two level systems (TLSs). The distribution of these TLSs is over barrier heights and widths, spatial displacements and energy differences between the two minima, etc. The nature of the displacement coordinate is open to speculation but might involve displacements of solvent (glass) molecules, a change in the internal conformation of solvent molecules, or, in the case of hydrogen bonded glasses, a reorganization of the hydrogen bonding network. The TLS model has been used to explain the anomalous low-temperature thermal properties of glasses (70,71), low-temperature structural relaxation in glasses (72), and other phenomena; and are now believed to be a universal accoutrement of glasses (73).

An impurity molecule is associated with the TLS in such a way that its electronic energy has two possible values depending on which of the two minima is occupied. Due to the distribution of barrier heights, for any arbitrary temperature there are some sites (impurity-TLS) which are in thermal equilibrium and others which are frozen into one of the

minima. For an optical experiment, the TLS potential must be considered for both the ground and excited states of the impurity molecule. NPHB is associated with those sites for which the TLS for the (impurity) excited state has a barrier low enough to allow transitions from one minima to the other, and for which the TLS for the (impurity) ground state has a barrier high enough to prevent transitions between the minima at the burn temperature on the time scale of the experiment. This situation is depicted in Figure 3. The TLS is initially in state I and the barrier is too high to allow transitions between I and II directly. The impurity is then excited to I' with a photon of frequency ω_I. The barrier between this state and II' is low enough to allow transitions between I' and II'. If such a transition occurs and the impurity molecule then relaxes from II' to II, the impurity molecule no longer absorbs at ω_I but to higher energy at ω_{II}, and hence contributes to a nonphotochemical hole at ω_I. The situation could just as easily be reversed with impurity starting in II and ending in I with a lower transition energy. Given a distribution of TLS energy splittings, it is clear that the absorption of sites burned at frequency ω_I would be spread over a region a few wavenumbers wide (recall the hole filling results) to either side of ω_I.

Hayes and Small observed (65) that for tetracene in 4:1 ethanol/methanol, holes burned at 2K were Gaussian with a laser-limited width of 0.88 cm^{-1} centered at the laser frequency. These holes broadened and filled as the temperature was raised, becoming undetectable by 10K. A hole burned at 13K was Lorentzian of width 5.33 cm^{-1} and was shifted

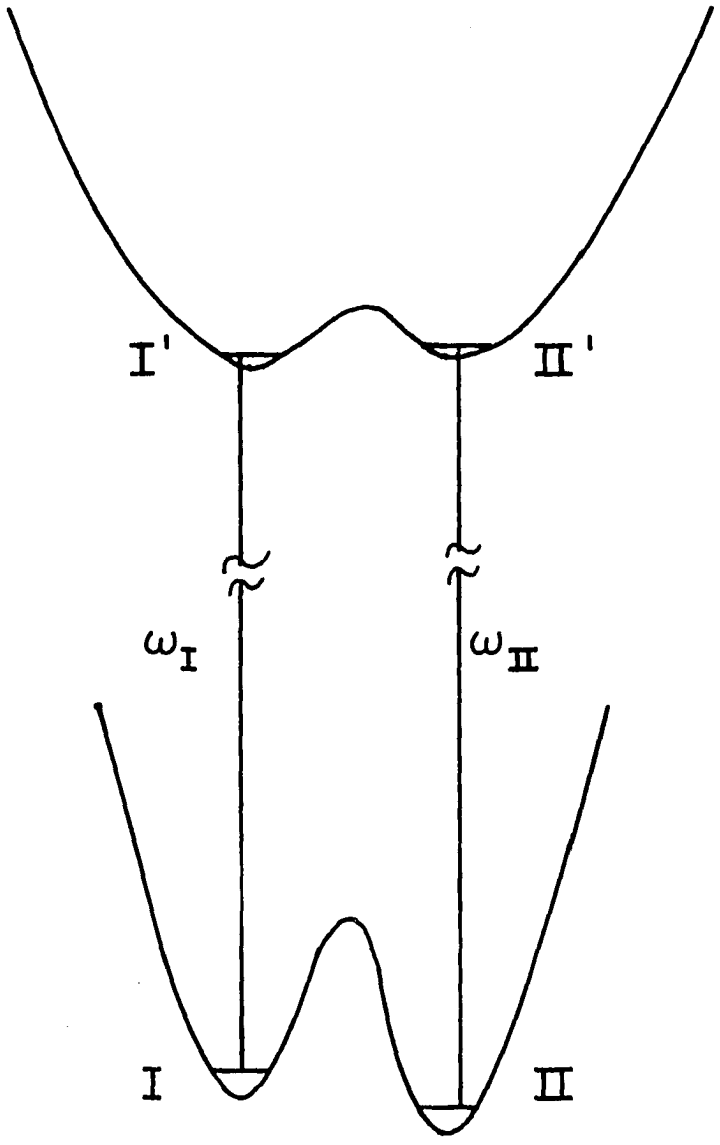

Figure 3. A schematic representation of a ground and excited state double well potential characteristic of the two level systems

1.32 cm^{-1} to lower energy than the laser. This hole disappeared with warming to ∿35K. When the sample was cooled to 2K after burning at 13K, the hole was unchanged. Irradiation at 2K produced a narrow hole superimposed on the broad one. Warming to 13K eliminated the narrow hole leaving the broad hole unchanged. It was concluded that at the two temperatures, different subsets of the sites absorbing at the laser frequency were being probed by NPHB.

We now focus on the transition from I' to II'. There are two possible mechanisms for this transition, a thermally activated transition over the barrier and phonon assisted tunneling (PAT) through the barrier. Theoretically, these processes are distinguishable through the temperature dependence of the burning rate. Thermal activation varies as $\exp(-\Delta E/kT)$, where ΔE is the barrier height (74), while PAT proceeds as $\coth(\Delta\omega/2kT)$, where $\Delta\omega$ is the difference in the zero-point levels of the tunnel states (65). In the first experiments, it was found that either equation gave a reasonable fit to the data over the limited temperature range where hole burning is observed (65).

It is useful here to return to the observations enumerated above. This TLS transition model depends on the existence of TLSs which only occur in amorphous solids. This model does not require the direct excitation of a phonon. The zero-phonon and pseudo-phonon holes arise naturally from this model and other considerations given above. The holes saturate because only some subset of the sites absorbing at the excitation frequency are associated with TLSs having (impurity) excited state barriers which permit TLS transitions and ground state barriers

high enough to render the holes persistent. Note that in systems with lower ground state barriers, the holes need not be persistent as observed by Dubs and Günthard (61,62) and Cuellar and Castro (28). Holes are eliminated when the available thermal energy becomes comparable with the ground state barrier height.

The effects of temperature on NPHB have also been studied (65,66, 75). For tetracene in ethanol/methanol, holes burned around 2K were Gaussians whose widths were strongly influenced by the glass cooling rate. Holes burned above 4K were Lorentzian and far less sensitive to the cooling rate. The hole widths for the Lorentzian holes were quite broad and increased linearly with temperature (75). It was first suggested that the Lorentzian width was due to the rate of site rearrangement leading to holes (65); the observed width of 5.3 cm^{-1} (T_B = 12K) indicating a rearrangement rate of 1.0 x 10^{-12} s^{-1} which seems inconsistent with the observed quantum yield for hole burning of $\approx 10^{-6}$ (65). A more satisfying interpretation (75) is that the Lorentzian widths are due to rapid interconversion of TLSs in thermal equilibrium which do not lead to hole burning, but which dephase the excited impurity molecule at the rate of 1 x 10^{-12} s^{-1}.

The linear dependence of hole widths on burn temperature, which has been found in another system as well (75, vide infra), was a surprising result. A nearly quadratic temperature dependence has been observed for the homogeneous fluorescence linewidths of metal ions in inorganic glasses (76-78), which has been interpreted by considering the dephasing of the excited states by TLS transitions (78-80). A

theory predicting a linear temperature dependence has recently been developed (75) which will be considered in detail in a later section of this dissertation along with a similar theory predicting a quadratic thermal behavior (80).

The temperature behavior for the annealing (filling) of previously burned holes has been reported (66,75). The integrated hole intensity was found to decrease linearly with increasing temperature with a concomitant increase in the hole width (75). The persistence of holes at T_B indicates that the burned sites have relaxation times which are, for all practical purposes, infinite. As the temperature is raised, a hole attains its new, higher temperature profile in a matter of a few minutes at most, implying an increase in the annealing rate of several orders of magnitude. These data cannot be explained by a decrease in site relaxation times with increasing temperature as was previously suggested (65), for either thermal activation or PAT relaxation. At present, the annealing of holes is not well understood and will be dealt with in a later section.

Amorphous Solids

Since NPHB has been found to depend on the nature of amorphous solids, a brief discussion of this state of matter is appropriate. Of the amorphous solids, glasses were most commonly used in this work and, since the topics to be discussed here are common to amorphous polymers as well, only glasses will be discussed here. A good introduction to the glassy state for the purposes of this dissertation is given in reference 81, chapter 1.

A suitable definition for a glass is an x-ray amorphous solid which exhibits the glass transition (82). This definition excludes those glasses, also called plastic crystals, which are x-ray periodic but whose molecules take on random orientations within the periodic lattice. Many glasses lack translational symmetry, but have local symmetries similar to the corresponding crystal; the local structure of glassy $ZnCl_2$, for example, is similar to the crystalline form (83). For molecular glasses like ethanol, the situation is more complex. The glass molecules may have random internal configurations as well which break down the site symmetry. In general, the short range order of the crystal is retained, to a greater or lesser degree, in the glass (81, p. 54).

The glass transition is defined (82) as "that phenomenon in which a solid amorphous phase exhibits with changing temperature a more or less sudden change in the derivative thermodynamic properties, such as heat capacity and expansion coefficient, from crystal-like to liquid-like values." Above the glass transition temperature, T_G, the liquid exists in an internal equilibrium, metastable with respect to the crystal. At T_G, the glass falls out of internal equilibrium as the relaxation mechanisms of the liquid are frozen out. It seems reasonable to assume that among the structural relaxations frozen out at T_G are relaxations associated with TLSs. It is also apparent that TLSs with relaxation times of picoseconds at 2K (vide supra) are not frozen out at T_G and, for relaxation and dephasing to occur, must still be in thermal equilibrium at 2K. We postulate then (75) that there are TLSs

with a distribution of barrier heights from near zero to kT_G. TLS relaxation may be the poorly understood high frequency β-relaxations known to exist in molecular and polymeric glasses (81, p. 709).

CHAPTER II. THEORY

A complete theory for nonphotochemical hole burning must be able to explain the kinetics and mechanism of the burning process, the width and shape of holes and the temperature dependence of hole profiles for both burning and annealing of holes. The burning process is adequately described by the mechanism of Hayes and Small previously discussed. Theories describing the kinetics of NPHB (84), the zero-phonon hole shape (84) and the zero-phonon plus phonon hole shape (54) have appeared. Reinecke (79) and Lyo and Orbach (80) have considered the effects of TLS dephasing on the homogeneous fluorescence linewidths of metallic ions in inorganic glasses. Neither of these theories, however, is consistent with the hole burning results.

Recently, the theory of Hayes and Small (64-66) has been extended (75,85) to describe the hole widths and shapes and their dependence upon burn temperature. This theory will be outlined and some connections between it and other theories discussed.

Effects of Two Level Systems on Hole Burning

The theory of Hayes, Stout and Small (75,85) assumes that PAT of glass TLSs which are coupled to an impurity molecule cause both NPHB of that impurity and dephasing of its excited state. It is argued that dephasing is due to TLSs which are in thermal equilibrium and hence cannot cause hole burning; while TLSs with higher barriers, leading to hole persistence in the ground (impurity) state, cause hole burning by PAT in the excited state at a rate (slow) consistent with the low

quantum yields for NPHB observed to date. An impurity molecule must, then, be surrounded by several TLSs, some giving rise to dephasing and others to hole burning; implying that the spatial extent of TLSs is small.

Two level system energetics and tunneling

We begin by considering the glass TLSs. Figure 4 shows the intermolecular double well potential for a TLS comprised of some "cluster" of glass molecules. The total electronic Hamiltonian for the TLS is

$$H = H_o + V_1 \tag{2.1}$$

where

$$H_o = \hat{T}_{el}(x) + V_{INT}(x,q,Q=0) \tag{2.2}$$

is the electronic Hamiltonian for the TLS with the glass molecules frozen in a suitable configuration, and is responsible for the potential surface in Figure 4.

$$V_1 = \sum_s \left(\frac{\partial V_{INT}}{\partial Q_s}\right)_{Q=0} Q_s \tag{2.3}$$

is the term giving rise to PAT. V_{INT} is the potential energy operator governing the interactions between TLS molecules and other glass molecules. Q represents the glass phonon coordinates, q the displacement coordinate for the TLS and x the electron coordinates.

Neglecting PAT, the tunnel states are linear combinations of the localized state $|L\rangle$ and $|R\rangle$ of Figure 4,

$$|A\rangle = a|L\rangle + b|R\rangle \tag{2.4a}$$

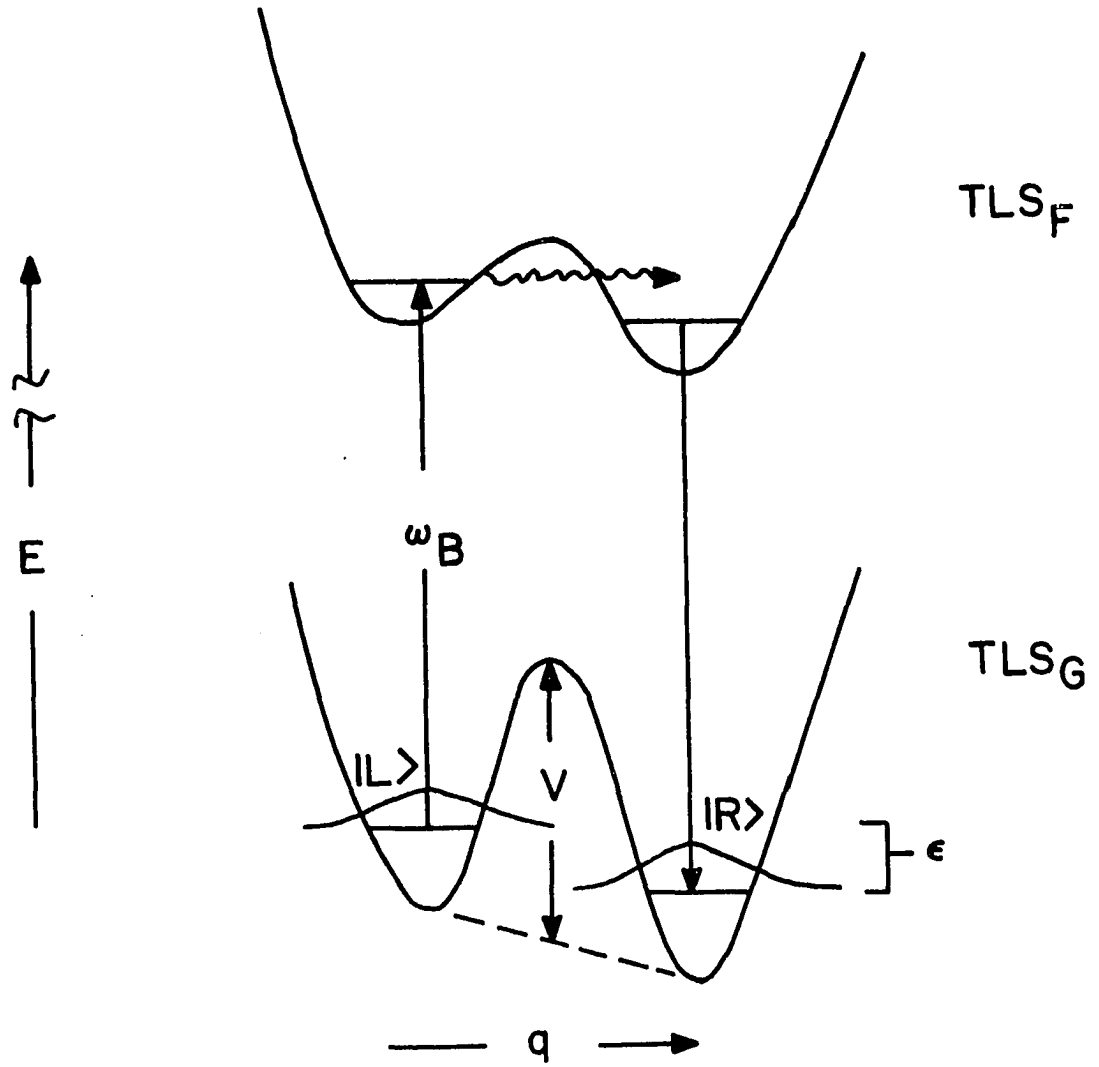

Figure 4. A more detailed look at a two level system potential showing the parameters relevant to the theoretical description of nonphotochemical hole burning

and

$$|B\rangle = -b|L\rangle + a|R\rangle; \tag{2.4b}$$

and are eigenfunctions of the Hamiltonian matrix (86)

$$\frac{1}{2}\begin{pmatrix} \varepsilon & \Delta \\ -\Delta & \varepsilon \end{pmatrix} \tag{2.5}$$

with eigenvalues

$$E_{A,B} = \pm 1/2\ E \tag{2.6}$$

where

$$E = (\varepsilon^2 + \Delta^2)^{1/2} \tag{2.7}$$

Δ is twice the tunneling frequency, approximated by

$$\Delta \approx \hbar\ \omega_o\ e^{-\lambda}, \tag{2.8}$$

with ω_o on the order of the zero-point frequency of the localized oscillators and

$$\lambda \approx d(2mV)^{1/2}/\hbar \tag{2.9}$$

where d is the distance between minima and m is the inertial mass of the tunneling unit. It is reasonable to assume that the potential barrier in Figure 4 varies from near zero to $kT_G \approx 100\ cm^{-1}$ for typical organic glasses. From Eqs. 2.8 and 2.9, one then expects the tunneling frequencies to vary several orders of magnitude.

Using the Fermi-Golden rule, the thermally averaged PAT frequency is given by

$$\langle \Gamma_{em} \rangle_T = \frac{2\pi}{\hbar} \sum_n W_n \sum_m |\langle GBm|V_1|GAn\rangle|^2 \times \rho(E_{A,n} - E_{Bm}) \tag{2.10}$$

for one-phonon emission-type transitions originating from $|A(g)\rangle|n(Q)\rangle$ and tunneling to $|B(q)\rangle|m(Q)\rangle$. $|G\rangle = |G(x,q,Q=0)\rangle$ is the TLS electronic eigenfunction. In the density of states function ρ, we have, for example, $E_{A,n} = E/2 + E_n$, where E is given by Eq. 2.7, and E_n is the energy of phonon state $|n(Q)\rangle$. W_n is an occupation probability for state $|n(Q)\rangle$. Integrating over electron coordinates

$$\langle \Gamma_{em} \rangle_T = \frac{2\pi}{\hbar} \sum_n W_n \sum_m \sum_s |\langle B|v_s^G(q)|A\rangle|^2 \times |\langle m|Q_s|n\rangle|^2 \rho(E_{A,n} - E_{B,m}), \tag{2.11}$$

where

$$V_s^G(q) = \langle G| \left(\frac{\partial V_{INT}}{\partial Q_s} \right)_0 |G\rangle. \tag{2.12}$$

Using the long wave approximation (87) and Eqs. 2.4

$$\langle \Gamma_{em} \rangle_T = \frac{\pi c^{-2}}{2\hbar} \left(\frac{\Delta B_G}{E} \right)^2 \sum_n W_n \sum_m \sum_s \omega_s^2 \times |\langle m|Q_s|n\rangle|^2 \rho(E - E_n + E_m), \tag{2.13}$$

with $E_m - E_n > 0$. B_G is the deformation potential for the TLS given by $\langle R|v^G|R\rangle - \langle L|v^G|L\rangle$ and c is the average sound velocity for the acoustical phonon branches. For $|m\rangle$ and $|n\rangle$ differing by one in the $k^{\underline{th}}$ mode and zero elsewhere, the phonon matrix elements may be evaluated in the harmonic approximation giving

$$\langle m|Q_k|n\rangle = \left(\frac{\hbar}{2M\omega_k}\right)^{1/2} (n_k + 1)^{1/2} \tag{2.14}$$

for a sample of mass M. Equation 2.13 becomes

$$\langle\Gamma_{em}\rangle_T = \frac{\pi c^{-2}}{2\hbar^4}\left(\frac{\Delta B_G}{\omega}\right)^2 \sum_s \left(\frac{\hbar\omega_s}{2M}\right) \times (\langle n_s\rangle_T + 1)\, \rho(\omega-\omega_s) \tag{2.15}$$

where $h\omega = E$ is the tunnel state splitting and $\langle n_s\rangle_T = [\exp(-\omega_s/kT) - 1]^{-1}$ is the thermal occupation number. Using a Debye density of phonon-states $(3V\omega^2/2\pi c^3)\delta(\omega-\omega_s)$ for $\rho(\omega-\omega_s)$ and integrating over s leads to

$$\langle\Gamma_{em}\rangle_T = \frac{3c^{-5}}{8\pi\rho\hbar^3}\Delta^2 B_G^2 \omega(\langle n_\omega\rangle_T + 1). \tag{2.16}$$

V is the sample volume and ρ, in Eq. 2.16, is the mass density. If the initial tunnel state lies lower in energy, then one-phonon absorption must be considered and one finds

$$\langle\Gamma_{abs}\rangle_T = \frac{\langle n_\omega\rangle_T}{(\langle n_\omega\rangle_T + 1)} \langle\Gamma_{em}\rangle_T \tag{2.17}$$

Hole widths due to PAT dephasing

We begin by considering an impurity molecule I to be part of the medium interacting with TLS^α through V_{INT}. $|G\rangle = |G(x,q,Q=0)\rangle$, then, represents the crude (with respect to phonon coordinates) electronic wavefunction for TLS^α for the ground state of impurity $I^-(TLS^\alpha_G)$ which yields the type of potential energy surface shown in Figure 4. $|F\rangle = |F(x,q,Q=0)\rangle$ is defined as the TLS^α electronic wavefunction where the impurity is electronically excited to state $|F\rangle$. The

potential surface of TLS^{α} for the excited impurity is given by $\langle F|H_0|F\rangle$ and is labeled TLS_F^{α} just as TLS_G^{α} is given by $\langle G|H_0|G\rangle$.[1]

Jones and Zewail (88) have found that the dephasing frequency of an impurity electronic transition is given by

$$\langle \Gamma_I^{\alpha} \rangle_T = \frac{2\pi}{\hbar} \sum_n W_n \sum_m |\langle FBm|\hat{T}|FAn\rangle - \langle GBm|\hat{T}|GAn\rangle|^2 \rho(E_{A,n} - E_{B,m}) \quad (2.18)$$

where the transition operator $\hat{T}$ (88) is accurate to all orders of the perturbation giving rise to the dephasing. Eq. 2.18 may be rewritten in a more convenient form as

$$\langle \Gamma_I^{\alpha} \rangle_T = \frac{2\pi}{\hbar} \sum_n W_n \sum_m |\langle Bm|\hat{V}(q,Q)|An\rangle|^2 \rho(E_{A,n} - E_{B,m}) \quad (2.19)$$

where the perturbation associated with $\hat{V}$ is

$$W(q,Q) = \delta U(q) + \delta v(q,Q). \quad (2.20)$$

In Eq. 2.20,

$$\delta U(q) = \langle F|H_0|F\rangle - \langle G|H_0|G\rangle \quad (2.21)$$

---

[1] Here we find that NPHB does depend upon electron-phonon coupling since TLS_F^{α} and TLS_G^{α} must be different for NPHB to occur. The differences between TLS_F^{α} and TLS_G^{α}, however, depend on the quadratic electron-phonon coupling (see, for example, reference 89), and we may still conclude that NPHB does not directly depend on the linear electron-phonon coupling (vide supra).

and

$$\delta v(q,Q) = \sum_s Q_s (v_s^F(q) - v_s^G(q)), \tag{2.22}$$

with, for example, $v_s^G(q)$ being given by Eq. 2.12. The integral in Eq. 2.19 is given to second order by

$$\langle Bm|\hat{V}|An\rangle = \langle Bm|W|An\rangle + \left\{ \frac{\langle Bm|W|An\rangle\langle Am|W|An\rangle}{\Delta E_{nm}} + \frac{\langle Bm|W|Bn\rangle\langle Bn|W|An\rangle}{\Delta E_{AB}} \right\}. \tag{2.23}$$

The leading term reduces to

$$\langle Bm|W|An\rangle = \langle B|\delta U|A\rangle\langle m|n\rangle + \sum_s \langle B|v_s^F(q) - v_s^G(q)|A\rangle\langle m|Q_s|n\rangle. \tag{2.24}$$

The first term, due to elastic scattering, does not lead to NPHB and will not be considered further. With the long wave approximation and Eqs. 2.4, we find

$$\langle Bm|W|An\rangle = \frac{\Delta_{\alpha,I}}{2c} (\delta\mathcal{B})_{\alpha,I} E_{\alpha,I}^{-1} \sum_s \omega_s \langle m|Q_s|n\rangle , \tag{2.25}$$

with

$$(\delta\mathcal{B})_{\alpha,I} = \mathcal{B}_{\alpha,I}^F - \mathcal{B}_{\alpha,I}^G \tag{2.26}$$

the change in the deformation potential accompanying electronic excitation of the impurity. In Eq. 2.25, the α and I labels are included as a reminder that the tunnel frequency Δ, $\delta\mathcal{B}$ and the tunnel state splitting E do depend on the impurity site I and the TLS to

which it is coupled. Using the procedure employed in deriving Eq. 2.16, $\langle\Gamma_I^\alpha\rangle_T$ is to first order

$$\langle\Gamma_I^\alpha\rangle_T^{(1)} = \frac{3c^{-5}}{8\pi\rho\hbar^3}\Delta_{\alpha,I}^2(\delta B)_{\alpha,I}^2\omega_\alpha(\langle n_{\omega_\alpha}\rangle_T + 1). \tag{2.27}$$

Since the TLSs leading to dephasing are assumed to be in thermal equilibrium, the Boltzmann distribution for a TLS, $\exp(-\beta\hbar\omega)/[1 + \exp(-\beta\hbar\omega)]$, is applied to Eq. 2.27 yielding

$$\langle\Gamma_I^\alpha\rangle_T^{(1)} = \frac{3c^{-5}}{16\pi\rho\hbar^3}\Delta_{\alpha,I}^2(\delta B)_{\alpha,I}^2\omega_\alpha\,\mathrm{csch}\left(\frac{\omega_\alpha}{kT}\right) \tag{2.28}$$

which is appropriate for both one-phonon emission and one-phonon absorption type transitions. It should be noted that for the case where the TLSs giving dephasing are not in thermal equilibrium (for example, at very low T), the dephasing frequency is given by Eq. 2.28 where the $\mathrm{csch}(\frac{\omega_\alpha}{kT})$ is replaced by $2\coth(\frac{\omega_\alpha}{2kT})$.

The tunnel frequency in this equation is that of TLS_G^α. This first order equation does not consider, for example, the change in tunnel frequency (potential barrier) accompanying electronic excitation. This change is due to $\delta U(q)$, Eq. 2.21, and appears in the second order contribution to the transition matrix element; the curly bracketed term in Eq. 2.23. Denoting this term by {}, one can show that in the long wave approximation

$$\{\} = \frac{(\delta B)_{\alpha,I}}{2cE_{\alpha,I}}\Delta'_{\alpha,I}\sum_s \omega_s\langle m|Q_s|n\rangle, \tag{2.29}$$

where

$$\Delta'_{\alpha,I} = 2\langle B|\delta U|A\rangle_{\alpha,I}. \tag{2.30}$$

Finally, the dephasing frequency correct to second order is given by

$$\langle \Gamma_I^{\alpha} \rangle_T^{(2)} = \frac{3c^{-5}}{16\pi\rho\hbar^3} (\delta B)_{\alpha,I}^2 (\Delta_{\alpha,I} + \Delta'_{\alpha,I})^2$$

$$\times \omega_{\alpha} \operatorname{csch}(\frac{\omega_{\alpha}}{kT}) \ . \qquad (2.31)$$

The burning of holes for TLS_{α}^{F} and their persistence for TLS_{α}^{G} indicate that Δ' is not small relative to Δ.

Considering the averaging of $\langle \Gamma_I^{\alpha} \rangle_T^{(2)}$ over α and I, one finds that exact averaging over α for a given I is not possible. If it is assumed that dephasing of site I is dominated on average by one TLS which has its PAT dephasing frequency lying in some "maximum" interval, the α-averaging is circumvented and

$$\langle \Gamma_I \rangle_T = \frac{3c^{-5}}{16\pi\rho\hbar^4} [(\delta B)_I (\Delta_I + \Delta'_I)]_{max}^2$$

$$\times \int_{\Delta_{min}}^{\infty} f(E) \, E \operatorname{csch}(\frac{E}{kT}) \, dE \qquad (2.32)$$

is the dephasing of site I undergoing hole burning, where Δ_{min} is the lower limit for the tunneling frequency. f(E) is the probability distribution for the TLSs and the integral accounts for the distribution of tunnel splittings that the TLS (dominating the dephasing) can have.

Using Eq. 2.7 where $\Delta = \Delta_{min}$ and a Gaussian distribution function $f(\varepsilon)$, Eq. 2.32 may be written in a more convenient form:

$$\langle\Gamma_I\rangle_T = \frac{3c^{-5}}{16\pi\rho\hbar^4}\left[(\delta B_I)\ (\Delta_I + \Delta_I')\right]^2_{max}$$

$$x\ \frac{1}{\sigma(2\pi)^{1/2}}\int_0^\infty \exp[-1/2(\varepsilon/\sigma)^2]\varepsilon\ \mathrm{csch}\left[\frac{(\varepsilon^2+\Delta^2_{min})^{1/2}}{kT}\right]d\varepsilon. \tag{2.33}$$

Note that for distributions narrow on the scale of kT, the high temperature limit of Eq. 2.33 is attained where $\langle\Gamma_I\rangle_T \propto T$. The low temperature behavior of this function is discussed later. Importantly, the onset of the linear behavior is related to the width of $f(\varepsilon)$. One observes that $\lim_{T\to 0}\langle\Gamma_I\rangle_T \neq 0$ which follows since downward PAT occurs even at T = 0.

Line shape of the zero-phonon hole

The observed zero-phonon hole is a superposition of the Lorentzian profiles of different impurity sites. A single impurity profile has a linewidth given by $\langle\Gamma_I\rangle_T$, Eq. 2.33. Defining Γ_{max} and Γ_{min} as the upper and lower limits for the "maximum" dephasing frequency interval, the line shape is given by

$$g(\omega) \propto \int_{\Gamma_{min}}^{\Gamma_{max}} \frac{\langle\Gamma_I\rangle_T\ d(\langle\Gamma_I\rangle_T)}{(\omega-\omega_B)^2 + (\langle\Gamma_I\rangle_T/2)^2} \tag{2.34}$$

$$= \ln\left[\frac{(\omega-\omega_B)^2 + (\Gamma_{max}/2)^2}{(\omega-\omega_B)^2 + (\Gamma_{min}/2)^2}\right]. \tag{2.35}$$

The linewidth of this function is $(\Gamma_{max}\Gamma_{min})^{1/2}$. Calculations have shown that for $\Gamma_{max}/\Gamma_{min} \lesssim 7.5$, it is difficult to distinguish $g(\omega)$ from a single Lorentzian of width $(\Gamma_{max}\Gamma_{min})^{1/2}$. For large values of $\Gamma_{max}/\Gamma_{min}$ $g(\omega)$ is more sharply peaked than a Lorentzian, falls off more slowly at intermediate $|\omega-\omega_B|$ values and converges to a Lorentzian for large $|\omega-\omega_B|$.

Connections with Other Theories

Reinecke (79) has considered the effects of TLSs on the time evolution of the homogeneous fluorescence linewidth of ions in hard (inorganic) glasses. He finds that for times longer than the maximum TLS transition time, a linear dependence of the linewidth on temperature is expected for a constant TLS distribution (over asymmetries) function. To explain the nearly quadratic temperature dependence observed (76,77), he notes that an energy dependence of the TLS distribution would yield an increased power in T. Although the different approach used by Reinecke makes a direct comparison of his theory and this one difficult, one major difference is apparent. He uses a constant TLS distribution which, while it may be appropriate for inorganic glasses at low temperatures (90) is inappropriate for the organic glasses used in NPHB (recall the hole filling results). To be fair to Reinecke, it should be pointed out that his theory was not developed for organic glasses or for hole burning. Lyo and Orbach (80) have developed a theory bearing a resemblance to that presented in this work, which explains the effect of TLSs on the homogeneous fluorescence linewidths

of ions in hard glasses. They express the coupling of the impurity to the TLS in terms of the local strain, making their equations appear quite different from those presented in this work which consider the coupling to be due to the system phonons. In the long wave approximation, however, the local strain can be written in terms of phonon operators (91), allowing the two approaches to be transformed each into the other.

Starting with Eq. 4 of Lyo and Orbach (80), their notation is converted to that used herein and the integrals evaluated (see Appendix) to give Eq. A9

$$\langle\Gamma_I\rangle_T = \frac{3}{\rho\pi\hbar^4 c^5} P(\varepsilon=0,\ \omega_o,\ \lambda=\lambda_{min})\ \frac{\Delta^2(\delta B)^2}{\omega}$$

$$\times \frac{\exp(-\beta\hbar\omega/2)}{\cosh(-\beta\hbar\omega/2)}\ (\langle n_\omega\rangle_T + 1), \qquad \text{(A9)}$$

which is compared with Eq. 2.32

$$\langle\Gamma_I\rangle_T = \frac{3c^{-5}}{16\pi\rho\hbar^4}\ [(\delta B)_I(\Delta_I + \Delta_I')]^2_{max}$$

$$\times \int f(E)\ E\ \mathrm{csch}\ (\frac{E}{kT})\ dE. \qquad \text{(2.32)}$$

Equation A9 does not agree in form to Eq. 2.32 or to Eq. 5 of Lyo and Orbach (80). The latter two equations have energy to the +1 power ($x = \beta E$ in Eq. 5 of Ref. 80), while Eq. A9 has energy to the -1 power. The discrepancy appears to be in the factor $(\hbar\omega_{\vec{q},s})$ in the denominator of Eq. 4 of Ref. 80, the origin of which is unclear. Dropping this factor, in the treatment of the Appendix, yields an equation consistent with Eq. 2.16 and Eq. 5 in Ref. 80.

In Eq. A8, the probability function $P(\varepsilon=0, \omega_o, \lambda=\lambda_{min})$ was assumed to vary only slowly in ε and λ, and integration over E has been done. The TLSs are assumed to be in thermal equilibrium and the term $\exp(-\beta\hbar\omega/2)/\cosh(-\beta\hbar\omega/2)$ is derived from the TLS partition function and the Boltzmann distribution function for the phonons. The exponentials in this term and in $(\langle n_\omega \rangle_T + 1) = [\exp(\beta h\omega) - 1]^{-1} + 1$ can be combined to give

$$\frac{\exp(-\beta\hbar\omega)}{1 - \exp(2\beta\hbar\omega)} \propto \operatorname{csch}(\beta\hbar\omega) \tag{2.36}$$

which is consistent with the exponentials in both Eq. 2.32 and Eq. 5 of reference 80. With this in mind, the main difference between Eqs. A8 and 2.32 is in the width of the distribution function over TLS asymmetries.

The final result of Lyo and Orbach (Eq. 6 of reference 80) reads (in the notation of this dissertation (see Appendix))

$$\frac{C(kT)^2(\delta B)^2}{96\, h^4\, \rho} \tag{A13}$$

where C is a constant. This equation is valid for temperatures below the Debye temperature or the maximum TLS asymmetry, whichever is lower; where it gives a quadratic temperature dependence. In the high temperature limit where this condition is not met, a linear dependence is found[2] (80). Thus for this limit, Lyo and Orbach's theory

---

[2]Note that for large T (small $\beta = (kT)^{-1}$), $\operatorname{csch}(\beta\hbar\omega) \sim (\beta\hbar\omega)^{-1} \propto T$.

predicts the same thermal behavior as the theory described here (vide supra). Computer modeling using Eq. 2.33 (to be discussed later) indicates that the quadratic temperature dependence may be due to the use of a constant TLS distribution function; a result that will tie these two theories even closer together.

The theory of Lyo and Orbach has been invoked to explain the observed quadratic temperature dependencies for the linewidths of homogeneous resonant fluorescence transitions of Eu^{+3} in silicate glasses (76,77), and of Pr^{+3} in BeF_2 and GeO_2 glasses (78). It has also helped to provide an understanding of the origins of homogeneous and inhomogeneous linewidths for fluorescence transitions of Eu^{+3} in several glasses at room temperature (92). Two of the temperature studies (77,78) covered ranges up to 300K, that of Hegarty and Yen (78) covering the entire range of 8-300K without a break in the quadratic behavior. While it is satisfying to explain all these data with a single theory, it seems unrealistic to invoke a constant distribution of TLS asymmetries over the range 0 to 300K. It seems even more improbable when one notes that the Debye temperature for most of the glasses used is below 300K. A new approach which uses the broadening theory described in this work for $T << \theta_D$ (Debye temperature) and the Raman broadening mechanism for $T \sim \theta_D$ will be described in a later section.

CHAPTER III. EXPERIMENTAL

Sample Preparation

The samples used in this research consisted of an absorbing guest dissolved into an amorphous solid, either an organic glass or an amorphous polymer. In the survey portion of this research, many different guests were studied, each being chosen from within a chemical class of compounds predominantly on the basis of favorable spectral overlap of the absorber's spectrum and the available laser light sources. The glasses and polymers were chosen for good optical quality at cryogenic temperatures and, in some cases, for particular chemical or physical properties

Guest species

Tetracene was the guest species most often used in this work since its absorption matched the argon laser lines well and it underwent such facile hole burning in the first several glasses studied. Indeed, it became a "benchmark" absorber, used to compare the hole burning characteristics of different glasses and to test new glasses for hole burning.

Tetracene, acridine orange (3,6-bis(dimethylamine)acridine), and acridine yellow (2,7-dimethyl-3,6-diaminoacridine) from commercial sources were used without further purification. Laser grade rhodamine 640 from Exciton was also used without purification. Benzophenone was recrystallized and zone refined. 2-Phenyl-1-azaazulene and 2-phenyl-1,3-diazaazulene, gifts from Dr. Yukichi Kishida, Sanleyo Co. Ltd.,

Tokyo, were used without purification. 2-Chloro-1-azaazulene, also from Dr. Kishida, was sublimed prior to use. Zone refined quinizarin (1,4-dihydroxy-9,10-anthracenedione) was obtained from D. Haarer, IBM Research Laboratories, San Jose, CA.

Potassium tetrachloroplatinate(II) (K_2PtCl_4) was obtained from Dr. Don S. Martin, Jr., Ames Laboratory, Iowa State University. Hexaaquacobalt(III) chloride ($[Co(H_2O)_6]Cl_3$), trisethylenediamine-cobalt(III) chloride ($[Co(en)_3]Cl_3$), potassium hexacyanocobaltate(III) ($K_3[Co(CN)_6]$), and hexaaquairon(III) chloride ($[Fe(H_2O)_6]Cl_3$) were either obtained commercially or synthesized by standard inorganic methods, and were recrystallized before use. cis-Dichlorobis (4,7-dimethyl-1,10-phenanthroline)iridium(III) chloride ([Ir(4,7-dimethylphen)$_2$Cl$_2$]Cl) was synthesized and purified after the method of Watts and Crosby (93) for the 4,7-diphenyl-1,10-phenanthroline complex.

Glasses and glass formation

The large number of glasses used precludes the discussion of each individually. In what follows, general considerations applicable to all the glasses will be given. Details about each particular glass, including composition, stability, and cooling procedures, are given in Table 1. It should be noted that glycerol was a valuable glass forming agent stabilizing many glasses, due in part to its high viscosity. For the glasses which are mixtures, the glass mixture was usually made up in bulk and used over periods of up to several months. Solutions of some of the guests in glass mixtures were made and used over several days. In these cases, it was shown that the properties

Table 1. Summary of the host glasses and polymers used

Symbol	Composition[a]	T_G(K)[b]	Cooling Rate	Stability
EtOH/MeOH	4:1 ethanol/methanol	100	slow[c]	usually cracks[d]
GLY/H_2O	5:4 glycerol/water	165	rapid[e]	consistently perfect[f]
GLY/EtOH	1:1[g] glycerol/ethanol	145	rapid	consistently perfect
GLY/H_2O/EtOH	5:2:2[g] glycerol/water/ethanol	160	rapid	consistently perfect
GLY/DMSO	5:4 glycerol/DMSO[h]	190	slow	usually cracks

[a]Composition by volume.

[b]Estimated from data in Angell, C. A., Sare, J. M., and Sare, E. J. J. Phys. Chem. 1978, 82, 2622.

[c]Cooled over 2+ hr. in a flow dewar, by stages in an immersion dewar.

[d]>75% of samples crack.

[e]Cooled over 0.5 - 2 hr. in a flow dewar, by transferring helium into an immersion dewar.

[f]>90% of samples form clear, uncracked glasses.

[g]These values are typical, the composition could be varied considerably with good results.

[h]Dimethylsulfoxide.

Table 1. (Continued)

Symbol	Composition[a]	T_G(K)[b]	Cooling Rate	Stability
GLY/DMSO/DMF	2:1:1[g] glycerol/DMSO/DMF[i]	175	rapid	consistently perfect
Benzophenone	pure	?	plunged[j]	usually perfect[k]
Decalin	pure	?	rapid	consistently perfect
o-Terphenyl	pure	?	plunged	usually perfect
P/MP/MC	2:3:3 pentane/2-methylpentane/ methylcyclohexane	85	rapid	usually perfect
PMMA[l]	polymer	---	rapid	---
PVK[m]	polymer	---	rapid	---
PC[n]	polymer	---	rapid	---

[i] N,N-Dimethylformamide.

[j] Room temperature sample plunged into liquid helium.

[k] >75% of samples form clear, uncracked glasses.

[l] Polymethylmethacrylate.

[m] Polyvinylcarbazol.

[n] Polycarbonate.

of these "aged" samples were identical to freshly prepared samples. In all cases where precision measurements were to be made, or if sample decomposition was suspected, fresh samples were made for each experiment.

The glass materials used were reagent grade or spectroquality as available; most were used without further purification. Decalin was a mixture of the cis and trans isomers. Benzophenone and o-terphenyl are room temperature solids. They were recrystallized twice each from ethanol and hexane and then zone refined 60-80 passes. The ethanol used was 95%, the water was distilled and deionized. All glass mixtures were optically transparent in the region of the guest's absorption. Most of the glass mixtures were contained in polystyrene tubes.[1] Two of the glasses, decalin and the pentane/2-methylpentane/methylcyclohexane mixture, dissolve polystyrene and were contained in polycarbonate tubes.[2] The benzophenone and o-terphenyl glasses were degassed by several freeze-pump-thaw cycles under dynamic vacuum in Pyrex tubes and then sealed off under vacuum.

The sample tubes were mounted either on a flat brass plate, or for all the temperature dependent studies, in a brass cylinder. Each holder had holes of 1/8" diameter for optical access to the sample and

---

[1] Falcon brand culture tubes, Oxnard, CA.

[2] Nalge brand centrifuge tubes, Sybron Corp., Rochester, N.Y.

to define the optical path through the sample. If a temperature sensor was used, it was mounted as near the optical path through the sample as was practical. With the cylindrical holder, the sensor was press fit into a hole drilled at the height of the optical path 90° away from the optical path.

The glass forming procedure used depended upon the particular glass and dewar involved. When a variable temperature dewar was used, the room temperature sample was introduced into the dewar and cooled slowly by throttling cold helium gas over the sample. The cooling rate chiefly depended upon the stability of the glass being used, although with all glasses cooled by this method, the cooling rate was limited to about 1K/min in the region of T_G. With a helium immersion dewar, three different cooling procedures were used. The easily formed glasses were introduced into the dewar at room temperature and cooled by transferring liquid helium into the dewar. This rapid cooling caused some of the glasses to shatter. These glasses were cooled much more slowly by introducing the room temperature sample into the top dewar partially filled with liquid helium. The sample was allowed to equilibrate at that position, then lowered in stages through the temperature gradient between the liquid helium and the top of the dewar, allowing the sample to equilibrate at each stage. Benzophenone and o-terphenyl required very rapid cooling to form optical quality glasses. For these two compounds, the supercooled liquid at room temperature was plunged directly into liquid helium to form the glass. The cooling procedure did not seem to affect the ability to burn holes

in any given sample, but did seem to affect the reproducibility of hole widths and intensities in some samples. Information on the cooling procedure for and the stability of each glass used is included in Table 1.

Polymers

Methylmethacrylate was vacuum distilled to remove the polymerization inhibitor. The purified monomer was kept away from light in a refrigerator. Polymethylmethacrylate (PMMA) samples were made by dissolving a guest species in the monomer at a concentration to give an optical density of 1 for a 2 mm thickness. Samples were sealed in a Pyrex tube under reduced nitrogen pressure and polymerized in an oven at 120°C for 24 - 48 hours. It should be noted that some absorbers, such as cresyl violet, strongly inhibited the free-radical polymerization while another, azulene, always decomposed, probably either thermally or by a free-radical mechanism. The polymerized samples were cut into slabs, the thickness of which (about 2 mm) were chosen to give a peak optical density of $\sim$0.8 for the guest's absorption. The surfaces of the slabs were smoothed using 600 grit sandpaper and polished on acetone and ethanol soaked tissues on a flat surface.

Polyvinylcarbazole (PVK), given to us by Dr. George Castro of the IBM Research Laboratory, San Jose, California, and polycarbonate (PC) were available in granular form. Samples were prepared for either host by dissolving 1 gram of polymer and the guest species in a minimum amount of tetrahydrofuran (THF). The guest concentration,

10^{-3} - 10^{-4} molar ratio with the polymer, was chosen to give an optical density near unity for a thickness of 100 μm. The sample solutions were placed into glass vials covered with a cap having a 1/4 inch hole drilled through it. The vials were placed in a desiccator modified to allow a slow passage of nitrogen gas over the samples. The THF evaporated over about 24 hours leaving a polymer film of varying thickness in each vial. A section of each film was chosen which gave a peak optical density ∿0.8 for the guest's absorption.

The samples of any of the three polymers were attached using General Electric adhesive and insulating varnish no. 7031 to a brass plate. Holes through the plate served to define the optical path through the sample. When used, the temperature sensor was mounted in thermal contact to the brass plate. The polymer samples were cooled over a period of 20 - 30 minutes to minimize thermal strain in the films or in the varnish. The polymers are included for reference in Table 1.

Cryogenic Equipment

Three different dewars were used in this study. The two variable temperature dewars used were a Janis Research Company model 10DT liquid helium dewar and a Janis model 8DT liquid helium dewar. Both dewars were equipped with the Supervaritemp Optical tail option. In these dewars, the sample is cooled by passing cold helium gas over the sample. A 20Ω heater is incorporated into the tail section which could be used to warm the gas passing over the sample. By varying the flow rate of helium and the heater current, the temperature could be varied from

4.2 K to room temperature. Temperatures were measured using a Lake Shore Cryotronics Model DT500 silicon diode temperature sensor calibrated over the range 1.5 to 300 K with a precision of 0.05 K or better below 25 K and 0.1 K from 25 to 300 K. The third dewar used was a 3 liter liquid helium immersion dewar from Pope Scientific.

Optical System and Light Sources

Optical system

The transmission spectra reported here were taken by focusing the output of a 600 W tungsten lamp (for visible spectra) or a 450 W Xenon arc lamp (for ultraviolet spectra) onto the sample. The transmitted light was collected and focused onto the slits of a Jobin Yvon HR-1500 spectrometer equipped with a 2400 lines/mm holographic grating. This system is capable of a resolution greater than 200,000 in first order. The light was detected photoelectrically using a cooled EMI 9558QB or 9659QB photomultiplier, the output of which was recorded on a strip chart recorder. When detecting holeburning by transmission, it is important that the excitation source irradiate the entire region probed by the continuum source. To this end, the continuum source was reflected onto the optical axis by a mirror with a small hole in its center. The laser excitation passed through this hole and then followed the same path as the continuum source. Care was taken to insure that the laser excitation was <u>not</u> focused onto the sample, but rather defocused so that it covered the entire region probed by the continuum source. To prevent bulk heating of the sample, the continuum

sources were filtered by 5 cm of water to remove infrared radiation. For all the temperature studies, a band pass filter was added which passed light only in the region of absorption of interest.

The fluorescence spectra were of two kinds, those excited using a continuous wave (cw) laser and those excited using a pulsed laser. When using cw excitation, the detection system was identical to that used for transmission. When using pulsed excitation, the output of the photomultiplier was directed to either a gated detection system designed and built in the Ames Laboratory or a Lambda Physik Laser Fotometer LF300 and then recorded on a strip chart recorder.

Fluorescence spectra were usually taken using the "straight through" excitation geometry with the laser passing through the sample on the optical axis and straight into the slits of the monochrometer. This method insured the alignment of the excitation and probe beams within the sample, but usually precludes the observation of fluorescence within 200 cm^{-1} of the laser frequency due to intense scattering of the laser. In these cases, care was taken not to scan the monochrometer across the laser line. When the observation of fluorescence was the intent of an experiment or when a clean fluorescence spectrum was desired near the laser frequency, a 90° excitation geometry was employed. In this case, the monochrometer's slits could be masked so that Rayleigh scattering of the laser and resonance fluorescence are the predominant signals at the laser frequency.

Laser excitation sources

Three laser sources were used during this work. The most frequently used was a Control Laser Corporation Model 553U argon ion laser designed to lase in the near ultraviolet or in the visible. In addition to the usual visible argon laser lines, a line at 528.69 nm could be made to lase using an output mirror for the yellow lines of a krypton laser. One pulsed laser used was a Chromatix Model CMS-4 flashlamp pumped dye laser which, with appropriate dyes, will lase across most of the visible spectrum to about 450 nm. To higher energy of 460 nm and into the near ultraviolet, a Molectron model DL-200 tunable dye laser pumped by a Molectron model UF14 pulsed nitrogen laser was used.

The Control and Chromatix lasers could each be used with an intracavity etalon. The holes burned with either laser which will be reported here were substantially broader than the laser linewidth without using an etalon. In addition for the careful study of tetracene in GLY/DMSO/DMF, it was shown that the narrowest holes of 0.85 cm^{-1} showed no dependence on the line widths of the argon laser line (0.009 cm^{-1} with the etalon, 0.2 cm^{-1} without). Consequently, the etalons were not generally used.

It has been shown (28) that above some threshold, the hole width for nonphotochemical holes increases with increasing laser power. This is thought to be due to local heating of the samples by the laser and that the hole burned is characteristic of some higher (local) temperature than the bulk temperature of the sample. In this work, it was

shown that for tetracene in GLY/DMSO/DMF hole widths were independent of laser power for powers below 50 mW. For the experiments reported here, the laser power was typically below 30 mW.

CHAPTER IV. RESULTS AND DISCUSSION

Nonphotochemically burned holes may be divided into four classes based on the type of hole produced. The first class contains the broad, shallow holes of which Figure 5 is an example. These holes are typically Gaussian in shape, representing an inhomogeneous broadening process, perhaps a redistribution of the initially excited isochromat. While the inhomogeneous broadening is interesting in itself, these holes do not provide any dynamical information and are considered uninteresting from the point of view of this dissertation. Carried to its extreme, a broad, shallow hole becomes no hole at all; the second class of holes. There are many possible reasons for the nonoccurrence of holes, some of which will be discussed shortly. The third class of holes, represented in Figure 6, includes the very deep, broad holes which cause gross changes in the absorption spectra. These holes are rather rare and, from the perspective of this work, are uninteresting. The most interesting and studied holes fall into the fourth class, that of the sharp holes typified by the example in Figure 7. These holes provide considerable information on the system under study as will be discussed shortly.

Survey of Nonphotochemical Hole Burning

Shallow, broad holes

Figure 5 shows the hole burned into 2-chloro-1-azaazulene in decalin at 5K. The hole is very nearly Gaussian with a width of

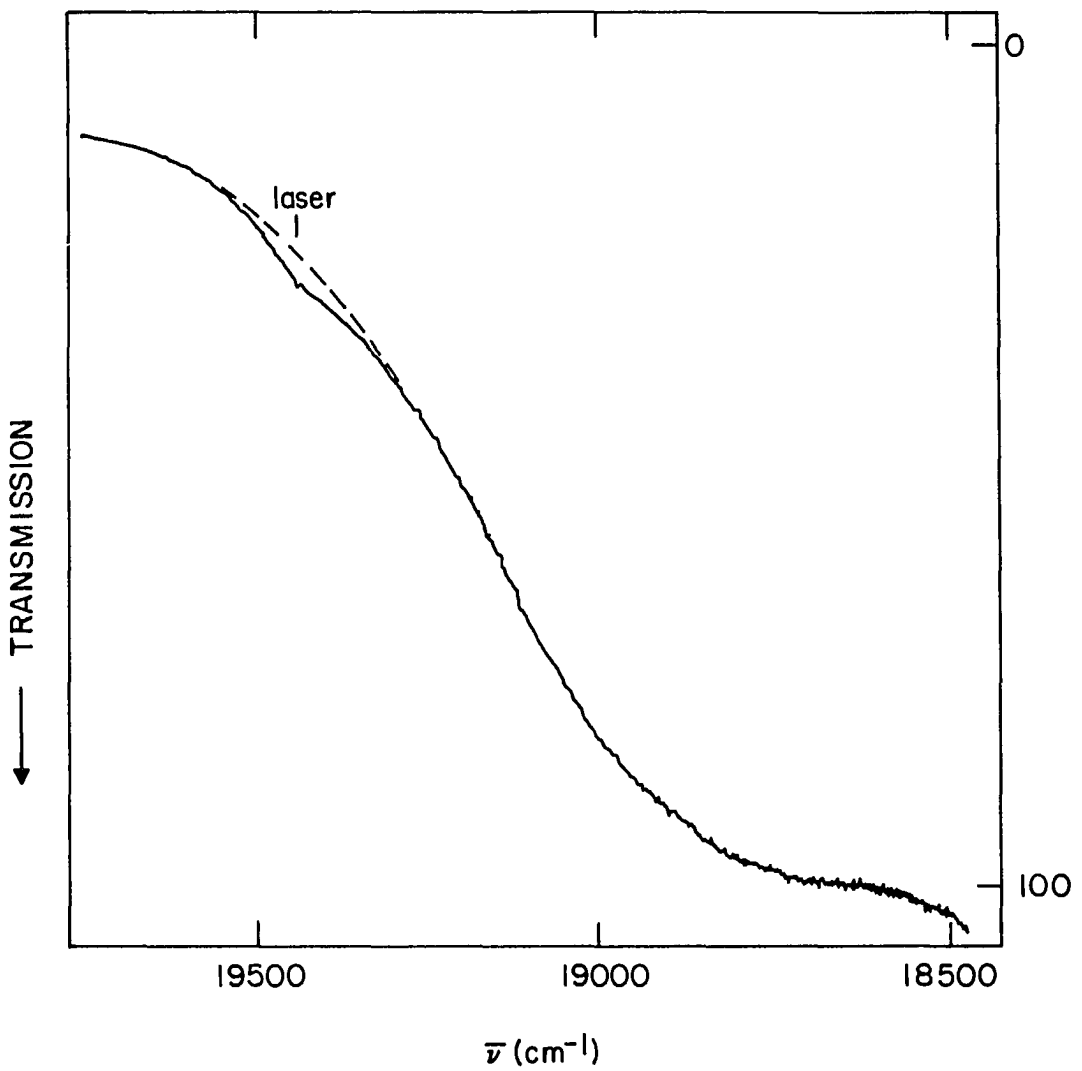

Figure 5. The hole burned spectrum of a 3 x 10^{-5} M solution of 2-chloro-1-azaazulene in decalin at 5K. The sample was irradiated at 19436 cm^{-1} using power densities ranging from 1.4 to 5.0 mW/cm^2

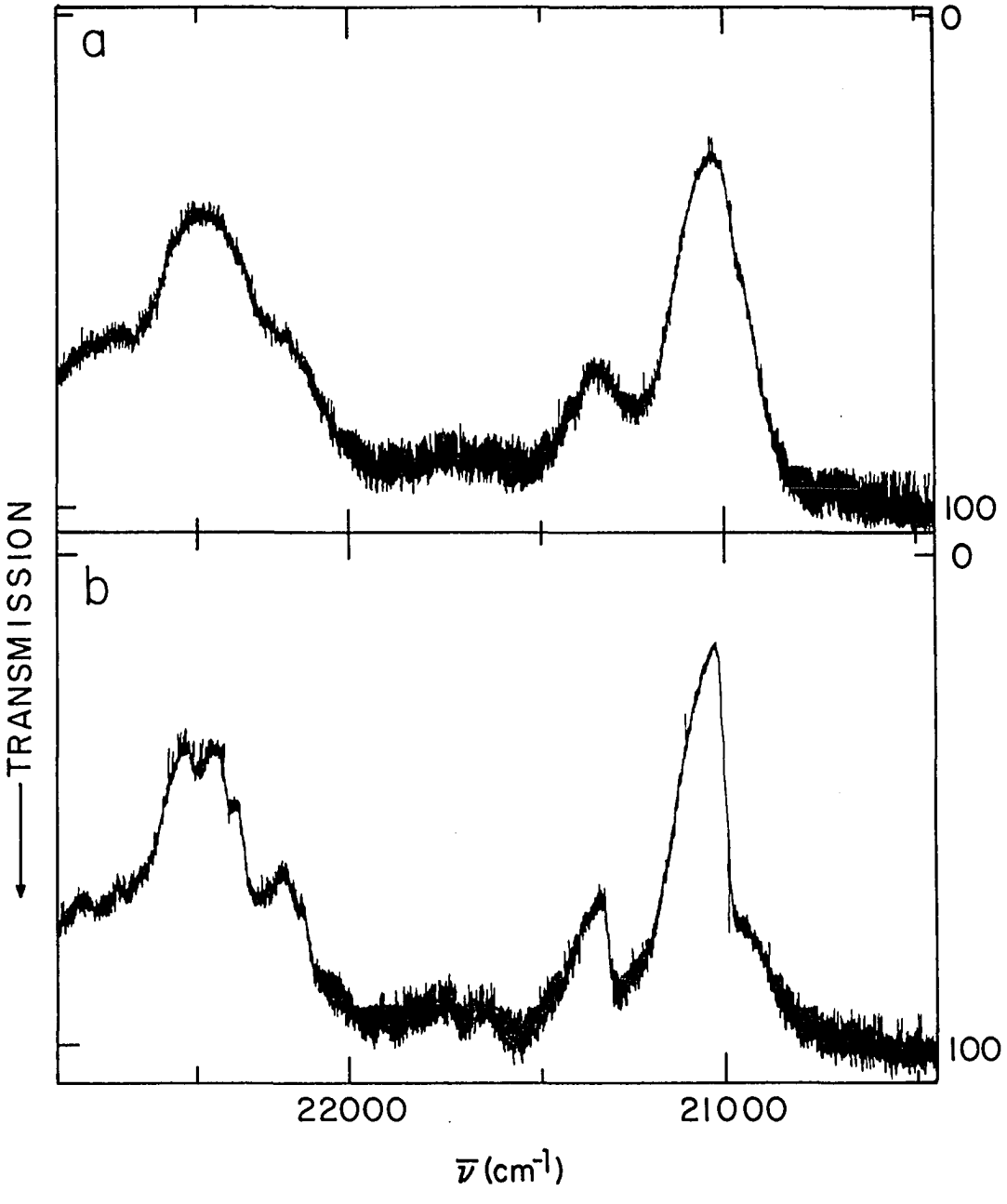

Figure 6. A hole burned spectrum of a 5 x 10^{-5} M solution of tetracene in 4:1 EtOH/MeOH at 2K. This sample reached hole saturation after 90 min of irradiation at 20987 cm^{-1} with a power density of 1.5 mW/cm^2. This spectrum is not typical for this system (see text for discussion)

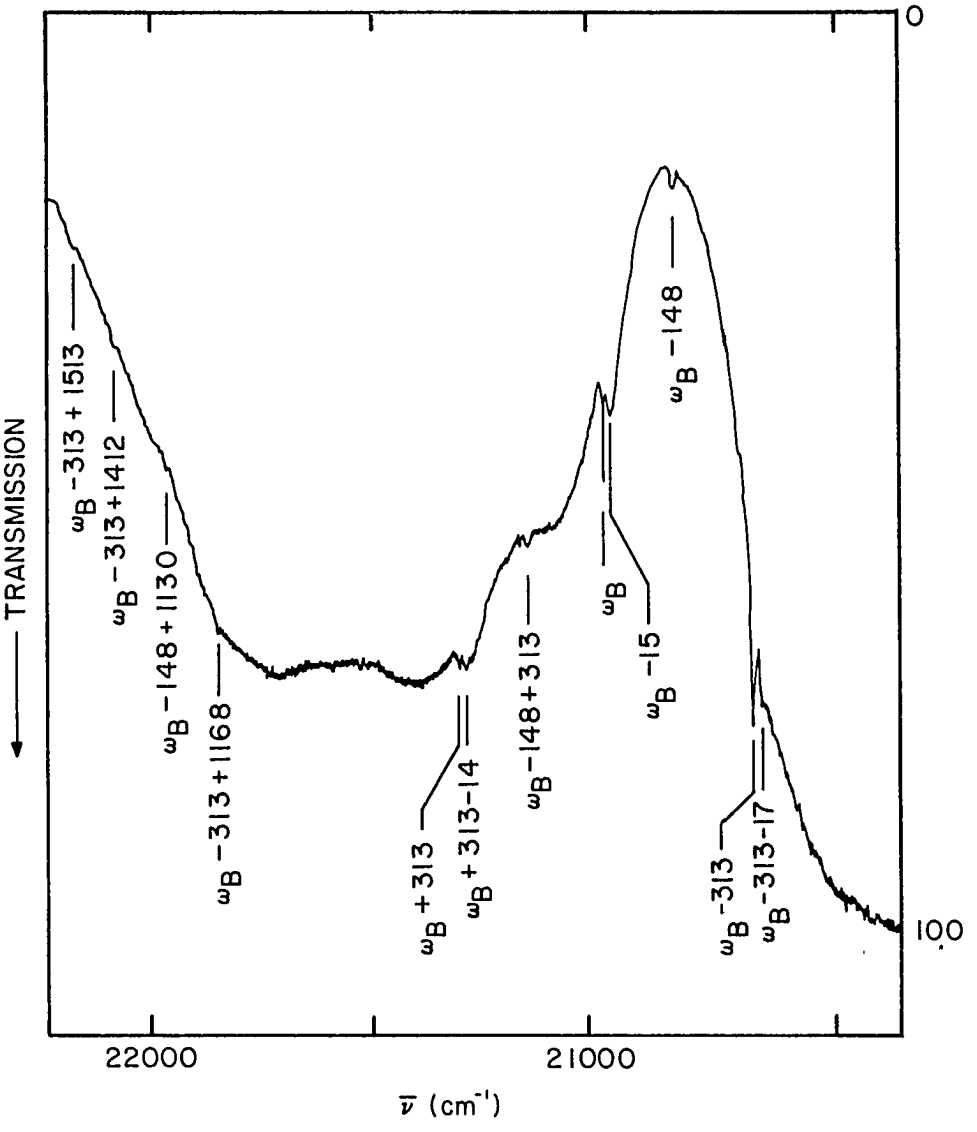

Figure 7. The hole burned spectrum of a 7 x 10^{-5} M solution of tetracene in 2:1:1 GLY/DMSO/DMF at 2K. The sample was irradiated for 80 min with a laser power density of 1.0 mW/cm^2 at 20987 cm^{-1}

140 cm^{-1}. Figure 8 shows a similarly broad hole burned into rhodamine 640 (R640) in polymethylmethacrylate (PMMA) at 2K which has a much narrower hole superimposed on it. The broad hole is fit to a Gaussian of width 100 cm^{-1}. The sharper hole is also Gaussian and is centered at the laser frequency with a phonon side hole to lower energy. Figure 9b shows the fluorescence obtained from R640 in PMMA at 2K for a different excitation frequency within the origin band. For comparison, the fluorescence of the same sample at room temperature is given in Figure 9a. The low temperature fluorescence shows a narrow feature, shown enlarged in the inset in Figure 9b, with a width of 12 cm^{-1} and a broader feature approximately 500 cm^{-1} in width.

One possible explanation for the broadness of these holes is suggested by the report of phonon assisted intersite energy transfer by Avouris et al. (94). In this mechanism, the excitation energy is transferred from an initially excited site to an unexcited, energetically inequivalent site with a phonon making up the energy difference. If this newly excited site then undergoes PAT leading to hole burning, the site contributes to an inhomogeneously broadened hole as in Figure 5. If the intersite energy transfer rate is fast compared to the hole burning rate, a broad hole is produced. If the two rates are comparable, a broad hole is produced by sites excited through energy transfer and a narrow hole is formed by those sites which have not undergone energy transfer. This mechanism is also capable of explaining the broadened fluorescence, Figure 9b, where the shift between the narrow and broad

Figure 8. The hole burned spectrum of rhodamine 640 in PMMA at 2K. The sample was irradiated for 40 min at 16649 cm^{-1} with an average power density of 1.8 mW/cm^2. The crosses represent a Gaussian fit with a width of 100 cm^{-1}

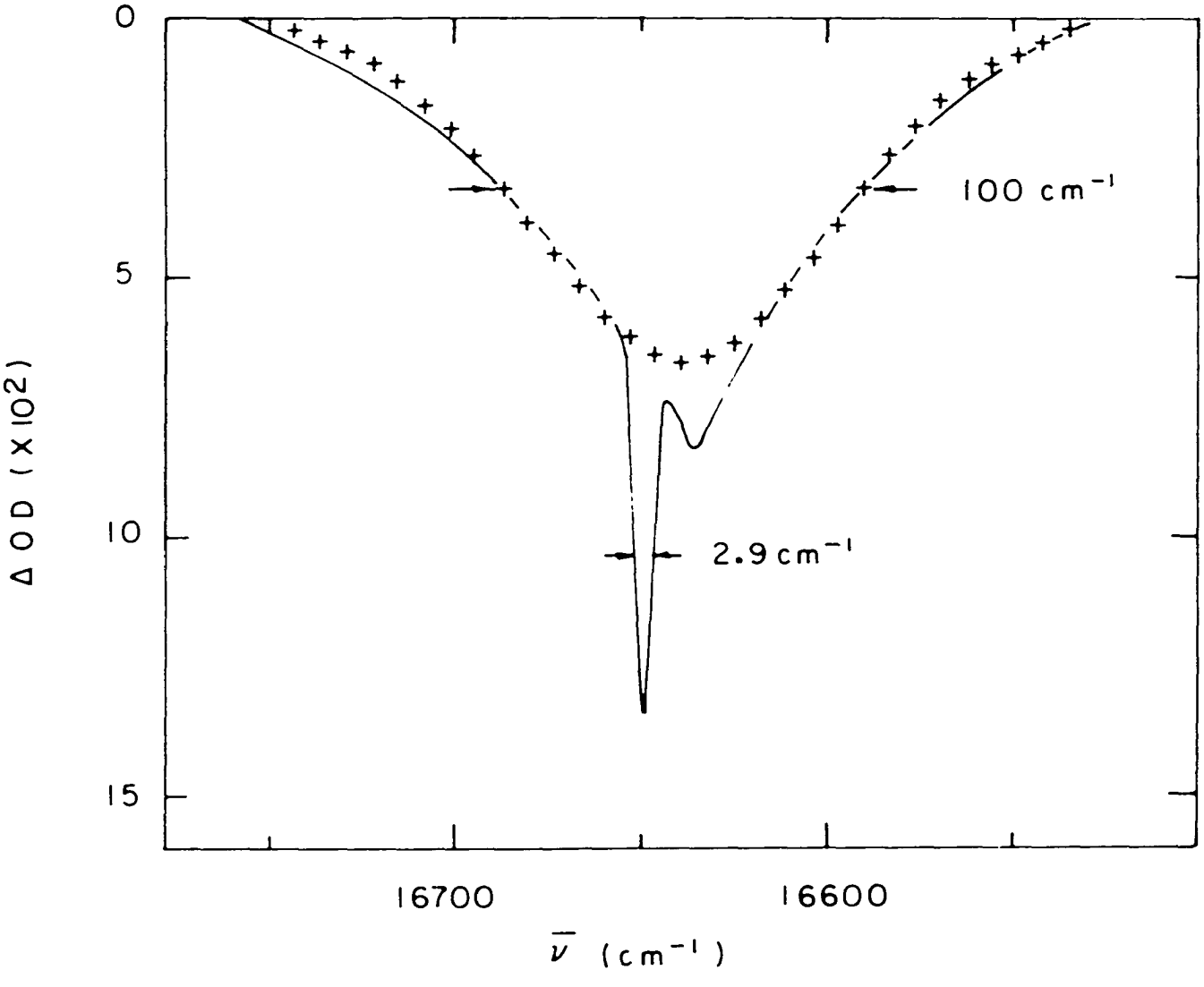
0
5
10
15
ΔOD (X102)
100 cm⁻¹
2.9 cm⁻¹
16700
16600
ν̄ (cm⁻¹)

Figure 9. Fluorescence spectra of rhodamine 640 in PMMA. (a) Room temperature fluorescence resulting from laser excitation at 16995 cm^{-1}. (b) 2K fluorescence spectrum excited at the same frequency. The narrow feature, shown enlarged in the inset, has a width of 12 cm^{-1}

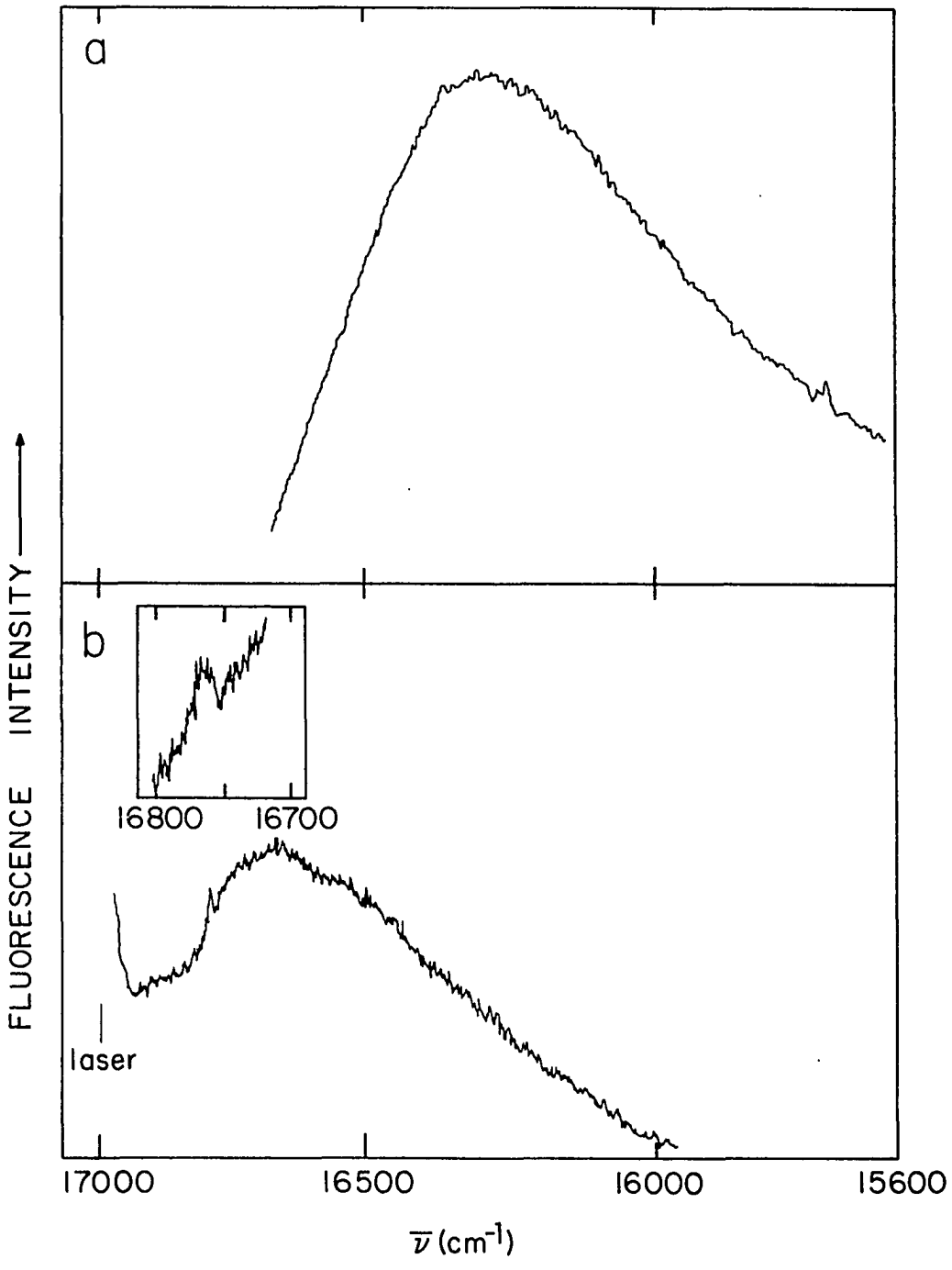
a
b
16800
16700
laser
FLUORESCENCE INTENSITY
17000
16500
16000
15600
$\bar{\nu}$ (cm^{-1})

peaks indicates that energy transfer to sites of lower energy with the concomitant emission of phonons is primarily occurring.

Another possible explanation must also be mentioned. A very small Debye-Waller factor would give a hole (fluorescence band) of predominantly phonon character which could be quite broad. This explanation is appealing for Figure 9b which has the general appearance of a zero-phonon line swamped by a phonon side band. For the broad holes, however, this explanation is less satisfactory. Phonon holes are weighted convolutions of the contributions from phonons of all available frequencies and are not usually Gaussian. In any event, a phonon (or pseudo phonon) hole would not be centered at the excitation frequency.

No holes

The original hole burning work by Hayes and Small (64-66) showed that NPHB was a result of the nature of the glass itself. It was assumed that NPHB could be observed in any glassy material under the proper conditions. It was somewhat surprising to find that NPHB did not occur in many systems, under a variety of conditions. While it may be argued that for these systems the proper conditions were not found, it seems that a more systematic explanation is necessary for at least some of the systems where hole burning does not occur.

In an attempt to extend NPHB to transition metal complexes, several metal-glass systems, summarized in Table 2, were prepared and tested for NPHB activity. In none of these systems was hole burning observed even after extended periods of laser irradiation under

Table 2. Summary of NPHB attempts on transition metal complexes in organic glasses

System Absorber/Glass	Temperature (K)	Laser λ (nm)
K_2PtCl_4/ GLY/H_2O[a]	77	337.1
	5	337.1
	25	476.4
	5	476.4
	2	476.4
$[Co(H_2O)_6]Cl_3$/ GLY/H_2O	5	514.5
	2	514.5
$[Co(en)_3]Cl_3$ GLY/H_2O	77	488.0
	5	488.0
	5	457.9
$K_3[Co(CN)_6]$/ GLY/H_2O	7	337.1
$[Cr(H_2O)_6]Cl_3$/ GLY/H_2O	5	457.9
	2	457.9
$[Fe(H_2O)_6]Cl_3$/ GLY/H_2O	5	363.8
	5	356.0
$[Fe(H_2O)_6]Cl_3$[b]/ EtOH/MeOH[c]	5	363.8
	5	351.0
$[Ir(4,7\text{-dimephen})_2Cl_2]Cl$[d]/ EtOH/MeOH	77	457.9
	5	457.9
	2	457.9
$[Ir(4,7\text{-dimephen})_2Cl_2]Cl$/ GLY/$H_2O$	77	457.9
	5	457.9
	2	452.9

[a] Glycerol/water 5:4.

[b] In this solvent, the water ligands may be partially exchanged for alcohol ligands.

[c] Ethanol/methanol 4:1.

[d] 4,7-Dimephen = 4,7-dimethyl-1,10-phenanthroline.

conditions which seemed appropriate for hole burning.[1] One explanation is that the presence of the metal complex changes the local structure of the glass around the complex by, for example, altering the TLS distribution such that each TLS is in thermal equilibrium rendering NPHB impossible. If this were the case, lowering the temperature sufficiently would cause some TLSs to fall out of thermal equilibrium, and hole burning might then be possible. If the complex had the opposite effect, causing the TLS barriers to become so large that hole burning could not occur, raising the temperature could then allow hole burning to commence. Although the lack of NPHB at relatively high temperatures, 77K, and low temperatures, $\lesssim$ 2K, tends to discount these mechanisms, a modification of the glass structure localized around the complex cannot be ruled out.

Another possible explanation is that spin-orbit enhanced intersystem crossing in these complexes allows the originally excited state to decay to lower states. Since an isochromat in one state need not be narrow in another, the intersystem crossing negates the (energy) site-selection process, and if a hole is burned at all, it would be quite broad. In support of this explanation, are the observed emissions of two of these complexes. The emission from the platinum complex was

---

[1] NPHB has been observed for organic impurities in the same glasses and, since hole burning is a characteristic of the glass, it seemed reasonable that if NPHB occurred for the metal complexes, it would occur under conditions similar to those used for the organic impurities.

quite broad, matching the classically excited emission spectrum, and was red shifted from the laser originating from the $^3A_{2g}$ (95) state rather than the ^3E_g or ^1E_g states which were excited. For the iridium complex, the excitation was into a superposition of the close-lying charge transfer and $\pi\pi^*$ states of the complex, while the emission was mainly $\pi\pi^*$ in character, matching the classically excited emission (96) quite closely. In each case, the observation that the laser excited emission matched the classically excited emission indicates that all the (energy) site-selection was lost.

There were also cases where NPHB of organic impurities in organic hosts was not observed. The most systematic of these cases of non-occurrence was in polymeric hosts. Except for R640 in PMMA, NPHB was not observed for the dye molecules R640 and 3,3'-diethyloxadicarbocyanine iodide (DODCI), and tetracene in PMMA, polyvinylcarbazole or polycarbonate. While the exact reason for this almost systematic non-occurrence of holes is not known, it is possible that the phonon assisted intersite energy transfer mechanism suggested as the cause of the broad, shallow holes is operative in these samples, and any holes produced are too broad to be observed. The R640/PMMA sample would then represent the case where the broadening did not proceed as far and the broadened hole was observable. Another viable explanation is that the polymers, being presumably more rigid than organic glasses, have barriers too high to allow NPHB at the low temperatures, 2-15K, used.

Other, more sporadic cases of the nonoccurrence of hole burning were found. For example, NPHB was not observed for tetracene in decalin, o-terphenyl or P/MP/MC.[2] Hole burning was also not observed for quinizarin in benzophenone (in which tetracene was not soluble at low temperature), decalin or o-terphenyl, but quinizarin in P/MP/MC did undergo NPHB. In these and other sporadic cases where hole burning did not occur, it seems that some property of the specific system under study causes holes not to burn.

There are, however, some interesting observations to be made in the cases of nonhole burning mentioned above. Figure 10 shows the laser-excited fluorescence of tetracene in o-terphenyl at 2K. Excitation is into the 310 cm^{-1} vibrational band of the first singlet state, S_1, of tetracene which relaxes to the zero vibrational level of S_1 allowing the fluorescence origin band near 20500 cm^{-1} to be observed without interference from the laser. This spectrum is reminiscent of the solution fluorescence spectrum of tetracene in cyclohexane (97) and clearly shows that no site-selection is occurring in this system, rendering hole burning impossible.

Tetracene in decalin did not exhibit NPHB, but the fluorescence spectrum of this system, shown in Figure 11b, is quite different from that just discussed. The transmission spectrum for this system, Figure 11a, above 20800 cm^{-1} resembles the transmission spectrum of

---

[2]For explanation of these and other glass symbols, see Table 1.

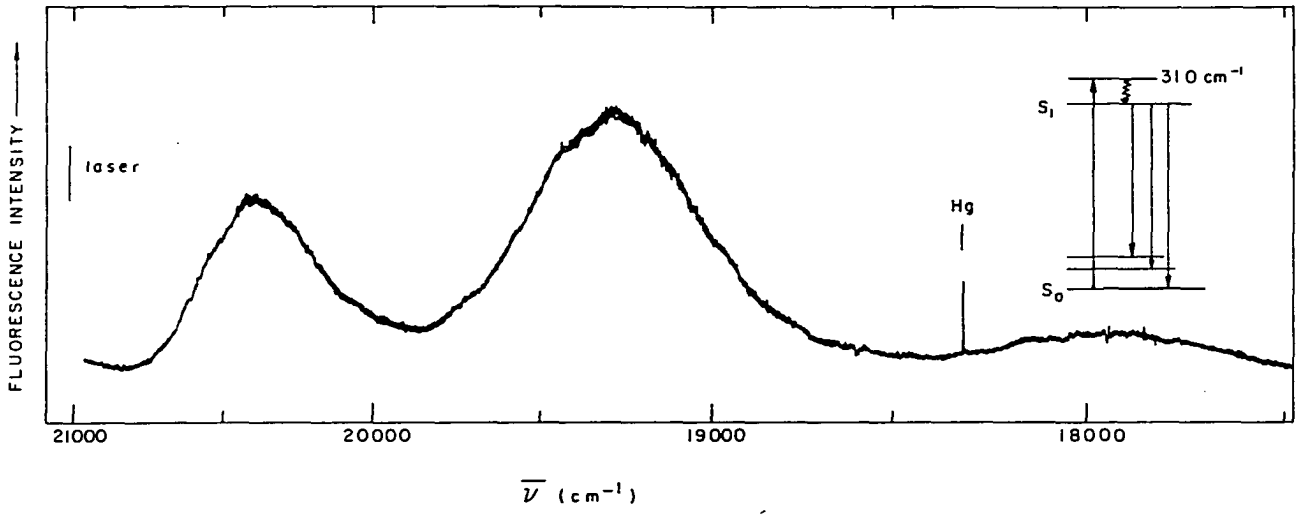

Figure 10. The fluorescence spectrum of a 2 x 10^{-5} M solution of tetracene in o-terphenyl at 2K. Laser irradiation at 20987 cm^{-1} with a power density of 2.1 mW/cm^2 produced no fluorescence line narrowing. The inset in the upper right depicts the excitation conditions and is explained in the text

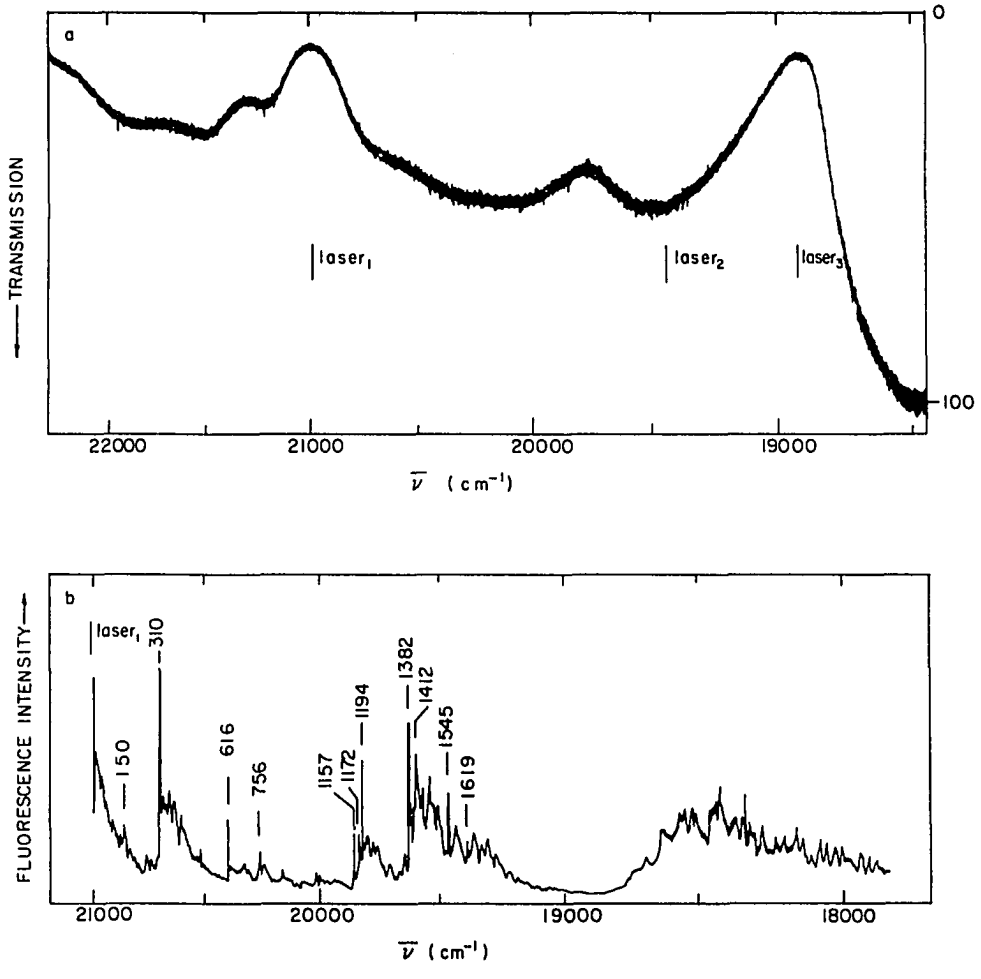

Figure 11. Transmission and fluorescence spectra of a $\sim 10^{-5}$ M solution of tetracene in decalin at 2K. (a) Transmission spectrum showing the three laser frequencies used for excitation. (b) Fluorescence spectrum excited at the frequency marked laser$_1$ (20987 cm^{-1}) with a power density of 1.4 mW/cm^2. See the text for a discussion of these spectra

tetracene in many other solvents. Excitation of the frequency marked "laser$_1$" into this absorption at 2K produces the line-narrowed fluorescence spectrum shown in Figure 11b. From 21000 to 19000 cm^{-1}, this spectrum can be easily assigned using the known vibrational frequencies of tetracene as is shown for the major features. Below 19000 cm^{-1}, the spectrum cannot be assigned to tetracene and remains uninterpreted. Interestingly, there was also absorption below tetracene's origin, down to 18500 cm^{-1}. Excitation into this absorption at the frequencies labeled "laser$_2$" and "laser$_3$" reproduced the fluorescence spectrum from $\sim$ 19000 cm^{-1} to lower energy shown in Figure 11b. The exact nature of this anomalous absorption and fluorescence is unclear, but it is quite possibly due to tetracene dimers. In this sample, site-selection is clearly occurring so that some problem in the hole burning process itself must account for the nonoccurrence of NPHB.

Laser excitation of quinizarin in decalin at 5K produced a weak, highly structured fluorescence. The vibrational frequencies observed in this spectrum were all some 20 cm^{-1} higher than those observed for quinizarin in n-heptane (51). Quinizarin in benzophenone at 2K exhibited a weak structureless fluorescence similar to that observed in 3:1 ethanol/methanol (51). Haarer and coworkers (50,51,53,54) have observed that for quinizarin in proton-accepting solvents at low temperatures, a structureless fluorescence is observed and photochemical hole burning (PHB) (vide supra) takes place. It, therefore,

seemed reasonable to expect PHB to occur in benzophenone. Surprisingly, it did not.

To begin the consideration of this result, recall that many glasses lack translational symmetry, but have local symmetries similar to the corresponding crystal (vide supra). If this holds for benzophenone, then it could be assumed that since the two molecules are nearly the same size, a quinizarin molecule would substitute for a benzophenone molecule in the locally ordered structure. For PHB to occur, the orientation of the molecules would have to be such as to allow the formation of a hydrogen bond between a hydroxyl proton on quinizarin and an oxygen on benzophenone. To examine the molecular orientations of quinizarin in benzophenone, a quinizarin molecule was substituted, mathematically, into a benzophenone unit cell.

Benzophenone is in the orthorhombic space group $P2_12_12_1$ with unit cell dimensions a = 10.30, b = 12.15 and c = 8.00 Å (98,99). The molecule lies mostly in the ab plane although the phenyl rings are rotated out of the plane. The four molecules in a unit cell are distributed along c according to z, 1/2 + z, $\bar{z}$, 1/2 - z. Figure 12 shows the projection of the benzophenone unit cell onto the ab plane with a quinizarin molecule substituted into one unit cell in position II. The apparent overlap between molecules is due to the projection. The quinizarin molecule and the benzophenone in position I just above it in Figure 12 are separated by 1/2 c = 4 Å along the c axis. The shortest interatomic distances for any pair of atoms, one from each molecule, is just over 3 Å. The dotted double bond on

Figure 12. A projection of the benzophenone structure onto the ab plane showing the substitution of a quinizarin molecule into the II position in one unit cell. The inter-oxygen distances relevant to the discussion of the nonoccurrence of holes in this system are shown

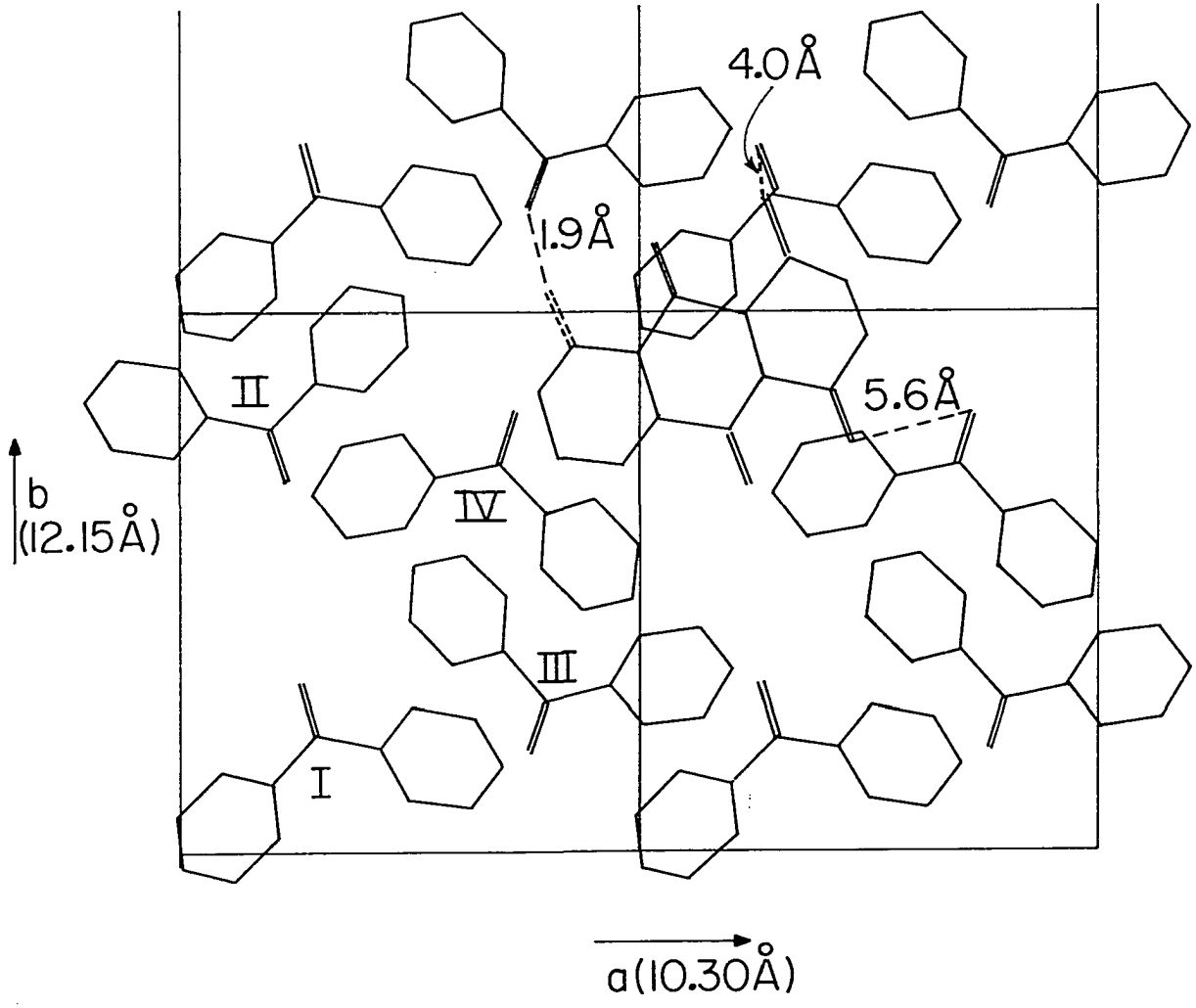
4.0Å
1.9Å
5.6Å
II
IV
III
I
b
(12.15Å)
a(10.30Å)

quinizarin shows one of the two hydroxyllic positions possible if the quinizarin molecule were rotated about its median axis in the site. The intermolecular distances do not indicate that either orientation should be preferred.

To investigate the possibility of PHB in this system, the inter-oxygen distances must be considered to determine if an intermolecular hydrogen bond is feasible. The distance between two hydrogen bonded oxygens in the quinizarin molecule is 2.68 Å. Any intermolecular hydrogen bond formed would be expected to have a similar inter-oxygen distance. The relevant distances are shown on Figure 12. (Note that only the oxygens in the 1 and 4 positions can hydrogen bond, and that they should be represented by single bonds and not double bonds.) Two of the distances, 4.0 and 5.6 Å, are clearly too great for the formation of an intermolecular hydrogen bond. The third, 1.9 Å, appears too short. This interaction is shown in more detail in Figure 13 where the proton is in its position in the quinizarin molecule. This proton is in an ideal position to hydrogen bond to both the quinizarin and benzophenone molecules, and it probably is bonded to both. This proton is also unable to cause PHB via the breaking of an intra- and formation of an inter-molecular hydrogen bond.

One other factor warrants consideration. The density of a glass is lower than that of the corresponding crystal. Assuming a volume increase of 25%, an increase in linear dimensions of 2.9% is found which does not significantly alter the preceding argument. To the extent that the local structure of benzophenone may be described by

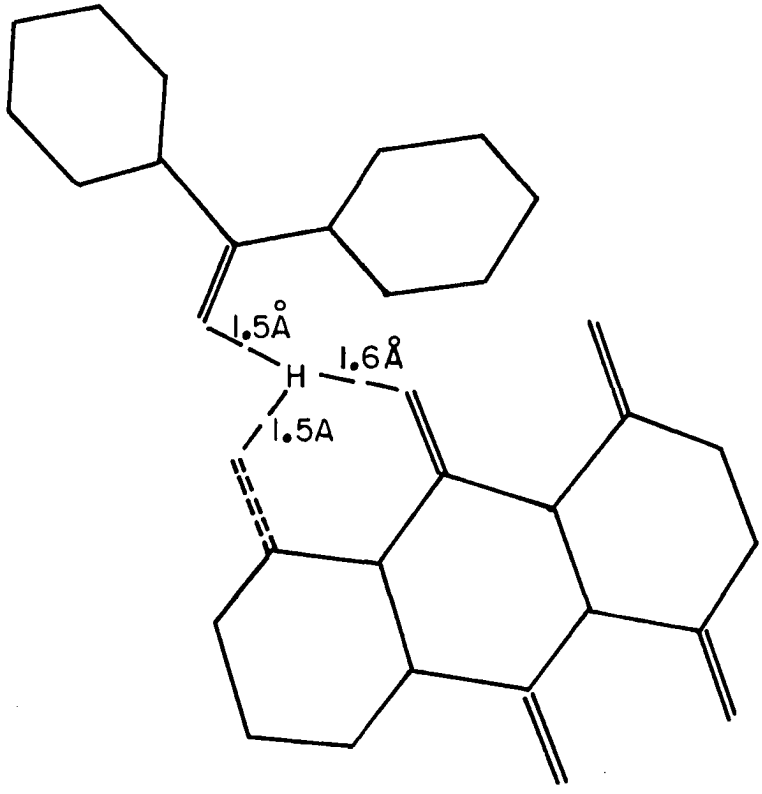

Figure 13. A closer view of the interaction of the quinizarin molecule in position II and the benzophenone molecule in position III. The proton is shown in the position it occupies in the quinizarin molecule. The distances between this proton and the relevant oxygens are shown

the unit cell structure of the crystal, the nonoccurrence of PHB for quinizarin in benzophenone appears quite reasonable. This may be a case where hole burning does not occur due to some specific property of the system under study rather than some more general effect.

Deep, broad holes

The extensive holes shown in Figure 6b were observed for tetracene in EtOH/MeOH at 2K. This type of spectrum was only observed for one sample and is not typical for this system. A similar example of an extensive hole was observed by Small (69) for cresyl violet in EtOH/MeOH at 10K. An explanation for these holes is that these samples have a small Debye-Waller factor and a moderately high hole burning efficiency, which would give deep holes of mostly (pseudo) phonon character. Referring again to Figure 6b, a zero-phonon hole is evident at the laser frequency just above 21000 cm^{-1}. The intense phonon hole to lower energy is the dominating feature to the point that its shape is not clearly seen, but rather the overall shape of the band seems to have changed.

Sharp holes

The sharp holes of the type shown in Figure 7 for tetracene in GLY/DMSO/DMF at 2K are by far the most useful. This spectrum contains a sharp hole at the burn frequency, ω_B, as well as satellite holes to both higher and lower energy, whose frequencies relative to ω_B give the vibrational frequencies for tetracene in good agreement with published values (100). The holes above ω_B in energy are vibronic holes, while

those below ω_B are origin holes formed by excitation of an isochromat in a vibronic band at ω_B which relaxes to the zero-vibrational level before undergoing hole burning. The hole at ω_B has contributions from an origin hole and in some cases several vibronic holes. The hole at ω_B-148 cm^{-1} gives a vibrational frequency which has not been previously observed for tetracene. Phonon holes appear to lower energy from the sharper holes, most notably the hole at ω_B.

From expanded recordings, hole shape information can be obtained. For this spectrum, the holes at ω_B and ω_B-313 cm^{-1} were analyzed, the hole at ω_B being fit to the line shape function given by Eq. 2.35 with a width of 0.85 cm^{-1} and the hole at ω_B-313 cm^{-1} being fit to a Gaussian 8.9 cm^{-1} in width. The shape and width of the hole at ω_B-313 cm^{-1} indicate that the isochromat excited at ω_B into the 313 cm^{-1} vibrational band, which is narrower than 0.85 cm^{-1} and probably laser limited at 0.2 cm^{-1}, undergoes an inhomogeneous redistribution over nearly 9 cm^{-1} upon relaxation to the zero-vibrational level. This type of site redistribution is known to occur for electronic states (101) due to differences in the interactions between differing electronic states of the impurity and the host medium. By burning into vibrational levels and observing the width and shape of holes at the burn frequency and in the origin band, the site distribution could be probed as a function of vibrational level.

The relationship of FLN to NPHB is illustrated by comparing Figure 7 to Figure 14 which shows the fluorescence spectrum obtained while the holes in Figure 7 were being burned. The two figures

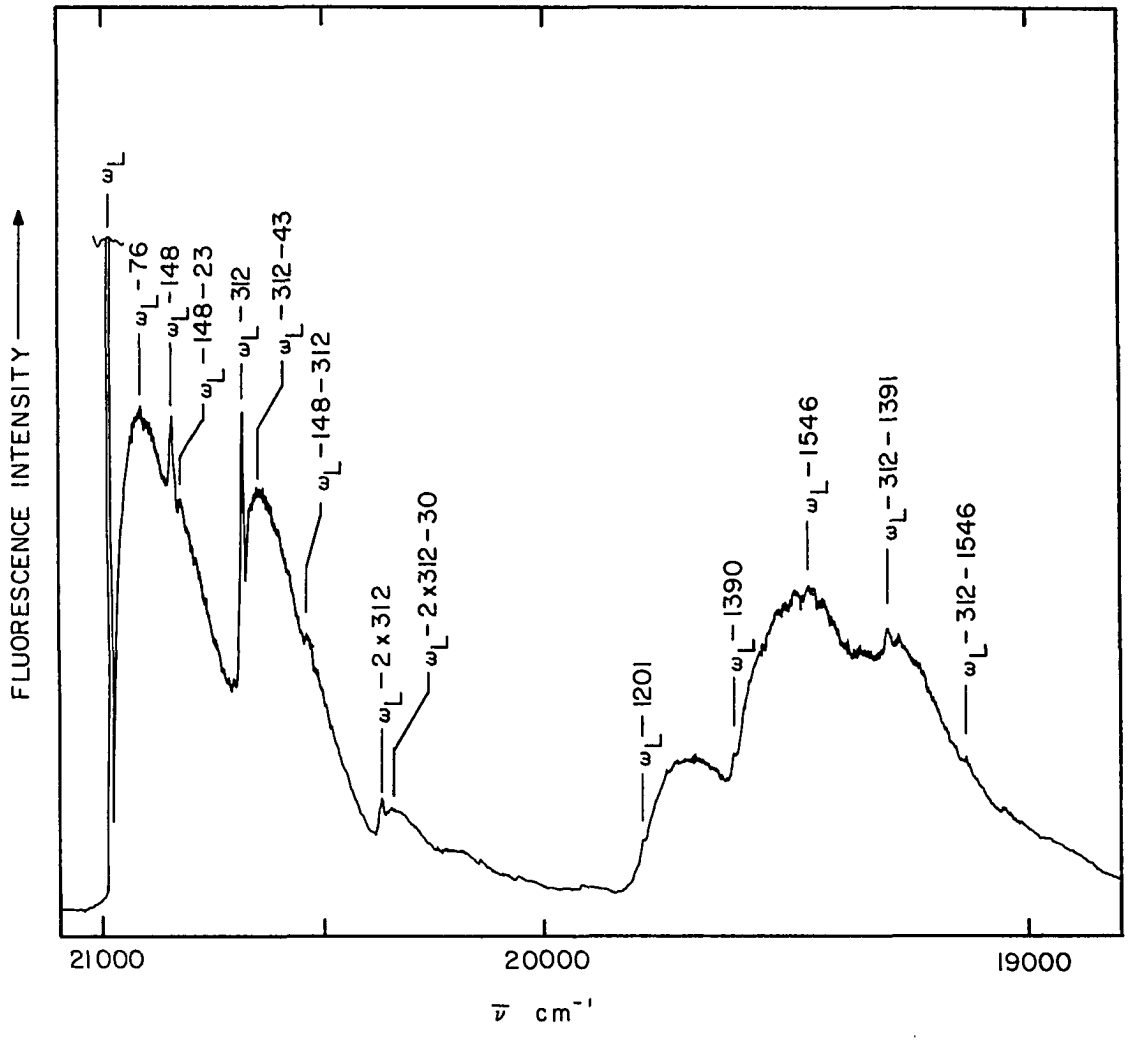

Figure 14. The fluorescence line narrowed spectrum of a 7 x 10^{-5} M solution of tetracene in 2:1:1 GLY/DMSO/DMF at 2K obtained while burning the holes shown in Figure 7. Excitation was at 20987 cm^{-1} with 1.0 mW/cm^2

contain the same information except that the fluorescence spectrum gives ground state vibrational frequencies rather than excited state frequencies.

Another hole-burned spectrum of the same type is shown in Figure 15 for 2-phenyl-1-azaazulene in GLY/EtOH/H_2O. Again, the vibrational frequencies agree with reported values (102). The number of holes below ω_B indicate that what appears to be the origin band can often be the superposition of several bands, here the origin and the 268, 426 and 645 cm^{-1} vibrational bands.

Often fewer holes are observed, as shown in Figure 16 for 2-phenyl-1,3-diazaazulene in EtOH/MeOH at 5K, and Figure 17 for quinizarin in P/MP/MC also at 5K. Another effect is seen here as well; the shallower the holes, the fewer that are visible. The excited isochromat tends to broaden with increasing vibrational energy as the energy site distribution changes. When fewer sites are burned (shallow holes), the holes for higher vibrational frequencies become harder to observe. If all the holes in Figure 15, for example, were 50% shallower, less than half of them would be easily seen.

Figure 17 has some other interesting aspects. Although these holes appear quite shallow, in one respect they are fairly deep. Because of the low optical density of the sample, even these shallow holes represent a considerable relative change in optical density. The hole at ω_B-323 cm^{-1}, for example, is burned to a depth of $\sim$30% of the original optical density. In this sample, the excitation at ω_B is into a vibrational band rather than the origin. The shallowness of

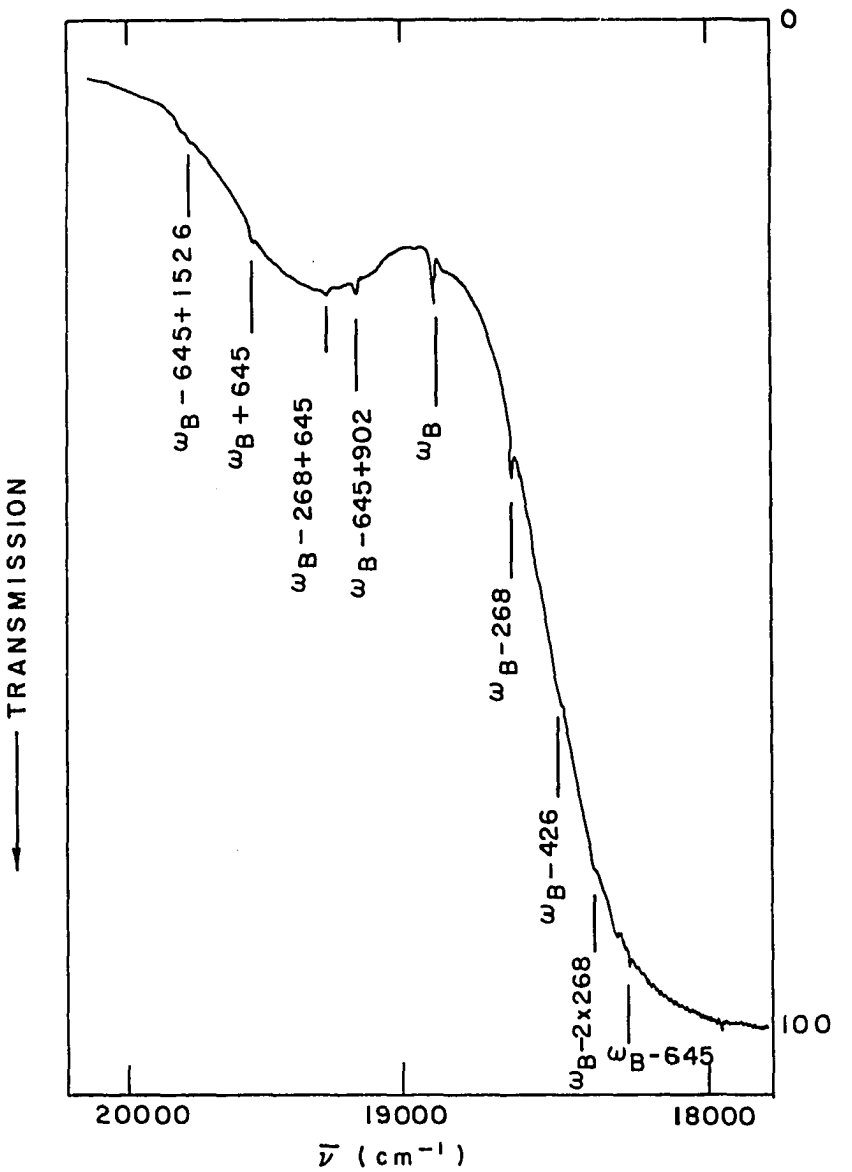

Figure 15. The hole burned spectrum of an 8 x 10^{-4} M solution of 2-phenyl-1-azaazulene in 2:2:1 GLY/EtOH/H_2O at 5K. Excitation was at 18914 cm^{-1} with 1.5 mW/cm^2

Figure 16. The hole burned spectrum of a 6×10^{-4} M solution of 2-phenyl-1,3-diazaazulene in 4:1 EtOH/MeOH at 5K. The sample was irradiated for 180 min at 23492 cm^{-1} with an average power density of 5×10^{-2} mW/cm^2

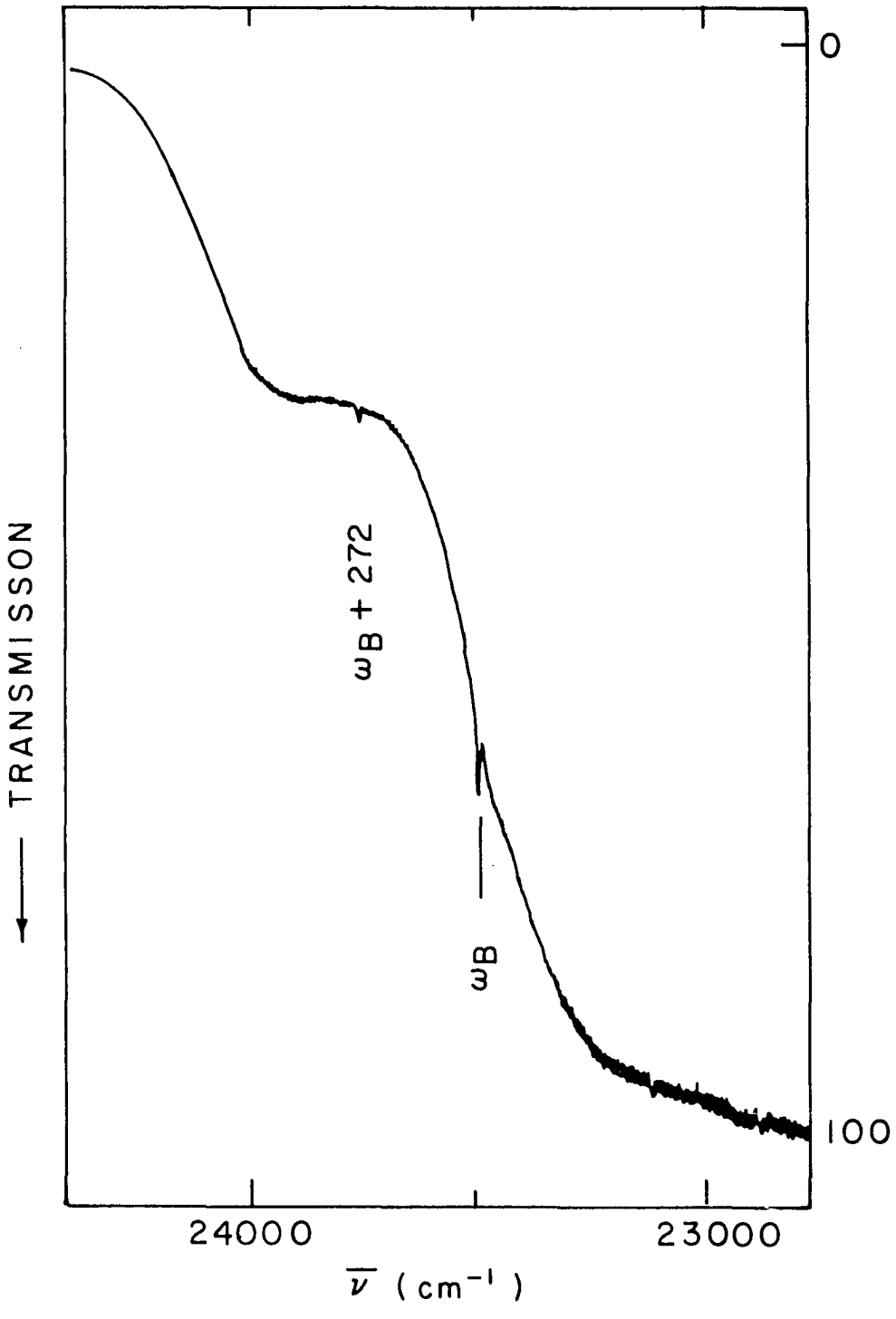
0
100
TRANSMISSON
$\omega_B + 272$
ω_B
24000
23000
$\bar{\nu}$ (cm^{-1})

Figure 17. The hole burned spectrum of a 10^{-5} M solution of quinizarin in 3:2:2 pentane/2-methylpentane/methylcyclohexane at 5K. The sample was irradiated for 50 min at 29436 cm^{-1} with 2.1 mW/cm^2. The pre-burn base line is given by the dashed line. The deviation of the base line from the dashed curve is discussed in the text

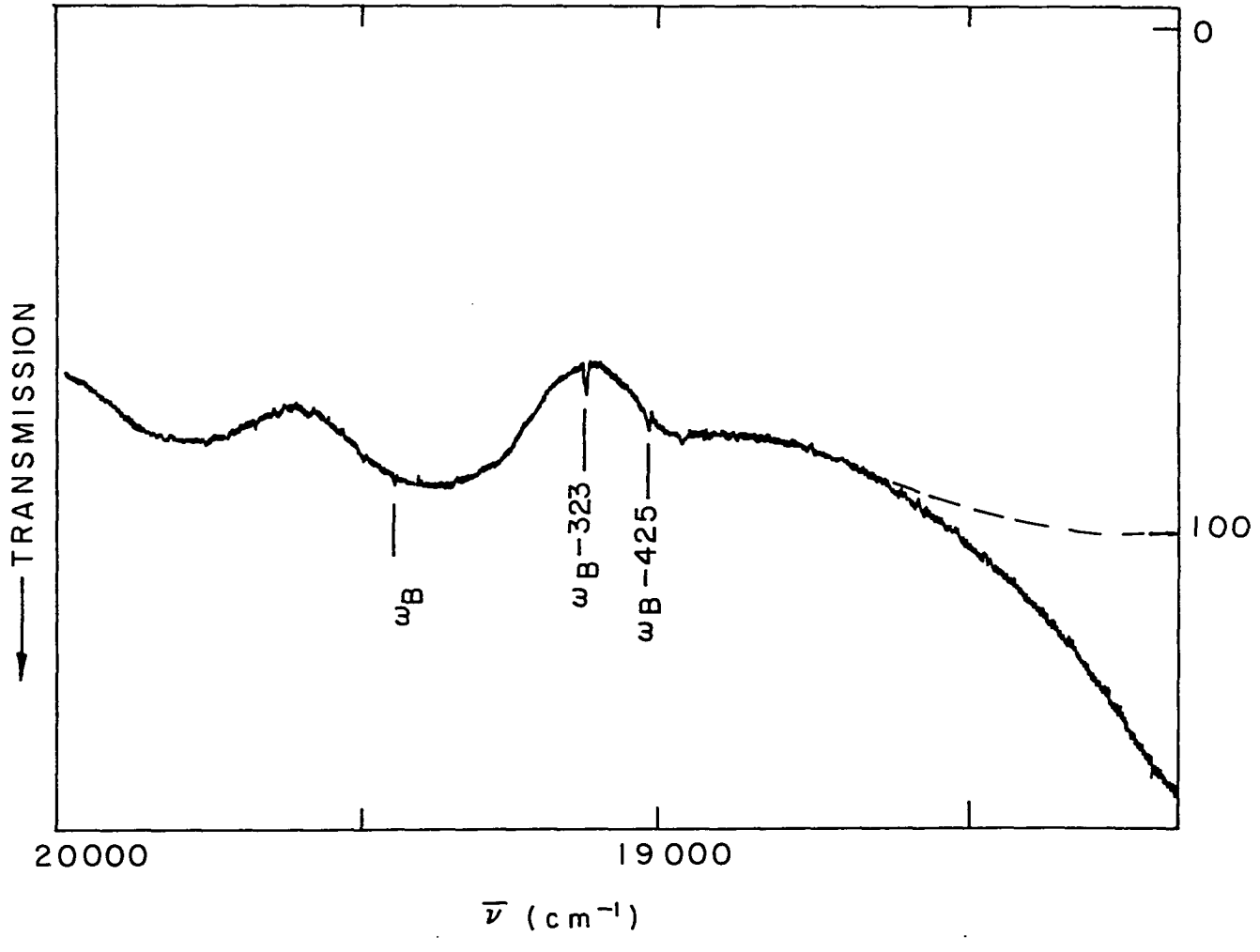
TRANSMISSION
0
100
20000
19000
$\bar{\nu}$ (cm^{-1})
ω_B
ω_B -323
ω_B -425

the hole at ω_B indicates that the vibrationally excited isochromat relaxed to the zero-vibrational level before substantial hole burning occurred. The increasing transmission below the origin is puzzling. Spectra taken before laser excitation did not show this behavior, but followed the dashed line. If the transmission was monitored following shuttering of the laser, it was observed to decrease in time back to the pre-excitation value. This effect did not appear to be due to the absorber, quinizarin, since it was observed even below the origin, but seems to be a broad-band increase in the transmission spectrum of the glass due to the excitation. The cause of this effect is unknown, but it was found that waiting $\sim$5 min between shuttering the laser and taking the spectrum eliminated the effect.

There were also cases where only a single sharp hole of the laser frequency was observed. One example for azulene in 3:1 ethanol/2-methyltetrahydrofuran at 4.5K is shown in Figure 18. Although difficult to measure because of the low signal-to-noise ratio, the hole, shown in an expanded scan in Figure 18b, appears to have a Lorentzian shape nearly 4 cm^{-1} in width.

Thermal Effects on Nonphotochemical Hole Burning

Hole burning

The effect of temperature on NPHB has proven critical to the understanding of the mechanism (64-66, 74, 75, 85). For this reason, a detailed study of the effect of temperature on NPHB in the tetracene-GLY/DMSO/DMF system was undertaken.

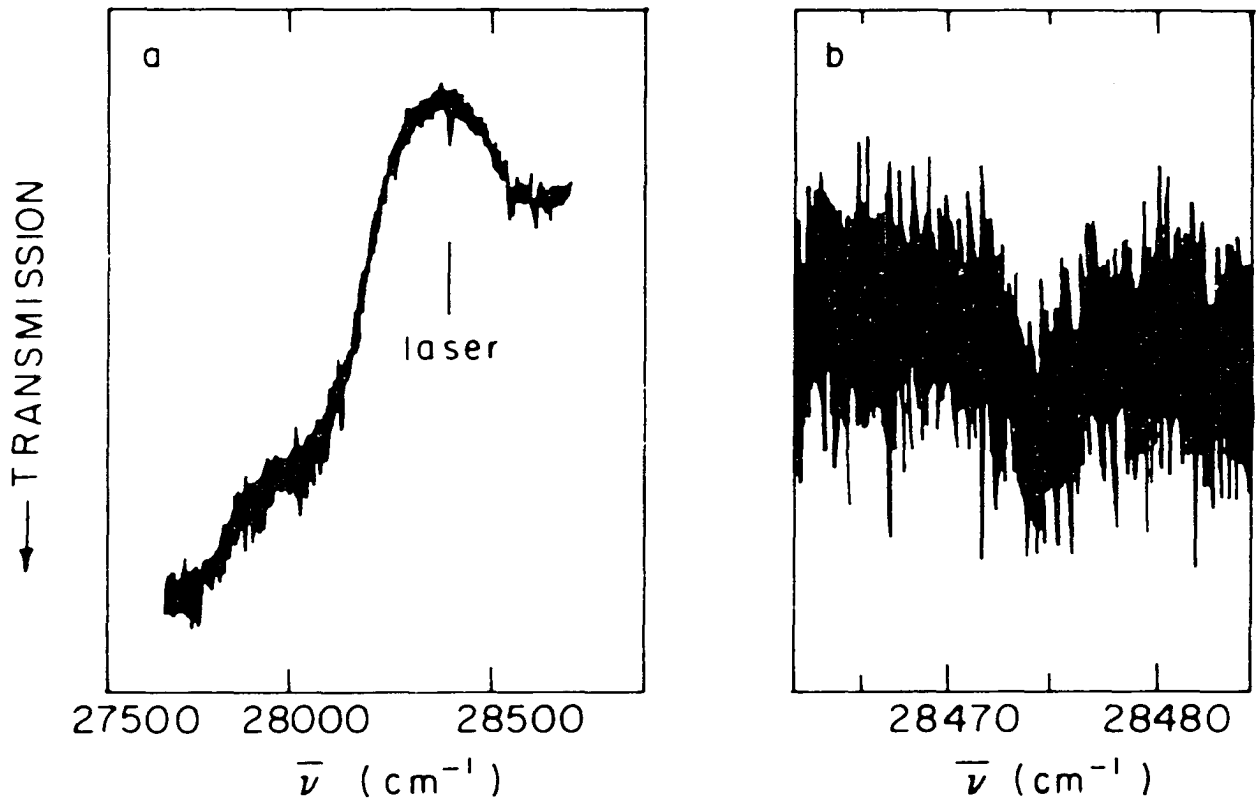

Figure 18. The hole burned spectrum of azulene. (a) The hole burned spectrum of the second singlet state of azulene in a 2×10^{-4} M solution in 3:1 ethanol/2-methyltetrahydrofuran at 4.5K. The sample was irradiated for 120 min at 28482 cm^{-1} with a power density of 1.4 mW/cm^2. (b) An expanded scan of the hole from which a width of 3.75 cm^{-1} was measured

Figure 19 shows the dependence of hole width on burn temperature for two samples of tetracene in GLY/DMSO/DMF. The holes represented in Figure 19 are homogeneous[3] as shown by Figures 20 and 21 for holes burned at 8.93 and 1.85 K, respectively. The holes are fit on the low energy side to a Gaussian, a Lorentzian and, for the lower temperature hole, the shape function given by Eq. 2.35. The high energy side was not fit due to interference from the phonon side hole, the intensity of which is observed to increase relative to the zero-phonon hole with irradiation time (see Figure 22). This effect, which has been carefully studied and explained by Friedrich et al. (54), occurs because fewer burnable sites may be excited through their zero-phonon line than through their phonon side band. Thus, the zero-phonon hole saturates first while the phonon side hole continues to burn.

The dependence of the zero-phonon hole width on T_B (Figure 19) is due to the temperature dependence of the pure dephasing of the impurity electronic transition by TLSs undergoing rapid PAT at the burn temperature. The pertinent equation is Eq. 2.33. Since in the high temperature limit ($[\varepsilon^2 + \Delta_{min}^2]^{1/2} << kT$), the csch function carries a linear dependence on T, the observed hole widths, $\langle\Gamma_I\rangle_T$, are expected to be proportional to T when the width of the TLS distribution function

---

[3]The true homogeneous line width for a site is approximated by $\Gamma_H = 1/2\ \Gamma_{obs}$ (103,104). Γ_H is used when a dephasing time is to be calculated, otherwise, the observed hole widths are reported.

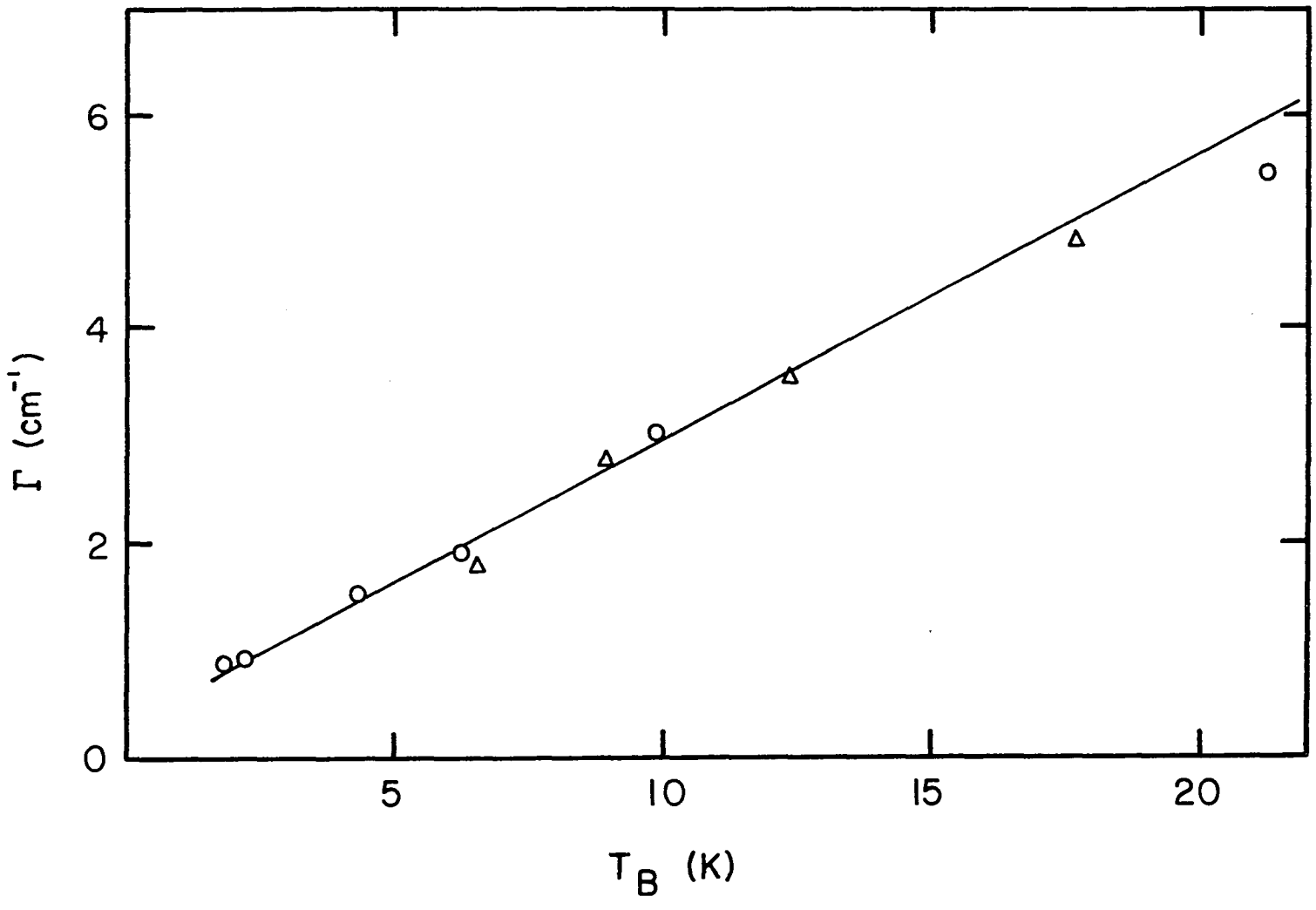

Figure 19. Holewidths at ω_B as a function of burn temperature for tetracene in GLY/DMSO/DMF

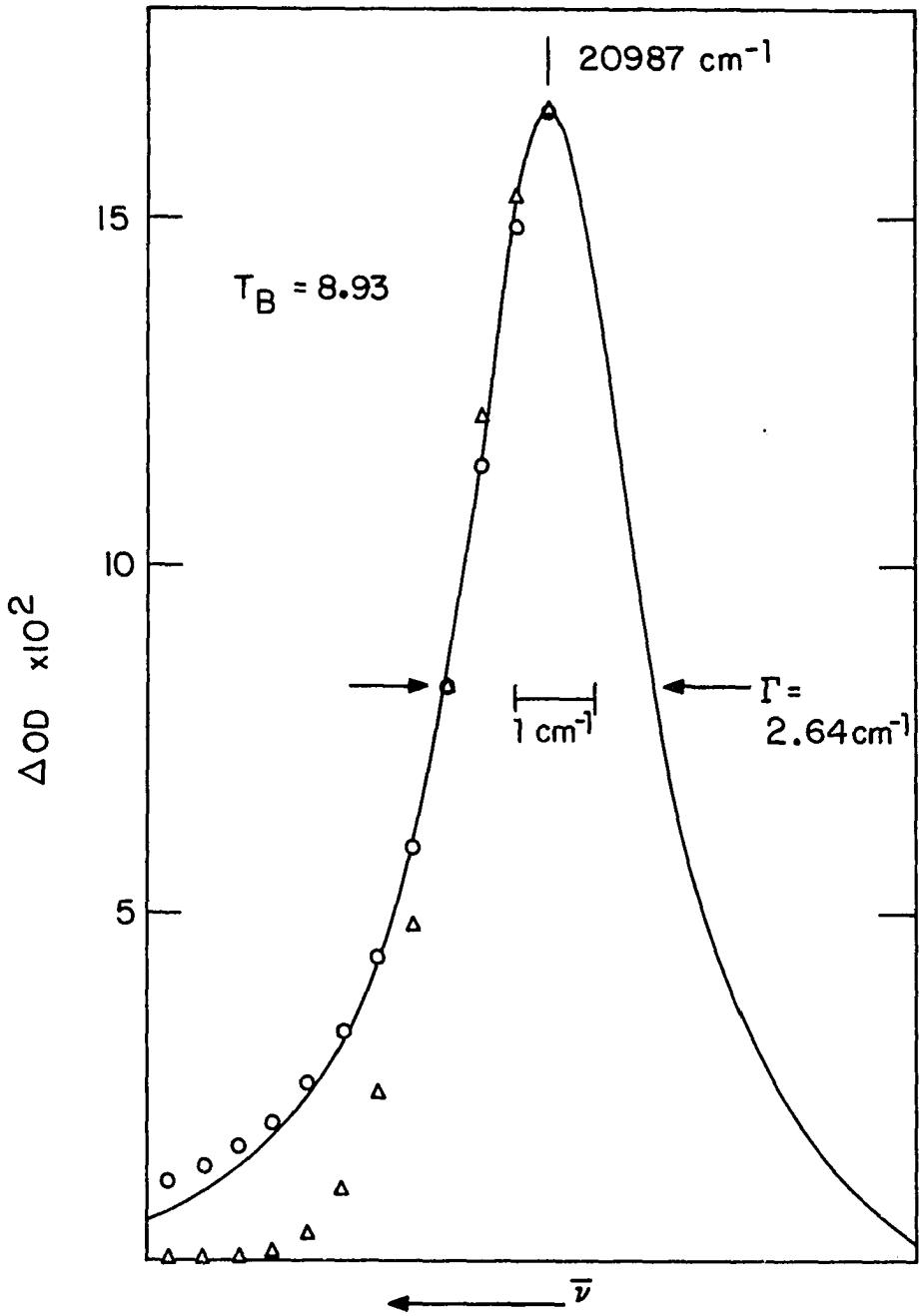

Figure 20. The hole profile for a hole burned in the origin band of tetracene in GLY/DMSO/DMF at 8.93K. The high energy side is fit to a Gaussian (Δ) and a Lorentzian (o) lineshape

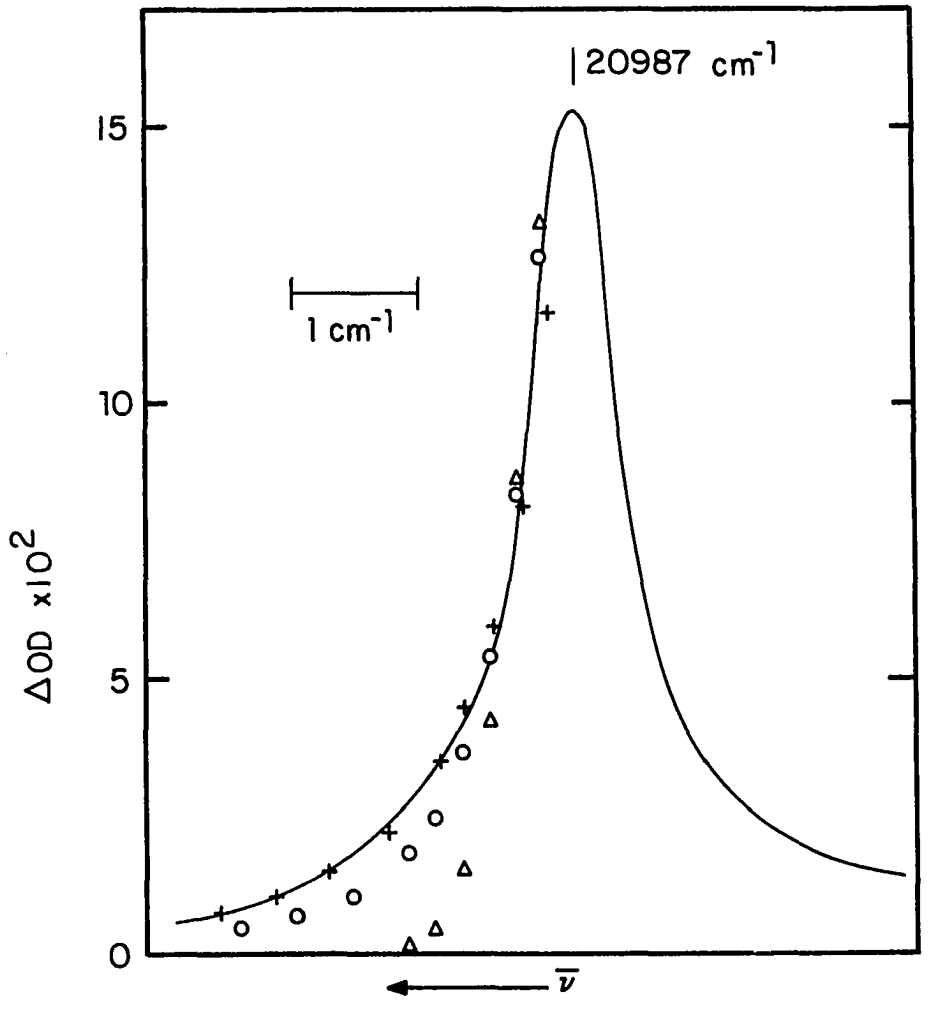

Figure 21. The hole profile for a hole burned in the origin band of tetracene in GLY/DMSO/DMF at 1.85K. The high energy side is fit to a Gaussian (Δ), a Lorentzian (o) and the lineshape function derived in the text (+) for $\Gamma_{max}/\Gamma_{min} = 20$

Figure 22. Transmission curves for holes burned in the origin band of tetracene in GLY/DMSO/DMF at 1.9K as a function of irradiation time. The zero-phonon hole shown at 130 min is saturated

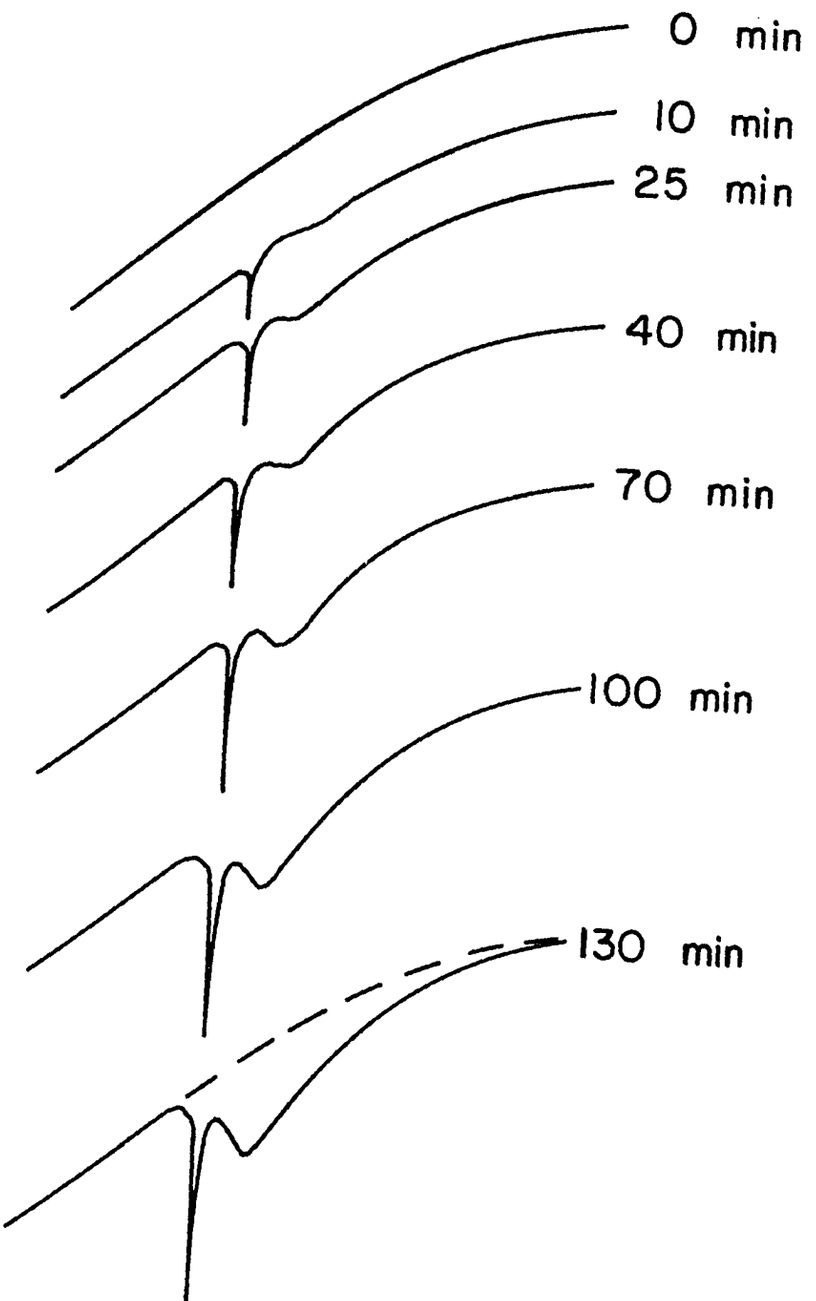
0 min
10 min
25 min
40 min
70 min
100 min
130 min

$f(\varepsilon) \sim \exp[-1/2\ (\frac{\varepsilon}{\sigma})^2]$ is narrow relative to kT. Numerical evaluations of the integral in Eq. 2.33 (vide infra) confirm this. Letting the half-width of the distribution be 0.5 cm^{-1} and Δ_{min} = 0.1 cm^{-1}, $\langle\Gamma_I\rangle_T$ becomes linear near 1.5K; which is consistent with the data in Figure 19, linear down to 1.85K. For tetracene in EtOH/MeOH (75), the onset for linearity was near 4K, which was predicted by Eq. 2.33 for σ = 2.0 cm^{-1} and Δ_{min} = 0.5 cm^{-1}. The narrow TLS distributions[4] obtained for both glasses are consistent with the hole filling experiments (64) on tetracene in EtOH/MeOH, which showed that appreciable filling of a primary hole at ω_B occurred when a secondary hole was burned within 2 cm^{-1} of the primary hole. If the line in Figure 19 is extrapolated to OK, a hole width of $\sim$0.5 cm^{-1} can be estimated at OK. This emphasizes an important feature of the TLS-PAT dephasing model; that due to phonon emission, the dephasing of the impurity excited state does not necessarily vanish in the limit as $T \to$ OK.

The zero-phonon hole shapes observed for tetracene in GLY/DMSO/DMF for $T \lesssim$ 2K (see Figure 21) also support the theoretical model given here in that they deviate from Lorentzian as predicted by Eq. 2.35. The observed hole shapes for $T_B \lesssim$ 2K are satisfactorily fit by Eq. 2.35 for $\Gamma_{max}/\Gamma_{min}$ between 15 and 20 and with a width $(4\ \Gamma_{max}\ \Gamma_{min})^{1/2}$ $\sim$1 cm^{-1}. From these values, the limits Γ_{max} and Γ_{min} of the maximum

---

[4]It should be noted that the width of the TLS distribution function calculated here is characteristic of the TLSs involved in the (fast) dephasing and may not be representative of the total distribution.

dephasing frequency interval (vide supra) are found to be 2 and 1.1 cm^{-1}, corresponding to minimum dephasing times of 2.6 and 48 ps. Friedrich et al. (44) have also observed a "super-Lorentzian" hole shape for phycoerythrin in a glycerol based glass at 1.8K.

It is instructive before leaving this discussion to do an approximate calculation using Eq. 2.33. A hole width of 1.5 cm^{-1} (dephasing frequency of 3.5 ps) is observed at 4K. Using these values, a distribution width of 0.5 cm^{-1} and Δ_{min} = 0.1 cm^{-1}, the normalized integral is found to be $\sim$6 cm^{-1}. Taking $(\Delta_I + \Delta_I')^2 \sim 1$ cm^{-1}, $c \sim 10^4$ cm s^{-1} and p = 1.5 g cm^{-3} gives a value of $\sim$9 cm^{-1} for $(\delta B)_I$, the change in the deformation potential. Given the definition of $(\delta B)_I$, Eq. 2.26 and the text after Eq. 2.13, the purturbation giving rise to it, Eq. 2.3, and the narrowness of the distribution function $f(\varepsilon)$, a value of this magnitude is reasonable.

The dependence of the integrated hole intensity on T_B is given in Figure 23. In the linear region below 10K, the number of sites which can undergo NPHB in a region dT_B about T_B is constant. Making the reasonable assumption that PAT is the first step to NPHB, and letting Δ^F and B^F label the excited state tunneling frequency and deformation potential, it is apparent that the number of sites with $\Delta^F B^F$ in the appropriate range for hole burning, and with ground state relaxation times long enough to cause hole persistence, in the range dT_B about T_B must also be constant. Given this, it is clear that the intensity data given above are related to the hole annealing data (vide infra). The bending over above 10K has contributions from two effects. Sites

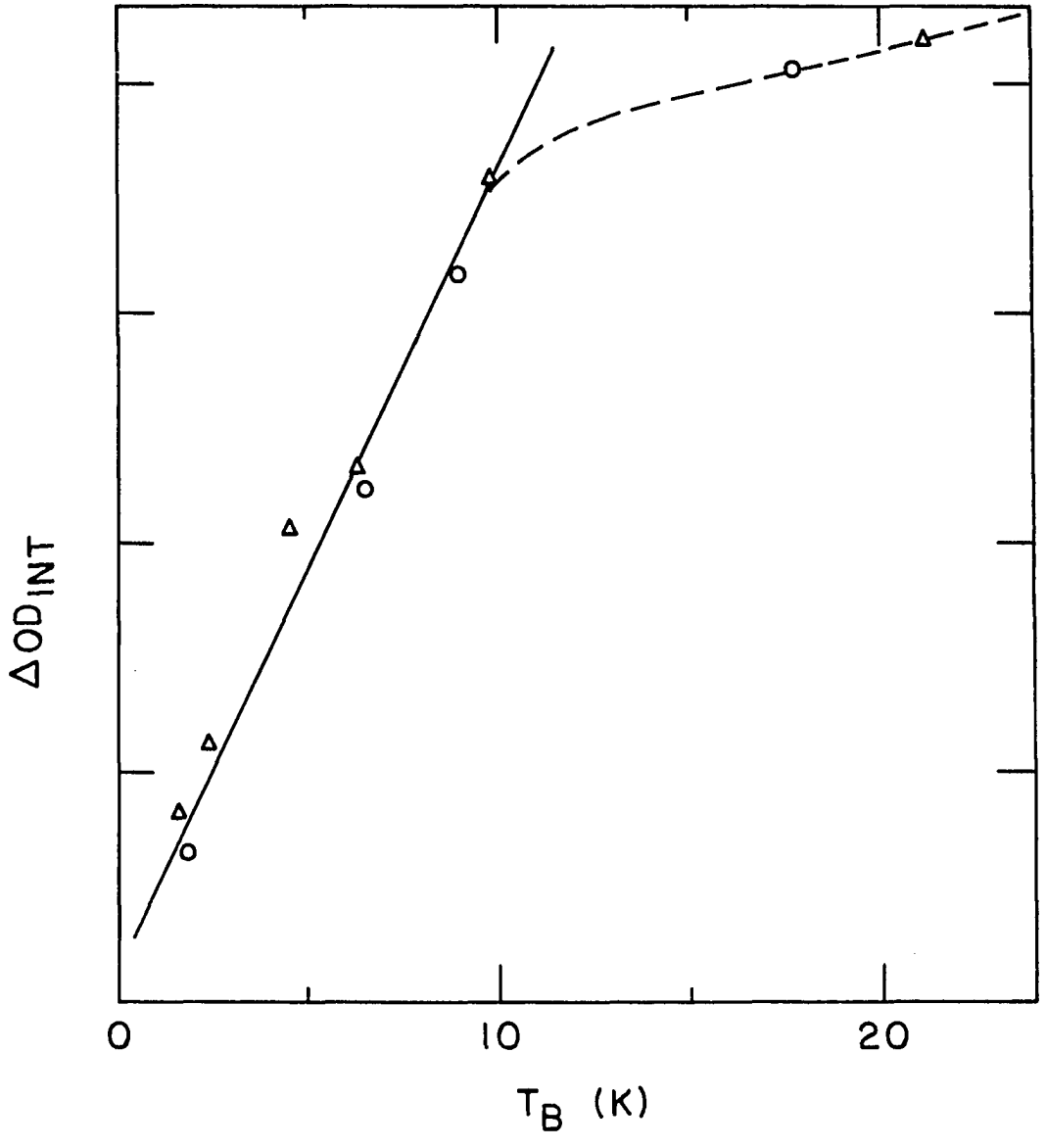

Figure 23. Integrated hole intensity for the zero-phonon hole in the origin band of tetracene in GLY/DMSO/DMF as a function of burn temperature

capable of being burned at the lowest temperatures, ∿2K, will also be burned and contribute to the hole intensity at intermediate temperatures, $2 < T \lesssim 10K$. Above 10K, however, these sites may be in thermal equilibrium in their excited states and hence not lead to hole burning. It may also be that sites burnable at 2K are in thermal equilibrium in their ground states at 10K. In either event, there are fewer burnable sites above 10K, and the integrated hole intensity falls off. The other effect is a saturation effect. There will be some maximum number of burnable sites, and for $T_B \gtrsim 10K$, the number of burned sites may be approaching this limiting value.

A temperature study similar to that discussed here has been done for NPHB of tetracene in EtOH/MeOH and has yielded similar results (75). These two studies led to development of the theory given here and in references 67, 75 and 85. These are the only temperature dependence studies of this type which have been reported, but there are other examples of hole profiles with a width of ∿1 cm^{-1} for burn temperatures ∿2K in other amorphous systems (28,43,44,50,51).

Annealing

Annealing, or (thermal) hole filling, is the process by which a hole irreversibly disappears as the temperature is raised above its burn temperature. Annealing occurs for all holes, either non-photochemically or photochemically burned, at sufficiently high temperatures, although for destructive photochemistry the annealing is due to diffusion of unburned impurities into the region of the hole and a net decrease in the integrated absorption of the band still

results (cf. reference 28). In some systems (see references 61, 62), holes are filled even at the burn temperature by a thermally activated barrier crossing. In most systems, the holes are persistent at T_B and are annealed by warming the sample or, in some cases (27,56), by irradiation with an intense, broad-band light source.

Annealing data for holes burned ∿6K in acridine orange in GLY/H_2O/EtOH are given in Figure 24. There appears to be two different mechanisms for annealing in this system, one giving a rapid intensity decrease with temperature and the other a slower one. More typical annealing data are shown in Figure 25 for tetracene in GLY/DMSO/DMF where both the hole intensity and width are given for $T > T_B$, and a uniform intensity decrease is observed. For each system, holes were found to be persistent at or below T_B for observation times up to six hours. When the sample was warmed from T_B to $T' = T_B + \Delta T$, such a warming typically taking 10-20 min, the holes were observed to be broader and shallower, and the "new" holes were persistent on a scale of hours. This process could be repeated until the holes disappeared, typically around 40K for these two systems. These observations imply that for sites annealed between T_B and T', the annealing rate changes from $\lesssim 10^{-5}$ s^{-1} at T_B to $\gtrsim 10^{-2}$ s^{-1} at T', while those sites which have not annealed have a rate $\lesssim 10^{-5}$ s^{-1} at T'. Since $\Delta T = T' - T_B$ was typically 2-5K, the annealing rate is seen to have a very large temperature dependence. For tetracene in GLY/DMSO/DMF, the situation is even more complex. For samples warmed until the holes disappear, $T \sim 40K$, and then cooled back to T_B, the holes partially reappear.

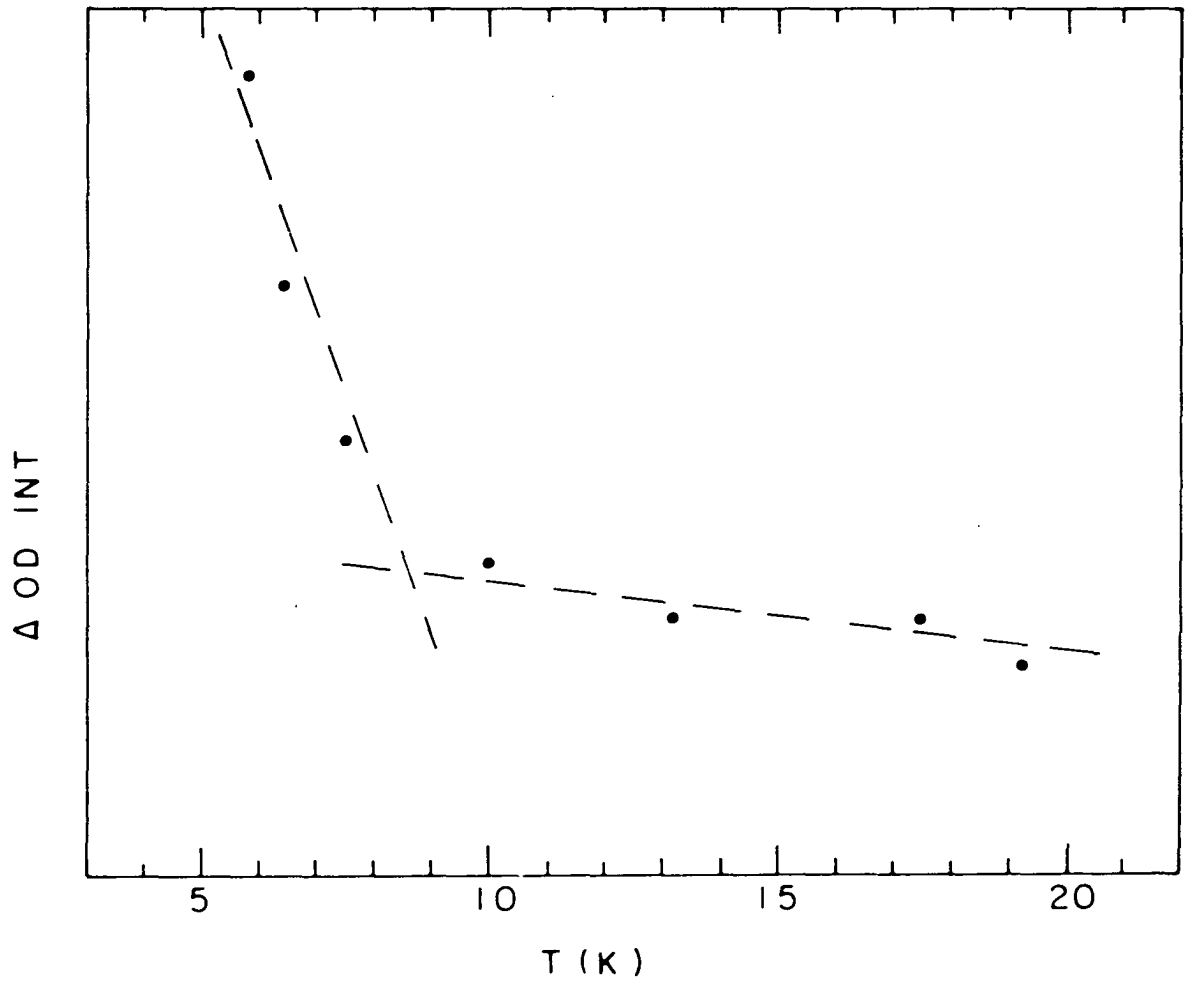

Figure 24. The integrated hole intensity as a function of annealing temperature for a hole burned at 5.8K in a 2 x 10^{-5} M solution of acridine orange in 2:1:2 GLY/H_2O/EtOH

Figure 25. Annealing data for the zero-phonon hole in the origin band of tetracene in GLY/DMSO/DMF as a function of temperature for a hole burned at 8K. The closed circles represent the integrated intensity and correspond to the left ordinate. The open circles represent hole width and correspond to the right ordinate

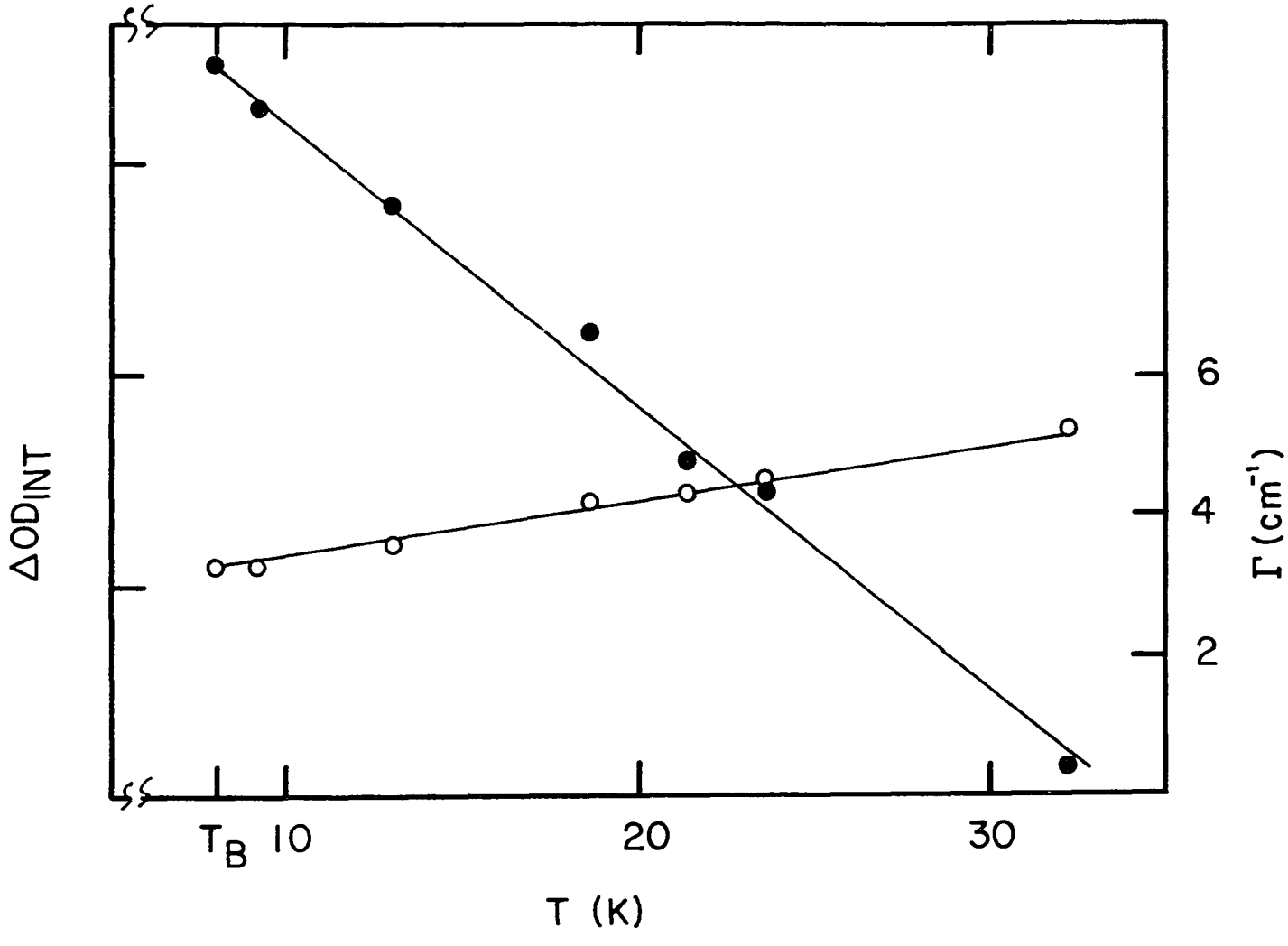
ΔOD_{INT}
$\Gamma\,(cm^{-1})$
6
4
2
T_B
10
20
30
T (K)

For the data in Figure 25, for example, the sample was warmed to 35K where no holes were seen and then cooled back to T_B = 8K. The hole reappeared to roughly 2/3 of its original integrated intensity and with a width of 3.9 cm^{-1}. They may be interpreted as an annealing process and a thermal broadening process operating simultaneously. An attempt was made to deconvolute these two processes experimentally (105) by cycling the temperature between T_B and successively higher temperatures, and measuring the hole profile at each temperature. Quantitatively, the experiment failed due to imprecision of the temperature control and reproducibility and lack of glass reproducibility (105). The qualitative results and the more usual annealing data are consistent with annealing and broadening mechanisms acting simultaneously.

The linearity in the annealing data, Figures 24 and 25, which is reminiscent of the burning data in Figures 19 and 23, suggests an annealing mechanism based on PAT of the TLSs for the ground (impurity) state (TLS_G). Sites which are burned via PAT of the TLS_Fs are returned to their original configuration through PAT of the TLS_Gs, where they again absorb at ω_B. This mechanism, despite its attractiveness, cannot explain the data. The highest temperature dependence for the PAT rate is a linear one (75)[5] which occurs in the high temperature limit. The other mechanism proposed for NPHB, thermal activation whose rate goes

---

[5]The PAT rate (Γ^{-1} of reference 71) goes as $\coth(\hbar\omega/2kT)$ which for $kT >> \hbar\omega$ is linear in T.

as exp[-V/kT], is similarly unable to explain the annealing. It is clear that the existing model for NPHB is unable to explain the annealing results, probably due to lack of sufficient detail. An extension to this model, or a new model, must be sought.

One extension which has been suggested (67,75) is that a local order-disorder transition (second order phase transition[6]) of the glass is responsible for the annealing. Such transitions are characterized by an order parameter S, which varies continuously from 1.0 at 0K to 0 at the critical temperature T_c. One typical order parameter is that for β-brass (106), which may be approximated by

$$S = \begin{cases} 1 - 0.182\ x & 0 \leq x \leq 0.55 \\ 0.9\left[1 - \dfrac{(x - 0.55)^2}{(0.45)^2}\right]^{1/2} & 0.55 < x \leq 1 \end{cases} \qquad (4.1)$$

with $x = T/T_c$. This function, graphed in Figure 26, is linear for $x \leq 0.55$ and is represented by one quadrant of an ellipse of eccentricity 0.87 for x between 0.55 and 1. Its strongest temperature dependence is in the region just below T_c. The order-disorder transition is assumed to alter the structure of the TLSs so that the barrier height, written $V = V_o S$, varies from V_o at 0K to zero at T_c.

---

[6]A general discussion of second order phase transitions is given in reference 107. A more theoretical discussion of one example, ferromagnetism, is found in reference 108.

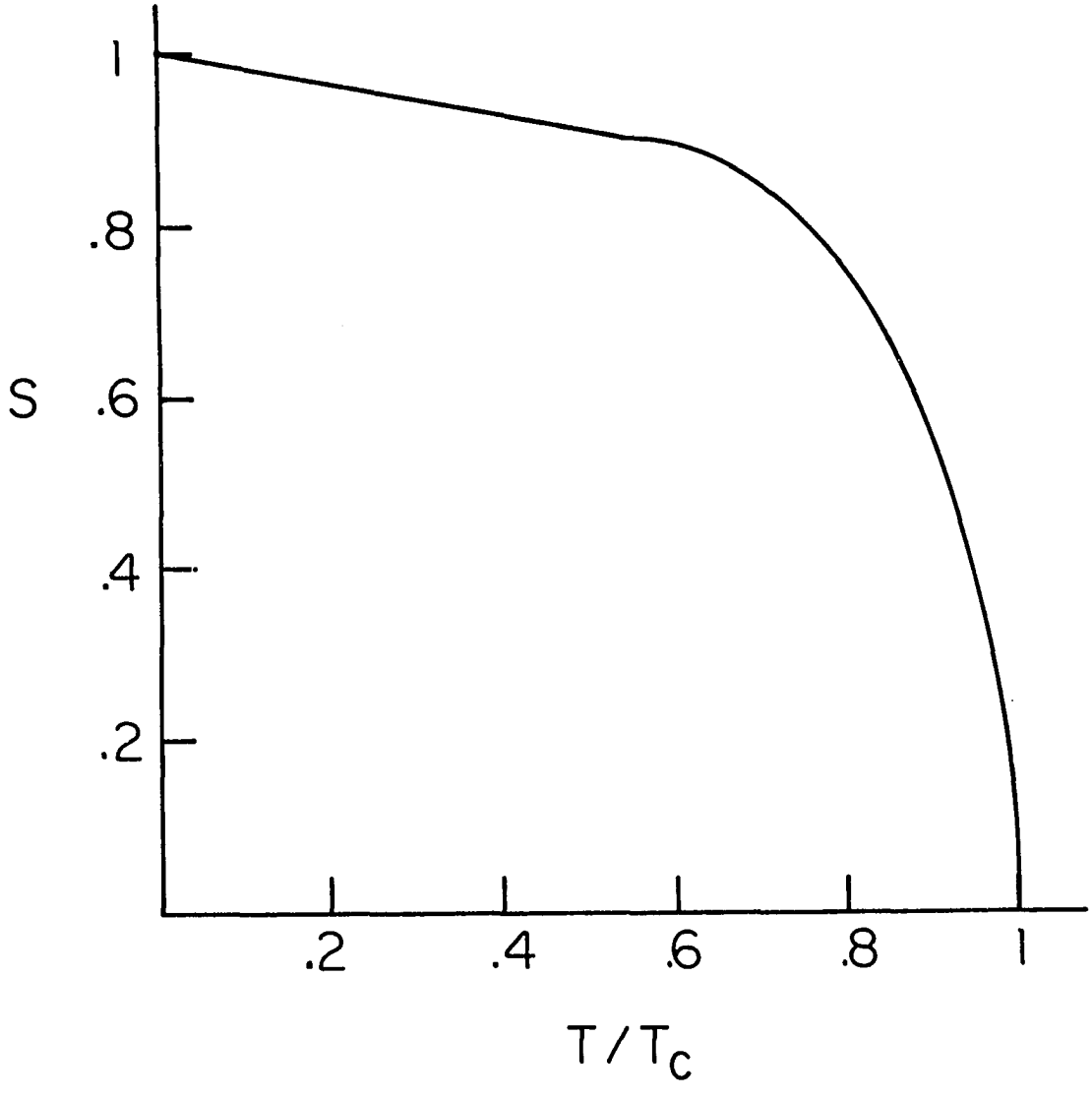

Figure 26. An approximation to the order parameter for β-brass (ref. 106) as a function of reduced temperature

Using a thermally activated annealing process, the rate for which is given by

$$k = A \exp[-V_o S/kT] \tag{4.2}$$

where S is given by Eq. 4.1, $A = 10^{10}\ s^{-1}$, $V_o = 200\ cm^{-1}$ and $T_c = 10K$, the annealing rates shown in Table 3 were calculated. These data show

Table 3. Thermally activated annealing rates calculated using equation 4.2

T (K)	S	k (s^{-1})
0	1.0000	---
1	0.9818	0
2	0.9636	6×10^{-51}
3	0.9455	4×10^{-30}
4	0.9273	1×10^{-19}
5	0.9091	2×10^{-13}
6	0.8944	2×10^{-9}
7	0.8485	7×10^{-6}
8	0.7483	2×10^{-2}
9	0.5657	1×10^{2}
9.5	0.4123	4×10^{4}
10	0	$10^{10} = A$

that below 8K the annealing is negligibly slow, while for T > 8K annealing occurs rapidly, almost instantaneously for $T \gtrsim 9.5K$. Notice also that $\Delta k/\Delta T$ for $T \lesssim 5K$ is very high due to the large relative change in temperature in this region. For lower barriers, $V_o \lesssim 40\ cm^{-1}$, the rate becomes significant at $T \sim 4K$ and $\Delta k/\Delta T$ remains high allowing the annealing of sites with low barriers at low temperatures to be explained by the normal thermal dependence of thermal activation. This model for annealing can explain the high dependence of the annealing rate on temperature only for very low temperatures, T < 5K, and in the narrow range just below T_c. It cannot offer an explanation for the linear intensity loss with temperature (Figures 24 and 25) observed over the range 5 - 30K. Similar results show that a PAT annealing process is also unable to explain the annealing data.

The critical temperature of an order-disorder transition is a measure of the energy necessary to randomize a structure along the symmetry coordinate associated with the transition. It is a measure of the "strength" of an ordering. Since glasses are locally ordered, but lack translational order (vide infra), it is reasonable to assume that the strength of the local ordering, and hence T_c, may vary within the glass. Allowing the barrier height to depend on S and using a thermally activated annealing process as before, a distribution of annealing temperatures is created based on the strength of local ordering around individual sites. Below its respective critical temperature, each site is stable towards annealing on a scale of hours. If the distribution of critical temperatures is constant, the number of sites capable of

being annealed at any temperature is also constant, and a linear intensity loss with temperature, as observed (Figures 24 and 25), is expected. This model explains the annealing data for tetracene in EtOH/MeOH (75) and acridine orange in GLY/H_2O/EtOH (vide supra), and with addition of a thermal broadening mechanism to explain the annealing hole widths and hole reappearance (vide supra), the annealing data for tetracene in GLY/DMSO/DMF.

This new annealing model, since it requires changes in the concept of a TLS, will affect the hole burning model as well. Assuming, as is reasonable, that the (impurity) excited state barrier height varies in the same way as the ground state barrier height, this model requires that different sites be active towards NPHB at different temperatures, but due to constant distribution of T_c's, there are a constant number of burnable sites at each temperature. A linear increase in the hole intensity with burn temperature is then expected as is observed (Figure 23). The theory for the hole widths and shape is unaffected by this model since the theory depends on TLSs in thermal equilibrium at T_B, implying that these sites have $T_c < T_B$. Thus, this annealing model is consistent with the theory for burning and explains the intensity vs. T_B data as well as the annealing.

The nature of the order-disorder transition is open to conjecture. There are no such transitions known for any of these glass solvents in their crystalline form, which implies that these transitions, as well as the two level systems, are characteristic of glasses. Given the coupling of the order-disorder transition and the TLSs in this model,

it seems plausible that the TSLs and the order-disorder transition may have the same or similar coordinates.

Computer Modeling

Numerical study of equation 2.33

While the high temperature ($kT >> \sigma$) behavior of Eq. 2.33 is easily deduced (vide supra), the behavior for lower temperatures can only be determined by numerical evaluation. In this region, the value of Eq. 2.33 depends strongly on the temperature, the TLS distribution width σ, and the minimum tunneling frequency Δ_{min}.

The temperature dependence of the integral (I) in Eq. 2.33 is given in a log-log plot in Figure 27 for different values of σ and integration limits of 0 and 10σ. The onset of linearity is shown to depend on σ, occurring for $kT \sim 2\sigma$. The curvature for $kT \lesssim \sigma$ is independent of σ. The dependence of I on Δ_{min} for $\sigma = 2\ cm^{-1}$ is given in Figure 28. For $\Delta_{min} < \sigma$, the onset of linearity is constant at $kT \sim 2\sigma$. For $\Delta_{min} \gtrsim \sigma$, Δ_{min} begins to dominate the csch term, moving the onset of linearity to higher temperatures. The value of I in the linear region also depends weakly on Δ_{min}, especially for $\Delta_{min} > \sigma$, for the reason explained above. The curvature below the linear region is strongly dependent on Δ_{min}. For $\Delta_{min} = 0.1\ cm^{-1}$, the data below 1K are fit quite well by a line of slope 2.0, indicating a quadratic temperature dependence for Eq. 2.33 for low temperatures. For larger Δ_{min}, both the curvature and the slope increase. With $\Delta_{min} = 2.0\ cm^{-1}$ ($\Delta_{min} = \sigma$), for example, the data below 1K (not all shown on Figure 28) are fit

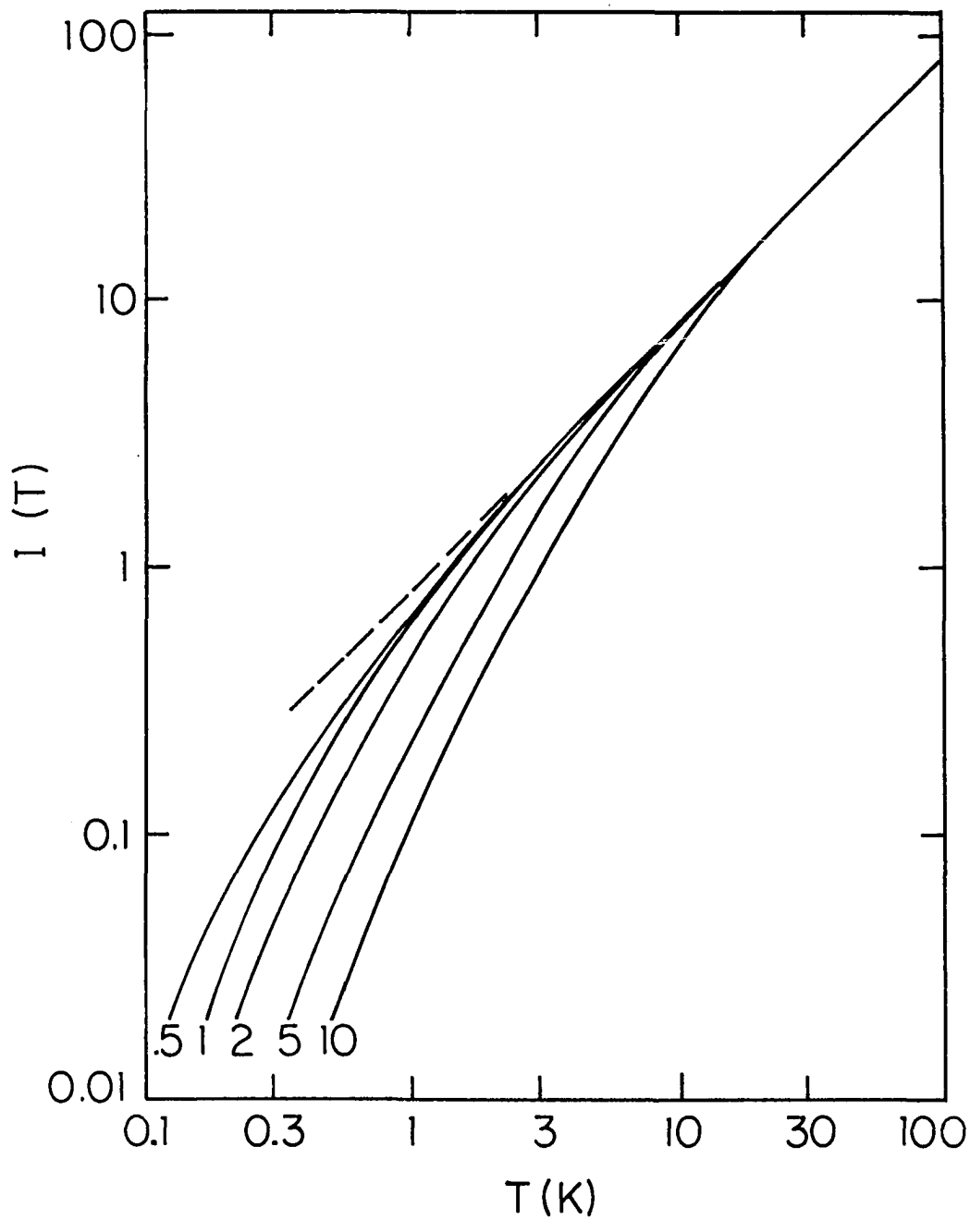

Figure 27. Numerical evaluations of the integral in Eq. 2.33 as a function of temperature for Δ_{min} = 0.1 cm^{-1}, and the σ values (in cm^{-1}) listed for each curve. The upper integration limit was taken to be 5σ

Figure 28. Numerical evaluations of the integral in Eq. 2.33 as a function of temperature for $\sigma = 2.0\ cm^{-1}$ and the Δ_{min} values (in cm^{-1}) listed for each curve. The upper integration limit was taken to be $5\sigma = 10\ cm^{-1}$

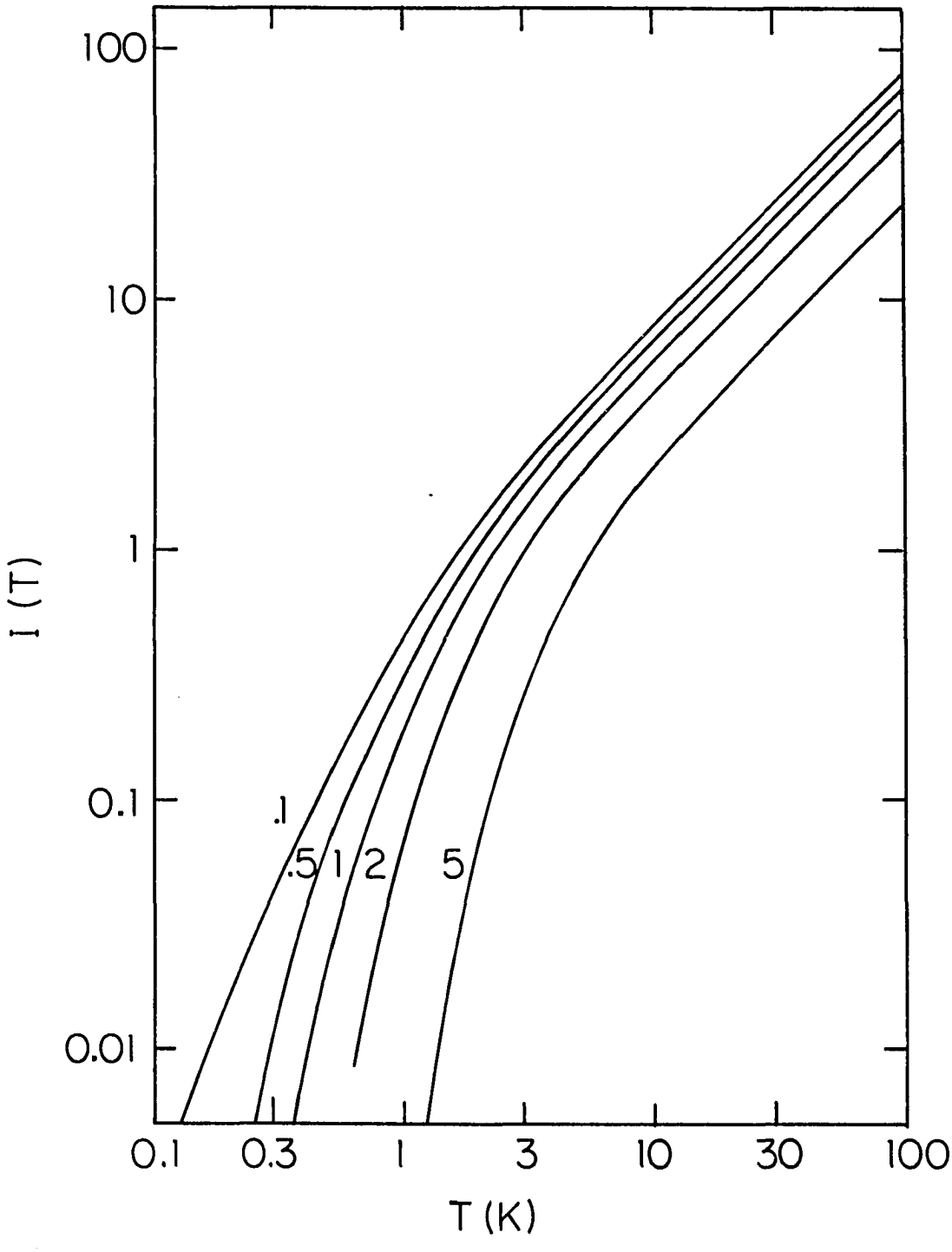
100
10
1
0.1
0.01
I (T)
.1
.5
1
2
5
0.1
0.3
1
3
10
30
100
T (K)

only moderately well by a line of slope 6.4. Similar data for σ = 10 and σ = 200 cm^{-1} indicate that Δ_{min}, σ and T all scale together so that all the data could be represented on a single graph with the curves labeled by the ratio Δ_{min}/σ and the temperature written as kT/σ. To review: for $kT > 2\sigma$ and $\Delta_{min} < \sigma$, Eq. 2.33 is linear with temperature. For $kT < 2\sigma$, the temperature dependence varies strongly with Δ_{min}/σ, but for $\Delta_{min}/\sigma \lesssim 0.1$, Eq. 2.33 is very nearly quadratic in temperature. For increasing values of Δ_{min}/σ, Eq. 2.33 shows increasing curvature and an increasing temperature dependence below the high temperature limit.

It has already been shown that the theory presented here is capable of describing the temperature dependence of NPHB hole widths using a narrow ($\sigma \sim 1$ cm^{-1}) distribution on TLS asymmetries. It is now useful to return to the comparison of this theory with that of Lyo and Orbach (80). Recall that their theory predicts a quadratic temperature behavior for temperatures below the Debye temperature (θ_D) or the maximum TLS asymmetry, whichever is lower. Above this limit, they find a linear temperature dependence. The Debye temperature is related to the maximum phonon frequency and serves as an upper bound for the integration. Applying these conditions to Eq. 2.33 using a constant TLS distribution ($\sigma = \infty$, $\Delta_{min}/\sigma = 0$) and $k\theta_D$ as the upper integration limit, a nearly quadratic ($T^{2.2}$) temperature behavior is found for $T \lesssim \theta_D/2$. For $T > \theta_D$, Eq. 2.33 is linear in temperature. Using a (Gaussian) TLS distribution width $\sigma > k\theta_D$ and 2σ as the upper integration limit, a nearly quadratic temperature behavior ($T^{2.1}$) is observed for $kT < 2\sigma$

where $\Delta_{min}/\sigma = 0.05$. $kT > 2\sigma$ yields a curve linear in T. These results show that the theory of Lyo and Orbach (80) and that given here (vide supra) are not only similar in form but also predict the same temperature dependence for optical linewidths due to dephasing by TLSs.

Comparison with experimental data

It is instructive to apply the theory described here to systems other than those for which it was derived. Selzer et al. (76) have observed a nearly quadratic temperature dependence ($T^{1.8 \pm 0.2}$) for the $^5D_0 \rightarrow {}^7F_0$ fluorescence transition of Eu^{3+} in silicate glass from 7 to 80K. As discussed above, in the theory presented here, for $kT < 2\sigma$ and $\Delta_{min}/\sigma \lesssim 0.1$ the linewidth depends quadratically on temperature. Using $\sigma \approx 30\ cm^{-1}$, this theory is consistent with the data presented by Selzer et al. (76). Similar data have appeared for the same system from 200 to 300K (77). These data can be fit by the TLS broadening mechanism described above using a very wide ($\sigma \approx 100\ cm^{-1}$) TLS distribution or by the two-phonon Raman broadening mechanism (reference 91, p. 347). For reasons to be discussed later, the Raman mechanism is preferable.

Hegarty and Yen (78) have reported homogeneous fluorescence linewidths for the $^3P_0 \rightarrow {}^3H_4(1)$ transition for Pr^{3+} in BeF_2 and GeO_2 glasses from 8 to 300K. They found a very nearly quadratic temperature dependence over this entire range, with no breaks in the curve. Above $0.5\ \theta_D \approx 150K$, the data are consistent with the two-phonon Raman broadening mechanism as observed for Pr^{3+} in crystalline LaF_3 (109,110). Below $T \approx 0.5\ \theta_D$, the linewidth due to the Raman mechanism rapidly falls below the observed widths since it goes as T^7 for low temperatures.

Hegarty and Yen (78) use the theory of Lyo and Orbach (80) to fit their data for low temperatures, calculating a linewidth at 10K in reasonable agreement with the experimental results. Hegarty and Yen remark that the theory of Lyo and Orbach assumes a constant TLS density of states (distribution), which, for high temperatures, may not be correct. In fact, for $T \approx \theta_D$, a constant TLS density of states is inconsistent with the Debye approximation used by Lyo and Orbach (and also in the theory presented here (vide supra)), and with the concept of TLSs in glasses.[7] Hegarty and Yen suggest that a decrease in the density of high-energy TLSs would lead to a decrease in the TLS contribution to the linewidth which, when added to the trend towards a linear thermal dependence at high temperatures, might give a smooth changeover from the low-temperature TLS broadening mechanism to the high-temperature Raman mechanism.

To examine this suggestion, the data of Hegarty and Yen (78) were fit using a linear combination of the linewidths predicted by the TLS broadening mechanism used here and the two-phonon Raman broadening mechanism. For the TLS mechanism, the integral of Eq. 2.33 was used where $\Delta_{min} = 1.0\ cm^{-1}$, the upper limit of integration was taken to be

---

[7] Recall the discussion of TLSs and glasses in Chapter I. It was postulated that TLSs begin to be "frozen out" at T_G, and that there existed a distribution of TLS barrier heights from zero to kT_G. The maximum barrier height kT_G serves as an upper limit for the maximum TLS asymmetry.

$k\theta_D$ and σ was varied to provide the best fit to the data. For the Raman theory, the pertinent equation is (reference 91, p. 350)

$$\langle\Gamma\rangle_R = A\left(\frac{T}{\theta_D}\right)^7 \int_0^{\theta_D/T} \frac{x^6 e^x}{(e^x - 1)}\, dx \qquad (4.3)$$

where A is a constant containing the transition matrix elements. Values of this integral including the $(T/\theta_D)^7$ term as a function of the ratio θ_D/T are tabulated in reference 91. The constant A was varied to obtain the best fit. The results are shown in Figure 29 where the data points are taken from Hegarty and Yen (78). "TLS" and "Raman" represent the appropriately scaled results of the TLS and Raman broadening mechanisms, and the dashed curve gives their sum. The fit to the data is quite satisfactory. The slight sigmoid character of the fit occurs because the Raman mechanism rises as T^7, faster than the TLS mechanism falls, as T. If, as Hegarty and Yen (78) suggest, the distribution of TLS asymmetries falls off sharply above some temperature, then the TLS broadening mechanism would fall off faster than T, and the fit could be improved. The values of A (see Eq. 4.3) obtained for the two glasses are consistent with that observed for the same transition in Pr^{3+}:LaF_3 (200 cm^{-1}) (109) given the differences in θ_D for these systems. For the BeF_2 glass, the linewidth at 10K was 0.03 cm^{-1}. The value of the normalized integral in the TLS mechanism for this temperature is 0.7 cm^{-1}. Using ρ = 2.0 g cm^{-3} and c = 3.02 x 10^5 cm s^{-1}, both taken from reference 111, the product $\delta B_I(\Delta_I + \Delta_I')$ was found to be 2 x 10^4 cm^{-2}. Taking d $\sim$ 1 Å, the mass of a fluorine atom

Figure 29. Theoretical fits to the fluorescence line width data for the $^3P_0 \rightarrow {}^3H_4(1)$ transition of Pr^{3+} in (a) BeF_2 and (b) GeO_2 as a function of temperature. The solid points are the data taken from reference 78. The solid curves are the results of the two-phonon Raman and the TLS broadening mechanisms. The dashed curve is the sum of the results of these two mechanisms

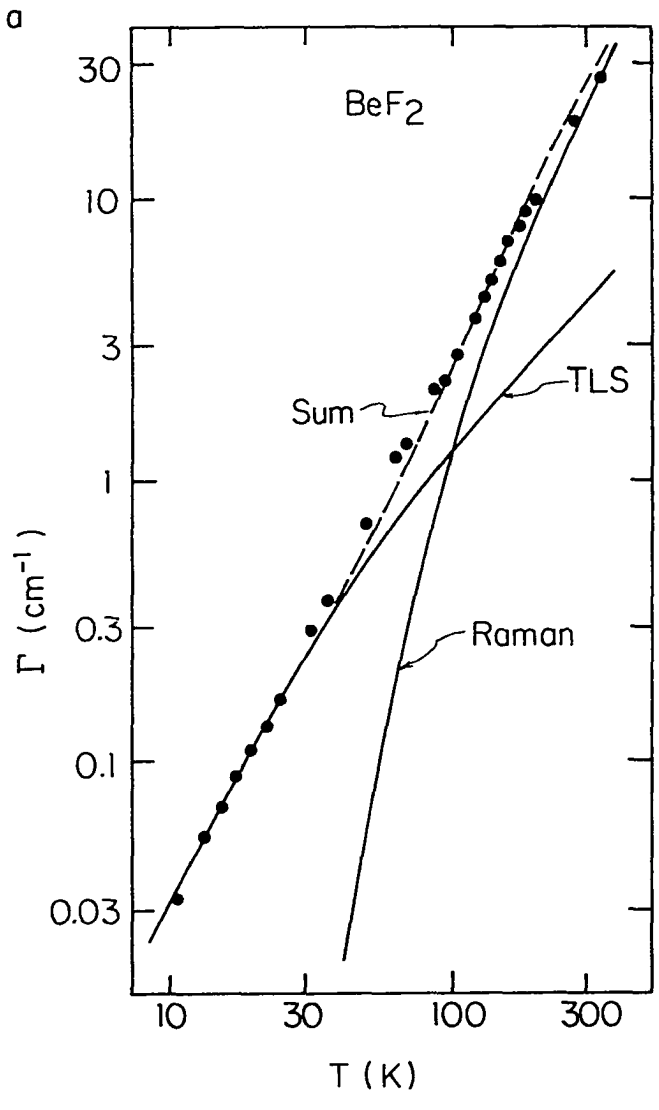
a
BeF2
Sum
TLS
Raman
Γ (cm-1)
T (K)
30
10
3
1
0.3
0.1
0.03
10
30
100
300

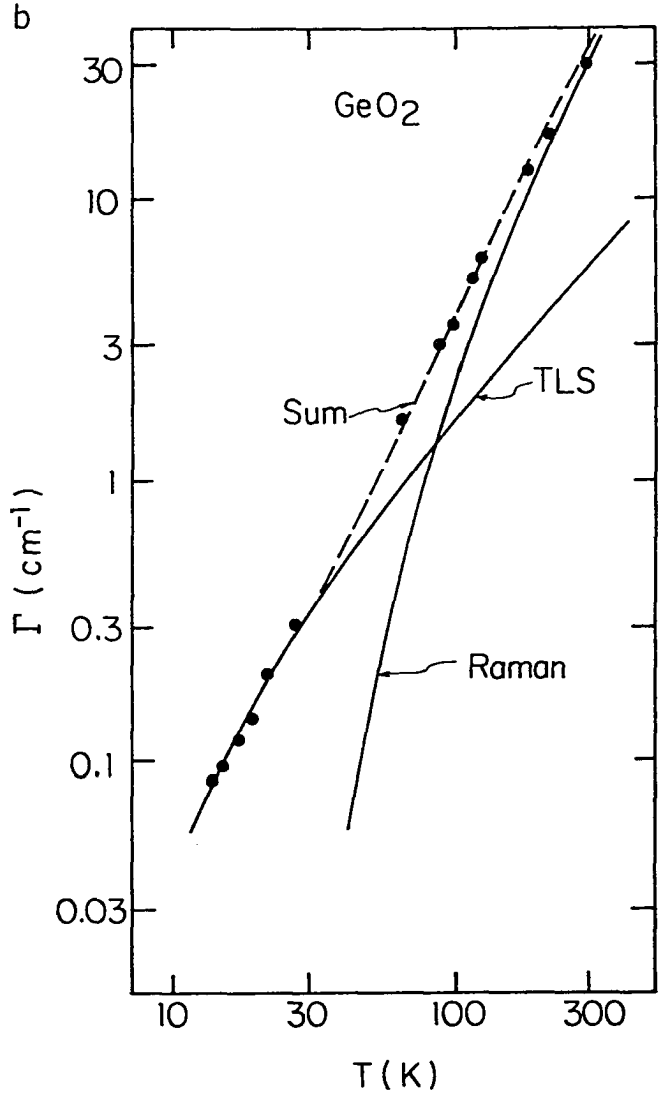
b
GeO2
Sum
TLS
Raman
Γ (cm-1)
T (K)
30
10
3
1
0.3
0.1
0.03
10
30
100
300

$(19/6 \times 10^{23})$ g for m, $V \sim 5$ cm^{-1} and $\hbar\omega_o \sim 10^{13}$ s^{-1} in Eqs. 2.8 and 2.9, Δ_I is calculated to be $\sim$30 cm^{-1}. Assuming Δ_I' to be on the same order, a value of $\sim$300 cm^{-1} is found for δB which is consistent with value of the deformation potential assumed for silicate glasses (70,71). A similar value of δB was calculated for the GeO_2 glass.

For both the BeF_2 and GeO_2 data, (Figure 29), $\sigma = 60$ cm^{-1} was found to give the best fit to the data. Making the assumption that the distribution of asymmetries is narrower than the distribution of barrier heights, and letting kT_G be the upper limit for barrier heights, 60 cm^{-1} is a reasonable value for σ. This value is also consistent with the probability distributions of V and ε derived for metallic glasses (112) if the distributions are scaled to $V_{max} \sim kT_G$.

Another consideration is the shape of the TLS distribution function. Here a Gaussian function peaked at $\varepsilon = 0$ was used. Several theories use a constant distribution (79,80). Experimentally, the distribution function is weakly quadratic (111) below 10K for many glasses. For higher temperatures, up to $\sim$100K, the distribution depends on ε^{α} with $\alpha \approx 0.2$ (113). These distributions share a common trait in that they are all approximately constant for small ε. In contrast, is the distribution used by Ngai (114) which is linear in ε for small ε and approximately Gaussian for large ε. The effect of using these distribution functions is (except for a constant distribution (vide infra)) unknown. It may be that the distribution function used in the TLS dephasing theory presented here is not characteristic of the entire TLS distribution (see footnote d of this chapter) and

could have a different shape than distributions measured by other techniques.

CHAPTER V. CONCLUSION

Nonphotochemical Hole Burning

Summing up

NPHB has been shown to occur in many impurity-glass (or polymer) systems. When it does occur, it is explained by a model based on two level systems which are thought to be characteristic of the glassy state. The impurity molecules are coupled to TLSs forming "sites". A subset of the TLSs have the following properties:

1) The ground (impurity) state barrier height is large enough to cause hole persistence.
2) The excited state barrier is low enough to allow relaxation, either by PAT or by thermal activation, from one minima to the other.

The relaxation of these TLSs alters the transition energy of the impurities coupled to them resulting in a decreased absorption, or a nonphotochemical hole, at the excitation frequency. The impurities are coupled to other TLSs which are in thermal equilibrium, leading to an ultra-fast dephasing of the impurity excited state. The dephasing, treated theoretically earlier (vide supra), gives broad ($\sim$1 cm^{-1}) homogeneous linewidths even at the lowest temperatures (Figure 21), a linear dependence of linewidth on temperature in the high temperature limit (Eq. 2.33, Figures 27-28, and Figure 19), and a super Lorentzian line profile (Eq. 2.35) as observed for $T \lesssim 2K$ (Figure 21).

Nonphotochemically burned holes are annealed out as the sample is warmed above the burn temperature. The data indicate that there is a very dramatic dependence of the annealing rate on temperature. The annealing is explained by postulating that the glass undergoes order-disorder transitions which alter the barrier heights of the TLSs. It is further postulated that there exists in the glass a constant distribution of critical temperatures for these transitions, predicting a linear decrease in hole intensities with annealing temperature (Figures 24 and 25), and a linear increase in hole intensities with burn temperature (Figure 23).

The explanations for NPHB, dephasing, and annealing are based on characteristics of amorphous solids. The study of NPHB had led to a greater understanding of the nature of these solids. The existence of NPHB and its explanation have helped to establish that TLSs are indeed characteristic of the glassy state. The linearity of linewidths as a function of burn temperature (Figure 19) indicates that the distribution of TLS asymmetries is quite narrow ($\sim$1 cm^{-1}), although this could be a measure of the TLSs important for dephasing and may not be characteristic of the total distribution of asymmetries. The requirement that an impurity molecule must interact with at least two TLSs, one leading to hole burning and the other to dephasing, led to the statements (75) that an "impurity is surrounded by several TLSs" and "the average spatial extent of the TLSs must be quite small." The number density of TLSs per unit energy can be obtained from the excess specific heat at low temperatures. This has been done for several inorganic glasses and

two polymers (72,73,111), all of which had number densities of 10^{32}-10^{33} erg^{-1} cm^{-3}. Assuming a similar density for the hosts used in this work and a typical impurity concentration of 10^{-4} M, one finds a density of $\sim 10^{-8}/cm^{-1}$ (impurity) molecule. Quite clearly, every impurity cannot be surrounded by several TLSs if their spatial extent is small. One could postulate that the presence of an impurity perturbs the host's structure, thereby inducing a higher density of TLSs. Another suggestion is that the spatial extent of TLSs is large and that a single TLS interacts with many impurity molecules. One educated guess as to the nature of the TLSs, at least for protic hosts, has the TLSs arising from the hydrogen bonding network of the host. If this is the case, it could well be that the TLSs are quite large and that an impurity molecule could "feel" a TLS relaxation spatially well-removed from itself. The proposed annealing mechanism is also based on an (unproven) assumption of the nature of amorphous solids. Further study of hole annealing should show whether or not this assumption is true, and if it is, could reveal the nature of the transition and of the microscopic structure of amorphous solids.

There were also many systems in which NPHB was not observed to occur. Although the nonoccurrence of holes was not systematically studied, some conclusions concerning reasons for hole nonoccurrence were drawn. Most of these conclusions involved properties of the host solid or the host-impurity interaction is some specific way. For example, it was suggested that some impurities alter the TLS distribution rendering NPHB impossible. In some samples, FLN was not

observed suggesting that a rapid intersite energy transfer might be dispersing the excited isochromat giving unobservably broad holes. For quinizarin in benzophenone, a hole nonoccurrence mechanism based on specific structural considerations was postulated. It seems likely that detailed study of the nonoccurrence of nonphotochemical holes would increase the understanding of the glassy state and of the host-impurity interactions.

What good is it?

It has been emphasized that NPHB can provide information about the nature of amorphous solids, much of which is difficult to obtain by other methods. NPHB, a new phenomenon discovered only a few years ago, has proven to be interesting in its own right, as its mechanism and its relation to the host material have been understood. Yet, there are always those who still ask "what good is it?"

Perhaps the simplest use of NPHB is to create very narrow bandpass optical filters. Given appropriate materials, it is conceivable that specialized filters could be made for a specific purpose. When finished with the filter, anneal it and make a new one. Such a narrow filter could be used, for example, in the satellite-to-submarine laser communication system currently under study by the Navy and Defense Advanced Research Projects Agency (115,116).

Another use for hole burning is in high density data storage. A group at IBM's San Jose Research Laboratory is studying the application of photochemical hole burning to data storage and has recently received

a patent on the concept (117). Simply, to write into a memory a tunable laser would scan a two-dimensional array on a burnable material and spectrally scan each point in this array, either burning a hole (1) or not burning a hole (0) at each point on the three-dimensional (two spatial, one spectral) array. To read the memory, a probe laser would be used to measure the absorption at each point in the larger array. The IBM group estimates that storage densities as high as 10^{15} bits m^{-2} could be achieved (117).

Where do we go from here?

Whenever a research project is ended, there is always more work which could be done. This project is no exception. The linearity of hole widths *vs.* T_B to below 2K for tetracene in GLY/DMSO/DMF (Figure 19) indicates that the TLS distribution width is exceedingly narrow, $\sigma \lesssim 1\ cm^{-1}$. An independent confirmation of this, perhaps by hole filling (64), would be useful. It would also be instructive to go to lower burn temperatures for this system to attempt to find the onset of linearity.

There are examples of hole burning which should be followed up. In particular, quinizarin in P/MP/MC (Figure 17) yielded quite deep holes and deserves further study. Hole burning in polymers was only briefly studied; this too should receive additional study. There are always new systems to study. Most of the NPHB work to date has been on polar glasses. A study of nonpolar glasses like P/MP/MC would be very instructive in light of the "educated guess" that the TLSs may be due to hydrogen bonding networks in glasses.

The temperature dependence of NPHB has only been studied for two very similar systems (75, vide supra). Further work on other systems is clearly in order to determine the general applicability of the hole burning theory, and to determine the validity and applicability of the annealing model presented here. The super Lorentzian hole profiles (Eq. 2.35, Figure 21) have only been observed and studied for one system; other examples would certainly be welcome.

One remaining question concerning NPHB is the nature of the TLS coordinate and the microscopic nature of the tunneling process. Work is currently under way using deuterium-substituted alcohols in an attempt to answer this question for the EtOH/MeOH glass. It is expected that if the tunneling group is deuterated, an isotope effect would show up in the burning rate and quantum yields for hole burning. This should prove a critical test of the importance of hydrogen bonding to the hole burning process.

NPHB has shown that the dephasing in organic glasses is much faster than that which occurs in many other systems (75,85), but is the only technique which has been used to measure these dephasing times. The photon echo technique also probes dephasing (118) and would be a very good complement to the hole burning studies.

Effects of TLSs have been observed for inorganic glasses by a wide variety of techniques; specific heat, thermal conductivity and ultrasonic attenuation (73,90) and fluorescence line narrowing (76-78). These effects have been explained by theories assuming a constant distribution of TLS asymmetries (70,71,80). In contrast, NPHB has

predicted a very narrow distribution for organic glasses (75, vide supra). Measurement of the thermal properties of these organic systems would serve as a critical test of these predictions, and should indicate if the TLS distribution measured by hole burning is characteristic of the dephasing process or of the entire glass.

REFERENCES

1. Hughes, T. P. Nature 1962, 195, 325.
2. Kisliuk, P.; Walsh, D. J. Bull. Am. Phys. Soc. 1962, 7, 330.
3. Tang, C. L.; Statz, H.; deMars, G. App. Phys. Lett. 1963, 2, 222.
4. Tang, C. L.; Statz, H.; deMars, G. J. App. Phys. 1963, 34, 2289.
5. Bennett, W. R., Jr. Phys. Rev. 1962, 126, 580.
6. Lamb, W. E., Jr. Phys. Rev. 1964, 134, A1429.
7. Danielmeyer, H. G. J. App. Phys. 1971, 42, 3125.
8. Lee, P. H.; Skolnick, M. L. App. Phys. Lett. 1967, 10, 303.
9. Hall, J. L.; Bordé, C. Phys. Rev. Lett. 1973, 30, 1101.
10. Szabo, A. Phys. Rev. B 1975, 11, 4512.
11. Macfarlane, R. M.; Shelby, R. M. Opt. Lett. 1981, 6, 96.
12. Szabo, A.; Kroll, M. Opt. Commun. 1976, 18, 224.
13. Szabo, A.; Kroll, M. Opt. Lett. 1978, 2, 10.
14. Muramoto, T.; Nakanishi, S.; Hashi, T. Opt. Commun. 1977, 21, 139.
15. Shelby, R. M.; Macfarlane, R. M. Opt. Commun. 1978, 27, 399.
16. Jessep, P. E.; Muramoto, T.; Szabo, A. Phys. Rev. B 1980, 21, 926.
17. Erickson, L. E. Phys. Rev. B 1977, 16, 4731.
18. Staerk, H.; Czerlinski, G. Nature 1965, 207, 399.
19. Laubereau, A.; Kaiser, W. Opto-electronics 1974, 6, 1.
20. Topp, M. R.; Lin, H. B. Chem. Phys. Lett. 1977, 50, 412.
21. Leung, M.; El-Sayed, M. A. Chem. Phys. Lett. 1972, 16, 454.
22. Zuclich, J.; von Schütz, J. U.; Maki, A. H. J. Am. Chem. Soc. 1974, 96, 710.

23. Avarmaa, R. A.; Mauring, K. Kh. Opt. Spectrosc. 1976, 41, 393.

24. Macfarlane, R. M.; Shelby, R. M. Phys. Rev. Lett. 1979, 42, 788.

25. Shelby, R. M.; Macfarlane, R. M. Chem. Phys. Lett. 1979, 64, 545.

26. deVries, H.; Wiersma, D. A. Phys. Rev. Lett. 1976, 36, 91.

27. Gorokhovskii, A. A.; Kaarli, R. K.; Rebane, L. A. JETP Lett. 1974, 20, 216.

28. Cuellar, E.; Castro, G. Chem. Phys. 1981, 54, 217.

29. Gorokhovskii, A. A.; Kaarli, R. K.; Rebane, L. A. Opt. Commun. 1976, 16, 282.

30. Gorokhovskii, A. A. Opt. Spectrosc. 1976, 40, 272.

31. Gorokhovskii, A. A.; Rebane, L. A. Sov. Phys. Solid State 1977, 19, 1966.

32. Gorokhovskii, A. A.; Rebane, L. A. Opt. Commun. 1977, 20, 144.

33. Voelker, S.; Macfarlane, R. M.; van der Waals, J. H. Chem. Phys. Lett. 1978, 53, 8.

34. Gorokhovskii, A. A.; Kikas, J. Opt. Commun. 1977, 21, 272.

35. Voelker, S.; Macfarlane, R. M.; Trommsdorff, H. P.; van der Waals, J. H. J. Chem. Phys. 1977, 67, 1759.

36. Voelker, S.; Macfarlane, R. M. Chem. Phys. Lett. 1979, 61, 421.

37. Dicker, A.I.M.; Noort, M.; Voelker, S.; van der Waals, J. H. Chem. Phys. Lett. 1980, 73, 1.

38. Kharlamov, B. M.; Bykovskaya, L. A.; Personov, R. I. Chem. Phys. Lett. 1977, 50, 407.

39. Maslov, V. G. Opt. Spectrosc. 1978, 45, 718.

40. Gutierrez, A. R. Chem. Phys. Lett. 1980, 74, 293.

41. Völker, S.; Macfarlane, R. M. J. Chem. Phys. 1980, 73, 4476.

42. Dicker, A.I.M.; Noort, M.; Thijssen, H.P.H.; Völker, S.; van der Waals, J. H. Chem. Phys. Lett. 1981, 78, 212.

43. Friedrich, J.; Scheer, H.; Zickendraht-Wendelstadt, B.; Haarer, D. J. Am. Chem. Soc. 1981, 103, 1030.

44. Friedrich, J.; Scheer, H.; Zickendraht-Wendelstadt, B.; Haarer, D. J. Chem. Phys. 1981, 74, 2260.

45. Hager, S. L.; Willard, J. E. J. Chem. Phys. 1974, 61, 3244.

46. Marchetti, A. P.; Scozzafava, M.; Young, R. H. Chem. Phys. Lett. 1977, 51, 424.

47. Davies, B.; McNeish, A.; Poliakoff, M.; Tranquille, M.; Turner, J. J. Chem. Phys. Lett. 1977, 52, 477.

48. Poliakoff, M.; Breedon, N.; Davies, B.; McNeish, A.; Turner, J. J. Chem. Phys. Lett. 1978, 56, 474.

49. Poliakoff, M. Chem. Phys. Lett. 1981, 78, 1.

50. Graf, F.; Hong, H.-K.; Nazzal, A.; Haarer, D. Chem. Phys. Lett. 1978, 59, 217.

51. Drissler, F.; Graf, F.; Haarer, D. J. Chem. Phys. 1980, 72, 4996.

52. Macomber, J. D. "The Dynamics of Spectroscopic Transitions"; Wiley-Interscience: New York, 1976; p 164.

53. Friedrich, J.; Haarer, D. Chem. Phys. Lett. 1980, 74, 503.

54. Friedrich, J.; Swalen, J. D.; Haarer, D. J. Chem. Phys. 1980, 73, 705.

55. Personov, R. I.; Al'shitz, E. I.; Bykovskaya, L. A. JETP Lett. 1972. 15, 431; Opt. Commun. 1972, 6, 169.

56. Personov, R. I.; Al'shitz, E. I.; Bykovskaya, L. A.; Kharlamov, B. M. Sov. Phys.-JETP 1974, 38, 912.

57. Kharlamov, B. M.; Personov, R. I.; Bykovskaya, L. A. Opt. Commun. 1974, 12, 191.

58. Kharlamov, B. M.; Personov, R. I.; Bykovskaya, L. A. Opt. Spectrosc. 1975, 39, 137.

59. Kharlamov, B. M.; Personov, R. I.; Bykovskaya, L. A. Opt. Spectrosc. 1977, 42, 445.

60. Kharlamov, B. M.; Bykovskaya, L. A.; Personov, R. I. J. App. Spec. 1978, 28, 570.

61. Dubs, M.; Günthard, Hs. H. Chem. Phys. Lett. 1979, 64, 105.

62. Dubs, M.; Günthard, Hs. H. J. Mol. Struc. 1980, 60, 311.

63. Edelson, M. C.; Hayes, J. M.; Small, G. J. Chem. Phys. Lett. 1979, 60, 307.

64. Hayes, J. M.; Small, G. J. Chem. Phys. 1978, 27, 151.

65. Hayes, J. M.; Small, G. J. Chem. Phys. Lett. 1978, 54, 435.

66. Hayes, J. M.; Small, G. J. J. Luminescence 1979, 18/19, 219.

67. Small, G. J. to appear in the volume "Molecular Spectroscopy"; Agronovich, V. M.; Hochstrasser, R. M., Eds., of the series Modern Problems in Solid State Physics; Agranovich, V. M.; Maradudin, A. A., General Eds.; North Holland Publishing Co.; 1981.

68. Small, G. J. J. Chem. Phys. 1973, 58, 2015.

69. Small, G. J. Department of Chemistry, Iowa State University, Ames, Iowa, unpublished results.

70. Anderson, P. W.; Halperin, B. I.; Varma, C. M. Philos. Mag. 1972, 25, 1.

71. Phillips, W. A. J. Low Temp. Phys. 1972, 7, 351.

72. Jäckle, J.; Pické, L.; Arnold, W.; Hunklinger, S. J. Non-Cryst. Solids 1976, 20, 365.

73. Hunklinger, S.; Arnold, W. In "Physical Acoustics", Thurston, R. N.; Mason, W. P., Eds.; Academic Press: New York, 1976; Vol. 12, p 155.

74. See any kinetics text, for example Moore, W. J. "Physical Chemistry", 4th ed.; Prentice-Hall: Englewood Cliffs, New Jersey, 1972; Chapter 9.

75. Hayes, J. M.; Stout, R. P.; Small, G. J. J. Chem. Phys. 1981, 74, 4266.

76. Selzer, D. M.; Huber, D. L.; Hamilton, D. S.; Yen, W. M.; Weber, M. J. Phys. Rev. Lett. 1976, 36, 813.

77. Avouris, P.; Campion, A.; El-Sayed, M. A. J. Chem. Phys. 1977, 67, 3397.

78. Hegarty, J.; Yen, W. M. Phys. Rev. Lett. 1979, 43, 1126.

79. Reinecke, T. L. Solid State Commun. 1979, 32, 1103.

80. Lyo, S. K.; Orbach, R. Phys. Rev. B 1980, 22, 4223.

81. Wong, J.; Angell, C. A. "Glass Structure by Spectroscopy"; Marcel Dekker: New York, 1976.

82. Materials Advisory Board, Nat. Acad. Sci. Res. Council 1968, MAB-243.

83. Vogel, W.; Gerth, K. Glastech, Ber. 1958, 31, 15.

84. deVries, H.; Wiersma, D. A. J. Chem. Phys. 1980, 72, 1851.

85. Hayes, J. M.; Stout, R. P.; Small, G. J. J. Chem. Phys. 1980, 73, 4129.

86. Jäckle, J. Z. Physik 1972, 257, 212.

87. Silsbee, R. H. In "Optical Properties of Solids"; Nudelman, Sol; Mitra, S. S., Eds.; Plenum: New York, 1969; p 607.

88. Jones, K. E.; Zewail, A. H. In "Advances in Chemical Physics"; Zewail, A. H., Ed.; Springer Series in Chemical Physics; Springer: New York, 1978.

89. Reissland, J. A. "The Physics of Phonons"; Wiley: New York, 1973; p 257.

90. Hunklinger, S. J. de Phys. 1978, 39, C6-1444.

91. Di Bartolo, B. "Optical Interactions in Solids"; Wiley: New York, 1968; p 342.

92. Morgan, J. R.; Chock, E. P.; Hopewell, W. D.; El-Sayed, M. A.; Orbach, R. J. Phys. Chem. 1981, 85, 747.

93. Watts, R. J.; Crosby, G. A. J. Am. Chem. Soc. 1971, 93, 3184.

94. Avouris, P.; Campion, A.; El-Sayed, M. A. Chem. Phys. Lett. 1977, 50, 9.

95. For state assignments, see Martin, D. S., Jr. Inorg. Chim. Acta Rev. 1971, 5, 107.

96. Watts, R. J.; Crosby, G. A.; Sansregret, J. L. Inorg. Chem. 1972, 11, 1474.

97. Berlman, I. B. "Handbook of Fluorescence Spectra of Aromatic Molecules", Academic Press: New York, 1965; p. 132.

98. Fleischer, E. B.; Sung, N.; Hawkinson, S. J. Phys. Chem. 1968, 72, 4311.

99. Brandon, R. W.; Closs, G. L.; Davoust, C. E.; Hutchison, C. A., Jr.; Kohler, B. E.; Silbey, R. J. Chem. Phys. 1965, 43, 2006.

100. Kruse, N. J.; Small, G. J. J. Chem. Phys. 1972, 56, 2985.

101. Griesser, H. J.; Wild, U. P. J. Chem. Phys. 1980, 73, 4715.

102. Eslinger, D. R. M.S. Thesis, Iowa State University, Ames, Iowa, 1973.

103. Kushida, T.; Takushi, E. Phys. Rev. B 1975, 12, 824.

104. Hegarty, J.; Brundage, R. T.; Yen, M. W. Appl. Opt. 1980, 19, 1889.

105. Stout, R. P. Quarterly Report, The Ames Laboratory, Iowa State University, Ames, Iowa, 6/1/80-8/31/80.

106. Bragg, W. L.; Williams, E. J. Proc. Roy. Soc. 1935, A151, 540.

107. Dickerson, R. E. "Molecular Thermodynamics"; Benjamin: Menlo Park, Calif., 1969; p. 238.

108. Huang, K. "Statistical Mechanics"; John Wiley: New York, 1963; Chapters 16, 17.

109. Yen, W. M.; Scott, W. C.; Schawlow, A. L. Phys. Rev. 1964, 136, A271.

110. Flach, R.; Hamilton, D. S.; Selzer, P. M.; Yen, W. M. Phys. Rev. B 1977, 15, 1248.

111. Stephens, R. B. Phys. Rev. B 1973, 8, 2896.

112. Banville, M.; Harris, R. Phys. Rev. Lett. 1980, 44, 1136.

113. Reinecke, T. L.; Ngai, K. L. Phys. Rev. B 1975, 12, 3476.

114. Ngai, K. L. Comments Solid State Phys. 1979, 9, 127.

115. Laser Focus 1980, 16(4), 14.

116. Laser Focus 1981, 17(4), 28.

117. Laser Focus 1978, 14(9), 30.

118. Zewail, A. H. Acc. Chem. Res. 1980, 13, 360.

ACKNOWLEDGMENTS

I am indebted to Dr. Gerald J. Small for his criticism and guidance throughout the course of this work. Thanks are also due to Dr. John M. Hayes for his help and advice and to the other members of the group, especially Carey Johnson and Sylvia Stevenson Adelman, for many enjoyable and helpful discussions. Thanks, too, to Dr. Steven Woodruff for his lunchtime company and the numerous incisive conversations.

To my wife, Linda, I give my sincere thanks for her constant love and support through this endeavor. Thank you Meleah for bringing so much serendipitous joy into our lives.

To the many friends I have had during my stay in Ames: for your friendship these past years which has served as a humanizing influence on what could otherwise have been a dehumanizing experience, I thank you.

APPENDIX

The purpose of this Appendix is to present the results of Lyo and Orbach (80) in a form which can be compared with the theory developed in this dissertation. The method used does not follow either their approach or that of the theory chapter of this work exactly, but draws on both.

Equation 4 of Lyo and Orbach (80) reads:

$$\Delta\omega = \frac{4\pi}{\hbar} \sum_{i,\vec{q},s} \int\int\int\int d\Delta d\omega_0 d\lambda df P(\Delta,\omega_0,\lambda,f)$$
$$\times \frac{[\hbar\omega_0 \exp(-\lambda)]^2 f^2 \langle (v_1 - v_0)_i^2 \rangle_{av} \Delta^2 \exp(-\beta E/2)}{E^4 (\hbar\omega_{\vec{q},s})^2 \cosh(\beta E/2)}$$
$$\times |\langle n_{\vec{q},s} + 1 | \varepsilon | n_{\vec{q},s} \rangle|^2 \delta(E - \hbar\omega_{\vec{q},s}) \qquad \text{(A1)}$$

where many of their symbols are different from those used in this dissertation. The following table lists those symbols which can be directly converted into the notation used here.

Table A1. Conversion of symbols in Lyo and Orbach (80) to those used herein

Lyo and Orbach	This work	Description
$\Delta\omega$	$\langle \Gamma_I \rangle_T$	Linewidth due to dephasing
Δ	ε	TLS asymmetry
$\hbar\omega_0 \, e^{-\lambda}$	$\Delta = \hbar\omega_0 \, e^{-\lambda}$	2 x tunneling rate
E	E	Tunnel state splitting
i	α	TLS label

Table A1. (Continued)

Lyo and Orbach	This work	Description
ρ	ρ	Mass density
$n_{\vec{q},s} + 1$	m	Phonon states
$n_{\vec{q},s}$	n	
$\Sigma_{\vec{q},s}$	$\Sigma_n\Sigma_m\Sigma_s$	Sum over phonon states
v	c	Average sound velocity

Writing the strain ε in terms of phonon creation and annihilation operators $\hat{b}^+_{\vec{q}}$ and $\hat{b}_{\vec{q}}$ (91) and using the conversions given above, Eq. A1 becomes

$$\langle\Gamma_I\rangle_T = \frac{4\pi}{\hbar}\sum_\alpha\sum_n\sum_m\sum_s\int\int\int\int d\varepsilon d\omega_0 d\lambda df P(\varepsilon,\omega_0,\lambda,f) \times \frac{\Delta^2 f^2 \langle(v_1-v_0)^2_\alpha\rangle_{av}\varepsilon^2 \exp(-\beta E/2)}{E^4(\hbar\omega_s)^2\cosh(-\beta E/2)} \times \frac{\hbar\omega_s}{2Mv^2}\,|\langle m|\hat{b}-\hat{b}^+|n\rangle|^2\,\delta(E-h\omega_s)\ . \tag{A2}$$

f, in these equations, is the difference in the phonon coupling strength to the two wells of TLS and $(v_1)_\alpha$, for example, is the difference in the coupling strength of the impurity state $|1\rangle$ to the two wells of TLS$^\alpha$. $(v_1-v_0)_\alpha$, then, is a difference of differences representing the change in the coupling of the two wells of TLS$^\alpha$ to the impurity excited ($|1\rangle$)

and ground ($|0\rangle$) states. The terms containing f and v_1-v_0 are contained in δB defined by Eq. 2.26 according to

$$\int df\ P'(f) f^2 \langle (v_1-v_0)_\alpha^2 \rangle_{av} \longrightarrow (\delta B)_\alpha \tag{A3}$$

where the probability function P'(f) has been extracted from the total probability function $P(\varepsilon,\omega_0,\lambda,f)$. Assuming that P varies only slowly in ε and λ (constant TLS distribution), the probability function may be approximated

$$P(\varepsilon,\omega_0,\lambda) \approx P(0,\omega_0,\lambda_{min}) \tag{A4}$$

where λ_{min} is the lower limit for the tunneling integral ($\int d\lambda$). The lower limit may be written in the form $\varepsilon > 2\hbar\omega_0 e^{-\lambda} = \Delta$ allowing the replacement of ε by E and the transformation of the ε integration into an integration over E. Recalling that on the average, one TLS dominates the dephasing, Eq. A2 becomes

$$\begin{aligned} \langle \Gamma_I \rangle_T = \frac{4\pi}{\hbar} \sum_n \sum_m \sum_s \int d\omega_0 \int d\lambda \quad & P(0,\omega_0,\lambda_{min}) \\ & \times \int dE\ \frac{\Delta^2 (\delta B)^2\ E^2\ \exp(-\beta E/2)}{E^4\ (\hbar\omega_2)^2\ \cosh(-\beta E/2)} \\ & \times \left(\frac{-\hbar\omega_s}{2Mc^2}\right) |\langle m|b|n\rangle - \langle m|b^+|n\rangle|^2 \\ & \times \delta(E-\hbar\omega_s)\ . \end{aligned} \tag{A5}$$

With the definitions of m and n given in Table A1, the phonon matrix elements may be evaluated

$$|\langle m|0|n\rangle - \langle m|b^+|n\rangle|^2 = |\langle m|m\rangle \sqrt{m}\ |^2\ . \tag{A6}$$

The sums in Eq. A5 are converted to integrals using a Debye density of phonon states $\frac{3V\omega^2}{2\pi^2c^3}$ for a sample volume V, and these integrals evaluated to give

$$\langle\Gamma_I\rangle_T = \frac{4\pi}{\hbar}\int d\omega_0 \int d\lambda\ P(0,\omega_0,\lambda_{min}) \times \int dE\ \frac{\Delta^2(\delta B)^2\, E^2\, \exp(-\beta E/2)}{E^4\,(\hbar\omega)^2\cosh(-\beta E/2)} \times \left(\frac{\hbar\omega}{2Mc^2}\right)\left(\frac{3V\omega^2}{2\pi^2c^3}\right)\left(\langle n_\omega\rangle_T + 1\right)\delta(E - \hbar\omega), \tag{A7}$$

where $\langle n_\omega\rangle_T = [\exp(\omega/kT) - 1]^{-1}$ is the phonon thermal occupation number. Finally, ω_0 and λ are contained in Δ which is in turn contained in E. In the theory presented in this work, ω_0 and λ are not explicitly averaged but are implicitly contained in the average over E and in the adoption of a "maximum" interval for the dephasing frequency prior to Eq. 2.32. The integrations over ω_0 and λ are, therefore, dropped and terms collected to obtain

$$\langle\Gamma_I\rangle_T = \frac{3}{\rho\pi c^5\hbar^2}\ P(0,\omega_0,\lambda_{min}) \int dE\ \frac{\Delta^2(\delta B)^2\omega}{E^2} \times \frac{\exp(-\beta E/2)}{\cosh(-\beta E/2)}\left(\langle n_\omega\rangle_T + 1\right)\delta(E - \hbar\omega)\ . \tag{A8}$$

Evaluation of the E integral gives

$$\langle\Gamma_I\rangle_T = \frac{3}{\rho\pi\hbar^4c^5}\,P(0,\omega_0,\lambda_{min})\,\frac{\Delta^2(\delta B)^2}{\omega} \times \frac{\exp(-\beta\hbar\omega/2)}{\cosh(-\beta\hbar\omega/2)}\left(\langle n_\omega\rangle_T + 1\right) \tag{A9}$$

which is compared with Eq. 2.32 in the main text.

Equation 6 of reference 80 is

$$\Delta\omega = \frac{(k_B T)^2 \eta D\langle V^2\rangle}{96 \hbar \rho B}, \tag{A10}$$

where η is a constant of order unity,

$$D = 3\pi B \iint d\omega_0 \, df \, P(0,\omega_0,\lambda_{min},f) f^2 , \tag{A11}$$

and B is a normalization factor given by

$$B \iiint P \, d\omega_0 \, df \, d\lambda \approx 1. \tag{A12}$$

Equation A9, written in the notation of this dissertation, reads

$$\langle \Gamma_I \rangle_T = \frac{c \, (kT)^2 (\delta B)^2}{96 \, h^4 \, \rho} \tag{A13}$$

where c is a constant incorporating terms from η, D and B.